AEOSR-TR- 91 0045

(2)

[redacted]

LMSC-F404864

HIGH TEMPERATURE INTERACTIONS OF METALLIC MATRICES WITH CERAMIC REINFORCEMENTS

AD-A232 967

CONTRACT #F49620-88-C-0021

AIR FORCE OFFICE OF SCIENTIFIC RESEARCH

ANNUAL TECHNICAL REPORT

for the period ending

December 31, 1990

DTIC
ELECTE
MAR 12 1991
S D
D

Prepared by

A. Joshi, T.C. Chou and J. Wadsworth

Lockheed Palo Alto Research Laboratory

3251 Hanover Street, Palo Alto, CA 94304

DISTRIBUTION STATEMENT A
Approved for public release
Distribution Unlimited

91 3 06 096

SECURITY CLASSIFICATION OF THIS PAGE

REPORT DOCUMENTATION PAGE

Form Approved OMB No. 0704-0188

1a. REPORT SECURITY CLASSIFICATION: Unclassified	1b. RESTRICTIVE MARKINGS: N/A
2a. SECURITY CLASSIFICATION AUTHORITY	3. DISTRIBUTION/AVAILABILITY OF REPORT: Unlimited
2b. DECLASSIFICATION/DOWNGRADING SCHEDULE	
4. PERFORMING ORGANIZATION REPORT NUMBER(S): LMSC-F404864	5. MONITORING ORGANIZATION REPORT NUMBER(S): ~~F49620-88-C-0021~~ AFOSR-TR- 91 0045
6a. NAME OF PERFORMING ORGANIZATION: Lockheed Missiles & Space Company; 6b. OFFICE SYMBOL (If applicable)	7a. NAME OF MONITORING ORGANIZATION: Air Force Office of Scientific Research
6c. ADDRESS (City, State, and ZIP Code): Lockheed R&D Division, 3251 Hanover Street, Palo Alto, CA 94304	7b. ADDRESS (City, State, and ZIP Code): Bldg. 410-NE, Bolling AFB, DC 20332
8a. NAME OF FUNDING/SPONSORING ORGANIZATION: AFOSR; 8b. OFFICE SYMBOL (If applicable): NE	9. PROCUREMENT INSTRUMENT IDENTIFICATION NUMBER: F49620-88-C-0021
8c. ADDRESS (City, State, and ZIP Code): Bldg. 410-NE, Bolling AFB, DC 20332	10. SOURCE OF FUNDING NUMBERS: PROGRAM ELEMENT NO. 61102F; PROJECT NO. 2306; TASK NO A1; WORK UNIT ACCESSION NO.

11. TITLE (Include Security Classification)

High Temperature Interactions of Metallic Matrices with Ceramic Reinforcements

12. PERSONAL AUTHOR(S)

A. Joshi, T.C. Chou and J. Wadsworth

13a. TYPE OF REPORT	13b. TIME COVERED	14. DATE OF REPORT (Year, Month, Day)	15. PAGE COUNT
Annual	FROM 1/1/90 TO 12/31/90	1990 December 31	77

16. SUPPLEMENTARY NOTATION

17. COSATI CODES		
FIELD	GROUP	SUB-GROUP

18. SUBJECT TERMS (Continue on reverse if necessary and identify by block number)

Nb, Co, Ni, Pt, SiC, Al_2O_3, stainless steel, composites, metal matrix, thin films, diffusion, diffusion couples, diffusion barriers, ceramics, reinforcement, kinetics, reactions, decomposition, interfaces, Auger electron spectroscopy

19. ABSTRACT (Continue on reverse if necessary and identify by block number)

Interfacial reactions of SiC with selected high temperature metals have been studied at temperatures between 800 and 1200°C for various times. The metals include Nb, a strong carbide former, Co, Ni, Pt, and stainless steel. Reactions of the metals with SiC in this temperature range were extensive; various metal silicides, metal carbides, ternary metal-silicon-carbides, and unreacted carbon were formed as layered reaction products in the reaction zones. Thin films of Al_2O_3 in the 100 to 500 nm thickness range are shown to be effective in minimizing the reaction between Nb and SiC. In some systems, massive or localized interfacial melting was observed as a result of metal-silicide formation. Reactions of SiC with Ni, Co, Pt and stainless steel resulted in the formation of clustered carbon precipitates with modulated or randomly scattered characters. The nature of the C precipitation behavior depends upon the specific metal system and is a function of distance from the reaction interfaces. In contrast, no unreacted carbon was found in the SiC/Nb system. The rate limiting step for the reactions of SiC with metals is discussed in light of the decomposition of SiC, which was sluggish in all cases. Discontinuous decomposition of SiC is proposed to explain the modulation of C precipitates.

20. DISTRIBUTION/AVAILABILITY OF ABSTRACT	21. ABSTRACT SECURITY CLASSIFICATION
☒ UNCLASSIFIED/UNLIMITED ☐ SAME AS RPT ☐ DTIC USERS	UNCLASSIFIED
22a. NAME OF RESPONSIBLE INDIVIDUAL: ~~A. Joshi~~ R. Rosenstein	22b. TELEPHONE (Include Area Code): ~~415-424-2206~~ 202-767-4939; 22c. OFFICE SYMBOL: NE

DD Form 1473, JUN 86 — Previous editions are obsolete. — SECURITY CLASSIFICATION OF THIS PAGE

CONTENTS

Accesion For
NTIS CRA&I ✓
DTIC TAB
Unannounced
Justification
By
Distribution /
Availability Codes
Dist | Avail and / or Special
A-1

QUALITY INSPECTED 3

LIST OF FIGURES

LIST OF TABLES

Section 1

INTRODUCTION

Advanced aerospace systems require low density materials with substantially improved high temperature mechanical properties and oxidation resistance. Metal matrices with ceramic reinforcements offer such potential. From a structural viewpoint, the metal/ceramic interface controls the transfer of load between a metallic matrix and its ceramic reinforcement and thereby influences the mechanical properties of a composite. Ideally, such an interface should be a mechanical continuum, but a chemical discontinuum, implying no interdiffusion between the matrix and the reinforcement. In most practical situations, however, compound formation occurs at the interface and results in some loss in mechanical strength [1]. Improved design of metal/ceramic materials is limited by the lack of understanding of fundamental interaction mechanisms between metal matrices and ceramic reinforcements. Such an understanding is highly desired to establish a scientific basis for the future selection of metal/ceramic systems.

Matrix/reinforcement systems may be separated into different classes based upon the nature and extent of reactions at their interfaces [2]. The vast majority of metal/ceramic systems of interest for aerospace structural applications are those in which the reinforcement and matrix chemically react to form compounds at the interface. In general, the various metal species which possess low density and high ductility (eg., Al and Ti), have a thermodynamic tendency towards compound formation with the most desirable reinforcement species. As a result, carbides, borides, or silicides are usually encountered in the interfacial reaction zone. Often, the formation of such layers degrades mechanical behavior [3]. Examples of recent studies in this class include SiC/Ti [4-6], SiC/Ti-6Al-4V [4,5,7,8], B/Ti [9], SiC/Al [10-12], C/Al [13], SiC/Ni [14], and Al_2O_3/Mg [11,15].

Most investigations on metallic matrices and ceramic reinforcements have been empirical and have emphasized bulk engineering materials. Furthermore, they have concentrated on reaction layer thicknesses which are convenient for study, i.e., in excess of 3-5 μm, but that are not necessarily appropriate for understanding fundamental metal/ceramic interactions. Reaction layer thicknesses on the order of only 0.3-0.5 μm can lead to significant degradation in both strength and ductility. For example, thin (0.4 μm) titanium diboride (TiB_2) reaction layers in commercial purity titanium (TI-40A), reinforced with 25 vol% B filaments) lead to significant degradation in room temperature strain to fracture of the filament [3] and a TiB_2 layer thickness of only 0.7 μm can be tolerated before significant degradation in the ultimate tensile strength. Thus, an understanding and control of interfacial reactions is essential to obtaining good mechanical properties in metal/ceramic systems.

In most practical situations, interdiffusion or compound formation occurs at the interface during either high temperature consolidation processes or engineering applications. Since most of the refractory metal matrices contain metal species (e.g., Ti, Nb, Ni, Fe, Al, V or Co) having a high affinity for the elements present in reinforcing fibers (e.g., Si, B or C), the composite systems must be treated as non-equilibrium systems [4] from a thermodynamic view point. In other words, the interdiffusion distance increases and the evolution of compound formation gets more complex as a function of time at elevated temperatures. Interdiffusion between the matrix and reinforcement, together with compound formation, may result in interfacial embrittlement and associated degradation of the overall properties of a composite. In order to improve the design of composites, a fundamental understanding of interfacial reactions of metal matrices with ceramic reinforcements is crucially needed.

This annual report summarizes the reaction kinetic studies of Nb (matrix material candidate) thin films with SiC, the effectiveness of thin film Al_2O_3 diffusion barriers in minimizing the reaction between Nb and SiC, as well as interfacial reactions of Nb, Ni, Co, Pt and stainless steel matrix materials with SiC, evaluated in the form of bulk diffusion couples. The bulk diffusion couples were prepared by diffusion bonding plate-shaped SiC with pure metals and then vacuum annealing at selected temperatures. The nature and extent of interfacial reactions were evaluated using optical metallography, x-ray diffraction (XRD), Auger electron spectroscopy (AES) for surface, interface and thin film chemical characterization, and scanning electron microscopy (SEM) and transmission electron microscopy (TEM) for detailed microstructural characterization.

Section 2

TECHNICAL BACKGROUND

2.1 Selection of Candidate Systems

The list of metal/ceramic combinations selected for study in the present program is shown in Table I. Two FCC metal matrices have been selected: Aluminum and Nickel. Aluminum is a key element as it is likely to impart oxidation resistance to, and decrease the density of, alloys or intermetallic compounds constituting the matrix of future engineering materials. Nickel was selected as a matrix material since many existing high temperature alloys are based on a nickel matrix. Cobalt, with a similar melting point and adjacent to nickel in the periodic table, was selected as a HCP matrix candidate. Stainless steel is selected as a multicomponent matrix candidate for evaluating the possible complex reactions. Ti and Nb, have been selected because their crystal structures are HCP and BCC, respectively, and their melting points are high enough to permit elevated temperature applications. They are also under active consideration as the basis of alloys for high temperature aerospace applications. Niobium is particularly interesting among the refractory metals due to its relatively low density (by comparison with Mo, W, and Ta). At the beginning of the present program, a niobium target, required for sputter deposition, could not be procured immediately. To minimize associated delays, experimental work was undertaken using tantalum, that was readily available, and for which most diffusional and reaction aspects are expected to be very similar to niobium. Selected tasks to evaluate the interaction between the intermetallic compound Ti_3Al and the reinforcements shown in Table I are also in progress.

SiC and Al_2O_3 are two of the most common reinforcement candidates because of their low density, good mechanical strength, and thermal stability at elevated temperatures. From considerations based on metal matrices, the most popular current materials used in the aerospace industry focus on nickel-, niobium-, and titanium- based alloys. In this work we emphasize the reactions of SiC with those elemental species which are contained in most of the refractory alloys. In addition, reactions of SiC with multi-element metal matrices were also studied to provide a fundamental understanding of SiC reaction behavior in the presence of various elemental species.

A few previous studies [6,16-32] have investigated the thermal compatibilities, fiber-matrix (FM) reactions, or solid state reactions of SiC with various high temperature metallic materials, e.g., Ti [6,16,17], Ni [18-20], Fe [18], Co [20], Nb [21-23], Pt [24,25], titanium aluminides [26-28], titanium alloys [27], nickel aluminides [29,30], and superalloys [31,32]. Most of these studies have been concentrated primarily on the determination of reaction products of metal/SiC reactions, and the growth kinetics of

reaction layers, which were deduced from the thicknesses of reaction layers as a function of reaction time. It is not the intent of this work to readdress or correlate those well-known phenomena.

The objective of this study is to explore a several fundamentally intriguing questions, e.g., the decomposition characteristics of SiC (in the presence of various metals), the effect of metal silicide formation (on interfacial properties), the thermodynamic driving force, and carbon precipitation behavior during SiC/metal reactions at high temperatures. To address these issues, elemental metals of Nb, Ni, and Co, and alloys of stainless steel (SS), containing Fe, Ni, and Cr, were reacted with SiC. Both thin film and bulk diffusion couples with plane interfaces, rather than consolidated metal powders with reinforcing fibers, were prepared to evaluate the metal/SiC reactions.

In addition to SiC and Al_2O_3, Si_3N_4, which does not contain the reactive elements C and O, was selected for additional evaluations. A tentative list of all the selected metal matrices and ceramic reinforcements are shown in Table I.

2.2 Summary of Previous Work

Interdiffusion and interfacial reactions occurring in candidate metal matrix and ceramic reinforcement materials were evaluated using diffusion couple specimens. Al, Ni, and Nb metal films were deposited on SiC and Si_3N_4 ceramic substrates, and vacuum annealed for selected times at elevated temperatures. The nature of diffusion, interfacial reactions and microstructural modifications were studied using optical microscopy, scanning electron microscopy, differential scanning calorimetry, Auger electron spectroscopy and transmission electron microscopy.

The reactions of Nb metal with a polycrystalline SiC substrate in the temperature range 800°C to 1300°C lead to the formation of layered structures. Detailed AES and TEM studies suggest a typical reaction sequence to be Nb/Nb_2C/Nb_5Si_4C/NbC/SiC. Variations to this sequence have been observed and were explained based upon extraneous (contaminant) phases present on the SiC surface. Reactions with the substrate resulted in formation of several phases, including NbC, Nb_2C, Nb_5Si_3 and Nb_5Si_4C. Reactions with the oxygen and carbon present in the vacuum annealing environment resulted in formation of NbO and NbC. Thermodynamic analysis and experimental studies of compatibility of Nb with Al_2O_3 indicate minimal reactions for temperatures up to 1200°C. In order to verify the effectiveness of Al_2O_3 as a diffusion barrier between Nb and SiC, a number of specimens were prepared with Al_2O_3 layers in the 100 to 500 nm range at the Nb/SiC interface. The usefulness of such interfacial barriers is discussed in the following section.

Interfacial reactions of Al with SiC and Si_3N_4 were studied utilizing ~1 μm Al films sputter deposited on the ceramic substrates. Reactions of Al/Si, Al-1wt%Si/Si are also being investigated to better understand the driving forces of these reactions and to evaluate the role of Si alloyed in Al on the interfacial reaction. The reaction of Al with SiC annealed for up to 2 h at 600°C was found to be minimal and did not result in the formation of Al_4C_3 or similar interfacial reaction products. In contrast, complete interdiffusion and eutectic reaction occurred in the Al/Si system. The reaction of Al with Si_3N_4 upon annealing for 1 h at 600°C resulted in near-complete disappearance of the Al metal from the surface. It is suspected that Al diffused into the substrate and formed AlN.

Reaction of Ni with SiC and Si_3N_4 substrates was evaluated at two temperatures, viz., 725°C ($0.5xT_m$) and 1160°C ($0.8xT_m$). Reaction with SiC at both temperatures resulted in formation of a layered structure similar to $NiSi_x/NiSi_xC_y/SiC$. The top layer contained little or no carbon and the second layer consisted of an estimated 30 to 40 at.% carbon. Even though the layered structures are similar, the lower temperature annealed specimen exhibited a thinner total reaction zone compared to the high temperature annealed specimen. The ternary phase diagram of Ni-Si-C at 1150°C does not exhibit any carbon-rich phases, which suggests that the $NiSi_xC_y$ region is possibly a physical mixture of carbon with $NiSi_x$. Such a phase would also be required to maintain a thermodynamic equilibrium between Ni and SiC. The interaction of Ni with Si_3N_4 at 1160°C was associated with extensive surface migration and reactions. Numerous $NiSi_x$ precipitates were observed on the surface. Nitrogen was observed throughout the film indicating the formation of a ternary phase or formation of islands of Si_3N_4 surrounded by $NiSi_x$ and Ni.

All the above results were obtained from the evaluations of thin film couple specimens. Bulk diffusion couple specimens are likely to compliment this information by providing information on more extensive reactions and in thoroughly characterizing the reaction products. They may also be helpful in simulating reactions in real composite materials. Reactions of Nb, Ni, Co, and stainless steel with SiC in bulk diffusion couple form are discussed in the following sections.

Section 3

EXPERIMENTAL

Evaluation of Al_2O_3 diffusion barriers in the Nb/SiC system was conducted using thin film couple specimens. All other studies reported in this period were conducted using bulk couples.

3.1 Preparation of Thin Film Couple

3.1.1 Substrate Preparation: SiC polycrystalline substrates were obtained from Carborundum (formerly Standard Oil Engineered Materials). They were 1 cm x 1 cm x 0.23 cm Hexoloy SA SiC Tiles and were fabricated from powders, which were formed into a green product and then sintered in argon or nitrogen at temperatures exceeding 2000° C. The SiC content of the Hexoloy is typically 99.2 weight percent and a representative chemical analysis, as supplied by the manufacturer, is given in Table II. Prior to metal deposition, the SiC substrates were step polished and finished with 0.25 micron diamond paste. The surface contaminants were then removed by immersion in a solution of one part concentrated HF and one part distilled water for 30 to 60 seconds. Subsequently, they were ultrasonically rinsed in methanol. The HF solution was selected as an etchant because it effectively removed surface contamination without attacking the substrate. Also, the stoichiometry of the surface composition was not affected by etching, as determined by Auger Electron Spectroscopy.

3.1.2 Thin Film Deposition: The Al_2O_3 and niobium metal were deposited on SiC substrates for evaluating the effectiveness of Al_2O_3 diffusion barriers. A CVC 601 Loadlock sputter deposition system was used for the sputter deposition of the Al_2O_3 film and the metal on the SiC substrates that were further cleaned by reverse bias sputter etching prior to the deposition.

Aluminum oxide films were deposited from a sintered Al_2O_3 target by RF deposition in a plasma containing argon and oxygen. The oxygen concentration in the gas, and the RF power and bias on the target were varied to obtain films of superior quality. Film quality was evaluated by pin hole density measurements in an electrochemical cell and by x-ray photoelectron spectroscopy (XPS) for compositional analysis. Typical deposition parameters include 2000 V RF power, 100 to 200 V RF bias and 2 to 4% oxygen in the $Ar+O_2$ plasma. The base pressure prior to deposition is 1×10^{-7} torr and gas pressure during deposition is 10 millitorr. For diffusion barrier application aluminum oxide films with 100, 200 and 500 nm thicknesses were deposited on SiC substrates, followed by 1 μm of niobium without exposing to ambient in between. All the films exhibited pin holes, with the least seen in the thickest of the films. Estimated pin hole density is 6 to 10 per cm^2 with a hole size of less than 2 μm

diameter. In order to determine the number of pin holes in an aluminum oxide film, the film deposited on a silicon substrate was made a cathode in an electrochemical cell. The electrolyte used is a 50:50 mixture of water and ethanol. A pointed copper electrode is used as an anode to probe H_2 evolution at the cathode. Assuming that hydrogen is evolved only from the conductive areas (or pin holes in the oxide film), the actual number of pin holes could be counted and their density estimated. A schematic of the electrochemical cell employed to measure the pin hole densities is shown in Fig. 3.1. This method is only semi-quantitative but was useful in quickly ascertaining the quality of the deposited films.

The Nb metal films were DC sputter deposited on the Al_2O_3 layers without exposing to the ambient. The procedures for the metal depositions are presented in previous reports.

3.2 Bulk Diffusion Couples

3.2.1 Preparation of SiC Ceramic: The polycrystalline SiC substrates, designated as Hexoloy, were obtained from the Carborundum Corporation. The substrates were 1 cm x 1 cm x 0.23 cm, and they were formed by sintering at temperatures exceeding 2000°C. The SiC content of the Hexoloy is typically 99.2 wt%. Prior to metal deposition or diffusion bonding, the SiC substrates were step polished and finished with a 0.25 micron diamond paste. The surface contaminants were then removed by immersion in a solution of one part concentrated HF and one part distilled water for 30 to 60 s, followed by ultrasonic cleaning in methanol and drying by compressed air.

For Co, Ni and Pt couples, the polycrystalline SiC was prepared by hot pressing, and was identified by x-ray diffraction (XRD) and Raman spectra to be primarily β-SiC. The density of the plates was at least 99.5 % of theoretical value. The SiC plates were then cut into small pieces of approximate dimensions of 10mm x 5mm x 1.5mm, and polished with a 15μm diamond disc. The polished samples were ultrasonically cleaned in acetone, rinsed in water, and then dried using compressed air.

3.2.2 Preparation of Metals: The metals (Nb, Ni, and Co), which are 99.99% pure, were purchased from Aldrich Chemical Co. The stainless steel bulk material has an approximate bulk composition of Ni 30, Cr 24, Fe 46 (in at%), and trace amounts of Mn and Ti, as revealed by energy dispersive x-ray microanalysis. The Pt metal is 99.9% pure and was received from Engelhard Corporation. The metal pieces were cut into a similar size to that of the SiC, mechanically ground with #600 SiC papers, polished by slurries containing 1 μm particle size alumina, fine polished with 1 μm diamond paste, and finished by ultrasonic cleaning in methanol and drying.

3.2.3 Formation of Bulk Diffusion Couples: To form a diffusion couple, reactant coupons of metals and SiC were stacked together, under a slight pressure (estimated 0.5 kg/cm^2) from a dead weight or by utilizing a pressure clamp, to achieve an intimate contact. For the Co, Ni and Pt couples with SiC,

diffusion anneals were performed in either a tube furnace, which was flushed with He gas, or in a vacuum of 5×10^{-7} torr. Upon completion of the diffusion anneals, the samples were quenched in either water or liquid nitrogen. Vacuum annealed samples, however, were furnace cooled. To facilitate the measurement of reaction zone thickness, metals of a slightly different area from SiC were used so that the original joining interface could be distinguished and serve as a reference boundary. The thickness of the reaction zones on both the metal and SiC sides were measured from this reference boundary.

3.3 Thermal Treatments

The thin film and the bulk diffusion couple specimens were annealed in vacuum with a base pressure of 5×10^{-6} torr at temperatures ranging from 600 to 1200° C for 1 to 12 hours. The specific treatments are included in the results and discussion section.

3.4 Characterization

The diffusion couples were transversely sectioned and reaction zones were analyzed by optical microscopy, scanning electron microscopy with EDS (energy dispersive spectrometry) microanalysis, x-ray diffraction, and scanning Auger microprobe. Electron microprobe analysis was conducted to establish quantitative atomic concentration profiles. The carbon precipitation behavior was examined by a laser Raman microprobe. Thin film metal/ceramic diffusion couples were characterized using optical metallography, x-ray diffraction, scanning electron microscopy (SEM), transmission electron microscopy (TEM) and Auger electron spectroscopy (AES). Altogether, they provided detailed topographical, compositional, and structural information of the reaction products.

Section 4

RESULTS AND DISCUSSION

This section discusses the continuing work on interfacial reactions in the Nb/Al_2O_3/SiC system, where Al_2O_3 thin films are employed as diffusion barriers, as well as reactions of SiC with metals Nb, Ni, Co and Pt in the form of bulk diffusion couples.

4.1 Nb/Al_2O_3/SiC System

AES profiles were obtained from Nb/Al_2O_3/SiC specimens containing 100, 200 and 500 nm thicknesses of interfacial Al_2O_3 layers. Figs. 4.1 and 4.2 show the profiles for specimens that were vacuum annealed for 2 h at 1200 °C. The niobium layer remained mostly unreacted in all cases, as indicated by the minimal build-up of silicon in the Nb film. In all instances both carbon and oxygen are seen in the films; this is likely to be a result of contamination occurring in the vacuum annealing system. Similar artifacts were observed in a number of specimens in the past. The reduction in the extent of interfacial reaction becomes more evident from a comparison of these profiles with those of Nb/SiC films in the as-deposited condition and after annealing for 2 h at 1200 °C. Fig. 4.3 also includes a Nb/SiC film for comparison. In the absence of an Al_2O_3 diffusion barrier, the reaction of Nb with SiC results in the formation of a sequence of reaction products, illustrated by Nb/Nb_2C/Nb_5Si_4C/NbC/SiC.

Several attempts were made to minimize the contamination occurring from the vacuum system during annealing at the elevated temperatures. These included improving the vacuum integrity of the annealing system and placing a diffusion barrier layer at the surface of the thin film specimen. A 20 nm Al_2O_3 cap layer applied to various specimens to achieve a thin film structure represented by Al_2O_3/Nb/Al_2O_3/SiC was found to be quite effective. AES results from a capped specimen which was subsequently annealed at 1200 °C for 2 hours is shown in Fig. 4.4. It is seen that both the carbon and oxygen levels in the Nb film are lower compared to the uncapped specimens. It is also noteworthy, in this film with a 100 nm Al_2O_3 diffusion barrier layer, that the reaction of Nb with SiC and the associated diffusion of Si into the Nb film is also lowered. These results indicate that a thin 100 nm Al_2O_3 diffusion barrier layer is effective in minimizing the interfacial reaction in the Nb/SiC system.

4.2 Reactions of Nb/SiC

Sequential annealing was conducted on Nb/SiC bulk diffusion couples at 1200 °C for 6, 18, 32, and 48 h; cross-sectional views of the reaction zones are shown in Figs. 4.5(a), (b), (c), and (d). Two layered

reaction products, as indicated by 1 and 2 in Fig. 4.5(a), were formed in the Nb/SiC reaction zone. The thicknesses of the two layers were more or less uniform across the interface. Layer 1, formed on the SiC side, was found to be thinner than layer 2 which was formed on the Nb side. In addition, a heterogeneously nucleated third phase (phase 3) was noted attached to the reaction front of layer 2.

The thicknesses (x) of both layers 1 and 2 increased as a function of reaction annealing time (t) and exhibited a parabolic relationship ($x^2 = k\,t$, where k is a reaction rate constant). Fig. 4.6 includes plots of x vs. $t^{0.5}$ and shows a linear relationship for both layers 1 and 2, from which the reaction rate constants of 6.7×10^{-13} and 5.3×10^{-12} cm^2/sec, respectively, were deduced. It appears that the growth rate for layer 1 is slower than that for layer 2. In contrast, the sizes of the heterogeneously nucleated phase 3 could not be directly correlated to annealing time. Nevertheless, it seems that the number of nucleating sites of phase 3 increases with annealing time. Since phase 3 was not connected to the Nb/SiC original joining interface, as indicated in Fig.1, but rather was attached to the migrating reaction front of layer 2, it is believed that phase 3 was nucleated at a later stage of the Nb/SiC reactions.

According to both AES and WDS x-ray analyses, the chemistry of reaction products 1 and 3 were similar; both phases were relatively rich in C and Nb, but poor in Si, compared to reaction product 2. Based on these analyses and earlier research on the Nb/SiC system [22,23], the phases 1 to 3 were determined to be NbC_x, $NbSi_yC_z$, and NbC_x, respectively. These observations suggest that the sequence of reaction products in the 1200°C heated sample is SiC/NbC_x(layer 1)/$NbSi_xC_y$(layer 2)/NbC_x(phase 3)/Nb. No unreacted C was observed in the reaction zone.

The mechanism regarding the heterogeneous nucleation of NbC_x is not clearly understood. It is likely to be a result of localized outward diffusion of C atoms, through interstitial sites, from layer 2 toward Nb. When the local C concentration reaches a certain supersaturation level, the NbC_x phase starts to nucleate and grow. This is supported by the observation of an increase of the number of NbC_x precipitates as a function of time. Also, based on an isothermal section (at 1300°C) of a Nb-Si-C ternary phase diagram [33], the Gibbs thermodynamic phase rule requires the presence of NbC_x at the Nb/$NbSi_xC_y$ interface. Hence, it is possible that there exists a thin but unresolved NbC_x layer all along the interface, which piles up occasionally as observed. The reason why NbC_x phase nucleates homogeneously at the SiC reaction front is attributable to the existence of a uniformly distributed high concentration of C from dissociated SiC.

4.3 Reactions of Co, Ni and Pt with SiC

The metal/ceramic reactions give rise to layered reaction products consisting of various metal silicides (as matrices) and free unreacted carbon (as precipitates); the unreacted carbon was identified by laser Raman microprobe. No carbide formation (i.e.,Ni_3C, Co_2C, or Co_3C) was detected by x-ray diffraction

or electron microprobe analysis with wavelength dispersive spectrometry (WDS). The formation of metal-silicides results in interfacial melting at certain temperatures. The carbon precipitates were formed either randomly or periodically in the reaction zones, depending upon the metal system as well as the location with respect to the SiC reaction interface. Detailed metal/ceramic reactions are described in the following subsections.

4.3.1 Co/SiC reactions at 1100 and 1210°C: A Co/SiC reaction zone after 1100°C annealing for 6 hrs is shown in Fig. 4.7(a). Immediately adjacent to the Co metal is a region relatively free from C precipitation that is designated as carbon precipitation free zone (C-PFZ). A phase boundary separating the unreacted Co and the C-PFZ was observed and is indicated in Fig. 4.7(a). Clustered voids were noted in some sections along this phase boundary. The thickness of the C-PFZ is typically less than 10 μm and increases with annealing time. Adjacent to the C-PFZ, a reaction layer with randomly scattered C precipitates was noted. A higher magnification SEM image of this random carbon precipitation zone (R-CPZ) is shown in Fig. 4.7(b). Concentration profiles, determined by electron microprobe analysis, of Co and Si across the reaction zone indicate the formation of Co-rich silicides (Co_2Si). Compositional discontinuities in the Co and Si concentration profiles at the phase boundary were also observed and, furthermore, diffusion of Si into the unreacted Co was detected.

No apparent melting/solidification was observed in the Co/SiC reaction zone at 1100°C. Ex-situ fractured Co and SiC reaction interfaces, however, do show signs of interfacial melting. A SEM micrograph from a fractured SiC interface is shown in Fig. 4.8. Granular particles with curved and smooth surface morphologies were observed at the interface. EDS x-ray microanalysis shows the presence of Co and Si from these particulate reaction products. The morphological characteristics of the reaction products suggest a pre-occurrence of interfacial melting and solidification.

Reactions between Co and SiC at 1210°C are extensive. A Co sample of 2 mm in thickness, as compared to a SiC of 0.87 mm, was consumed completely after a reaction at 1210°C for 4 hrs. Massive interfacial melting followed by solidification was observed and is shown in Fig. 4.9(a) and (b), which differ by the stacking sequence of the Co metal and the SiC. Droplet-like reaction zones, as a result of a surface tension effect, were noted. Regardless of the relative position of the metal component with respect to the SiC component during diffusion bonding, the SiC reaction interface shows a concave contour. Moreover, the amount of SiC consumed during the reactions is exactly the same in the two different reaction geometries. The effect of gravity on the interface morphology, and SiC decomposition kinetics, is believed to be negligible. XRD results show that cobalt silicide (Co_2Si), a solid solution of Si in Co [Co(Si)], and free carbon (C) were all formed in the reaction zone. Cross-sectional optical micrographs, as shown in Fig. 4.10, of the reaction zone show the presence of C-PFZ as well as random carbon precipitation zone (R-CPZ). In the areas remote from the SiC reaction interface, two coexisting phases, featured by the light and gray areas in Fig. 4.10(f), were noted. Electron microprobe

analysis indicates that the light phase (as a matrix) is Co(Si) while the gray one is Co_2Si. A major portion of the reaction zone is physically separated from the unreacted SiC as a result of a weak Co/SiC interface. No distinguishable C-PFZ was observed in the region close to the Co because of the complete consumption of the Co layer during the metal/ceramic reaction.

4.3.2. Ni/SiC reactions at 1100 and 1170°C: The Ni/SiC reactions at 1100°C, as shown in Fig. 4.11(a), (b) and (c), generate similar patterns to those in the Co/SiC reactions. In addition to the formation of C-PFZ and R-CPZ, a modulated carbon precipitation zone (M-CPZ) was also generated in the region adjacent to the SiC component. High magnification SEM micrographs of the Ni/SiC reaction zone are shown in Fig. 4.12(a), (b) and (c). It is noted that the M-CPZ, see Fig. 4.12(a), is composed of patches of very fine C precipitates. At locations farther removed from the SiC reaction front, from which the C was decomposed, the C starts to redistribute and exhibit a more random pattern, as shown in Fig. 4.12(b) and (c). Moreover, the C precipitates appear more globular and to increase in size as a function of distance from the SiC reaction front. The thickness of the C-PFZ in the Ni/SiC reaction zone is in the same range as that in the Co/SiC; it also increases with annealing time. The C-PFZ is separated from the Ni component by a phase boundary which is clustered with voids.

Quantitative electron microprobe analysis across the Ni/SiC reaction zone, see Fig. 4.13, indicates that the C-PFZ is composed of Ni_3Si, while the CPZ (which includes M-CPZ and R-CPZ) is primarily Ni_5Si_2 phase. An inward diffusion of Si into the Ni was also noted. No obvious compositional discontinuity, however, was observed at the phase boundary; this result is not clearly understood at this time. Thickness measurements of the reaction zone on the Ni and SiC sides show that the reaction zone on the Ni side is thicker than that on the SiC side.

The Ni/SiC reactions at 1170°C give rise to massive interfacial melting, which is characterized by the formation of a teardrop-shaped reaction zone and porosity as a result of solidification. The Ni sample is 2 mm in thickness, as compared to the SiC sample which is 1 mm, and was consumed completely during the reaction. In the reaction zone, non-planar reaction interfaces as well as microcracks were generated. The generation of microcracks is suggested to be a result of mismatch of the thermal expansion coefficients between the reaction products and SiC. By XRD analyses, see Fig. 4.14, $Ni_{31}Si_{12}$ and C were identified to be present in the reaction zone. Cross-sectional views of the reaction zone show the formation of M-CPZ and R-CPZ, as shown in Fig. 4.15. A C-PFZ was not observed in this case because the Ni component was consumed completely during the reaction.

4.3.3. Pt/SiC reactions at 900, 1000 and 1100°C: The Pt/SiC reactions at 900, 1000 and 1100°C were found to be very similar to each other. Interfacial melting was observed, as marked by arrows in Fig. 4.16, for all the samples annealed in these temperature regimes. This suggests that either the melting point of the reaction product(s) is lower than the respective annealing temperatures, or that the enthalpy

of Pt/Si solid state intermixing is high. XRD analysis of the Pt/SiC reaction zones shows the formation of Pt_3Si, Pt_2Si, and a mixture of Pt-silicides upon annealing at temperatures 900, 1000 and 1100°C, respectively. The XRD spectra are shown in Fig. 4.17 (a), (b) and (c).

Cross-sectional views of the Pt/SiC reaction zones show three distinguishable reaction layers. SEM micrographs of a Pt/SiC reaction zone after 1100°C annealing are shown in Fig. 4.18. Starting from the Pt reaction interface [Fig. 4.18(a)], a 1st layer containing alternate Pt-silicide/C-decorated Pt-silicide bands [Fig. 4.18(b),(c) and (d)] is followed by a 2nd layer with clustered discrete C bands [Fig. 4.18(e) and (f)], and a 3rd layer consisting of randomly scattered C precipitates in the areas adjacent to the SiC interface [Fig. 4.18(f)]. In the areas adjacent to the Pt component, a large volume of porosity was generated. There is also a microcrack, running parallel to the reaction interface, formed within the 2nd layer.

It is noted in Fig. 4.18 that the frequency of the presence of the discrete C bands, which formed in the 2nd layer, decreases as a function of distance from the Pt reaction interface. As the Pt interface is approached, see Fig. 4.19(a), (b), (c), and (d), clustered discrete C bands disappear and C-decorated granular Pt-silicide layers evolve. The granular microstructure develops as a result of the formation and subsequent grain growth of Pt-silicide. Carbon is found to decorate the microstructure either along grain boundaries or within the grains, presumably on defect sites. The thickness and grain growth phenomena of the granular layers become more prominent at locations farther away from the SiC reaction front. The transition from discrete C layers into C-decorated granular layers was noted and is evident in Fig. 4.19(b) and (c). As the reaction temperature decreases, similar phenomena were also observed, but to a much lesser extent than those at high temperature.

The pre-occurrence of melting/solidification during the Pt/SiC reactions is evidenced by the microstructure in the reaction zone from as-reacted Pt/SiC samples. A typical example is shown in Fig. 4.20 of the microstructural change as a function of distance from a Pt/SiC diffusion couple after reaction at 1000°C. A dendritic-shaped reaction zone (Pt_2Si) was noted to be generated in front of a microcrack, which is adjacent to alternating layers of Pt-silicide and C. The dendrites are oriented perpendicular to the reaction interface. In other words, the growth orientation of the dendrites is parallel to the direction of thermal conduction during the cooling of the interfacial melt.

In the area (which corresponds to a 3rd layer in a Pt/SiC diffusion couple) immediately adjacent to the unreacted SiC, clustered granular particles were noted to form on a matrix which has a similar granular microstructure to the SiC. A high magnification backscattered electron image of the 3rd layer is shown in Fig. 4.21. A brighter contrast was observed from this layer than from the SiC, indicating that the average atomic density of the layer is greater. Inward diffusion of Pt into the 3rd layer was detected by EDS. The smooth surface morphology of those clustered particles suggests that they have undergone

melting/solidification. Based on EDS microanalyses, the particles were identified as having a chemistry close to Pt_2Si.

A similar microstructure between the 3rd layer and the unreacted SiC suggests that the phase transition from SiC to Pt-silicides in the 3rd layer is incomplete. Raman microprobe analyses from the 3rd layer, however, indicates the presence of C only. Neither SiC nor Si characteristic peaks were detected.

A list of major reaction products and interfacial phenomena observed from the samples which were diffusion annealed at various temperatures for different times is given in Table III. For all the Co/SiC, Ni/SiC, and Pt/SiC reactions, Raman microprobe analyses indicate that C precipitates exist in a mixed glassy/graphitic state. A series of Raman spectra are shown in Fig. 4.22 (a),(b),(c), and (d), which were obtained from C precipitates, located both in regions close to the SiC and farther away, in the Pt/SiC reaction zone after diffusion annealing at 1000°C. In the regions close to the SiC reaction interface, the C exists primarily in a glassy state. Graphitization of the C occurs, however, as its location is farther removed from the SiC interface. The formation of glassy carbon is characterized by the presence of a Raman peak at 1354 cm^{-1}, whereas graphitization of the glassy carbon is indicated by a decrease of the intensity ratio between the 1354 and 1585 cm^{-1} Raman peaks [33b].

4.3.4 Reaction products and interfaces: Co, Ni and Pt metals are known to react with Si and to form various silicides. According to the present experimental results, these metals also react with SiC ceramics and form various silicides. In addition, free unreacted C is also generated as a result of the metal/ceramic reactions. It is clear that the source of Si atoms originates from a decomposition of the SiC. The decomposition of the SiC therefore provides not only Si but also C. The decomposed Si atoms readily react with the metals to form silicides, whereas no carbide formation was detected. This may be attributed to a lower reaction affinity of the respective metals for carbon than for silicon. Thermochemistry data [34] show that the Gibbs free energies of Co_2C and Ni_3C formation at 1100 and 1200, and 727°C are +1090 and +880, and +6410 cal/mole, respectively. No data are available for Pt-carbides and Co_3C, or Ni_3C formation at temperatures above 727°C. The present study indicates that only metal-rich silicide phases were formed during the metal/ceramic reactions between 900 and 1200°C. The reaction is sluggish at temperatures below 900°C. However, the temperature at which decomposition of SiC can occur during a metal/SiC reaction has been reported to be as low as 500°C based on interfacial reactions between Ni and Pd thin films, of about 100 nm in thickness, on SiC substrates [19].

Considering the overall reactions between SiC and the metals of interest, SiC + M (Ni, Co, Pt) $\longrightarrow$ M_xSi_y + C, a negative Gibbs free energy of the reaction is necessary to assure the formation of metal silicides as well as of C. The decomposition of SiC into Si and C exhibits positive Gibbs free energies at all the temperatures being studied. In addition, the presence of unreacted C precipitates, which appear

to be an inert species within these material systems, in the metal silicide matrices requires the formation of interfacial energy. Both the positive Gibbs free energy of the SiC decomposition, and the total interfacial energy required between the C precipitates and metal silicide matrices, are factors that inhibit the metal/ceramic reactions. In order for the reactions to proceed, it is clear that Gibbs free energy of metal silicide formation must be highly negative in order to provide the thermodynamic driving force for the metal/ceramic reactions. Table II lists calculated Gibbs free energy for the decomposition of SiC at different temperatures. Experimental thermochemistry data for those metal silicides which were formed in the present studies, however, were not available.

According to the present results, two types of interfacial morphologies were observed. Planar interfaces were observed when solid state interdiffusion occurs alone. On the other hand, non-planar interfaces were generated when interfacial melting occurs. The non-planar interfaces show a concave contour with respect to the SiC component. Analogous to the grain growth phenomenon, the presence of a curved grain boundary (interface) is always associated with a net driving force (ΔP) which drives atomic diffusion fluxes from the convex side (positive curvature) toward the concave side (negative curvature). The driving force can be expressed by $\Delta P = \gamma_i/r_i + \gamma_j/r_j$, where $\gamma_{i,j}$ and $r_{i,j}$ are the interfacial energy and radius of curvature, respectively, of two orthogonal contours (i and j) of an interface. The presence of curved interfaces is expected to affect the interdiffusion rates of the constituents from either side of the concave reaction interface. Based on the interface morphologies observed in the present study, it is suggested that diffusion rates of the metal species (which lie in a positive curvature side) is further assisted by the creation of a non-planar interface.

It has been reported [35] that molten metals (i.e., Ni, Co, Pt, Fe, and Cr) attack SiC ceramic regardless of its high degree of chemical stability. Although no further details on the attack phenomenon and mechanism were given, it is believed that the attack is mediated through the formation of low melting point eutectic silicides. All of the listed metals are well-known to form various silicides across wide compositional ranges. It is suggested that once the silicide phase forms, which gives rise to interfacial melting and concave interfaces in SiC, the metal/SiC reaction is expedited and propagates until the SiC is consumed.

To understand the rate limiting step for the present metal/ceramic reactions, the thicknesses of the reaction zones on metal and ceramic sides were measured and correlated with the reaction time. When no interfacial melting occurs, it is noted that the thickness of the reaction zone on the SiC side is thinner than that on the metal side. In most cases, a parabolic growth rate law ($x^2 = kt$, where x is the thickness of reaction zone, k the reaction rate constant, and t the annealing time) is not obeyed according to the measured thickness of the reaction zone as determined from the SiC side. When interfacial melting occurs, the thickness of the reaction zone on the center of SiC, which shows the greatest thickness due to a concave interfacial morphology, is still much thinner than that of metal

counterpart. Based upon these observations, it is suggested that the metal/ceramic reaction is limited by the decomposition of SiC rather than interdiffusion of the constituents. This is further supported by the fact that the diffusion rates of metal and Si constituents in the reaction zone, which exists in a molten (or partially molten) state, are not expected to be slow.

In contrast to the present results, a diffusion limited parabolic growth rate was reported in the SiC/Ni [36] at 800°C, SiC/Ni alloys [32] at temperatures between 700 and 1150°C, and SiC/Ni and SiC/Co-1wt%Cu composites [20] at temperatures ranging from 1000 to 1200°C. It is not clear why there is a discrepancy in the relationship between the thickness of reaction zones v.s. reaction time among the different studies. It is believed that the conflicting results may originate from the surface characteristics (e.g., order and stoichiometry) as well as crystal structure of the SiC being used. For example, the formation of Al carbide (Al_4C_3) has been reported in an annealed Al thin film on Ar^+-ion bombarded single crystalline α-SiC [37] but not in an Al film on ordered and stoichiometric β-SiC(001) [38] under similar conditions. In view of the fact that interfacial melting was observed in Ni/SiC and Co/SiC systems in the present study, but not in those of previous studies in a similar temperature region, a direct comparison of the data from different studies is difficult.

A thinner reaction zone in the SiC than in the metal suggests that the diffusion distance of metal atoms is shorter than that of Si atoms. This raises an interesting question regarding the predominant diffusing species during high temperature metal/ceramic reactions. It was reported that the Ni atoms are more mobile than the Si atoms during Ni/SiC reactions at 850°C [18], in which similar reaction products of Ni_3Si, Ni_5Si_2, Ni_2Si and C were generated. Assuming that Ni is at least as mobile as Si at higher temperatures, a comparable or greater reaction zone thickness in the SiC side (as compared to that in the metal side) would be expected providing that SiC is readily decomposed. A shorter diffusion length of Ni atoms suggests that the interaction between metal atoms and SiC at the SiC reaction interface may be a rate limiting step for the metal/ceramic reactions. This may well explain why the thickness of the reaction zone on the SiC side is smaller than that on the metal side.

In all of the three metal/ceramic systems, the silicide phases formed in the reaction zones at various temperatures are metal-rich. No Si-rich silicide phases (e.g., $CoSi_2$, $NiSi_2$, and PtSi) as reported in the metallization of Si for contact and/or interconnect applications were detected. The reason why metal-rich silicides, rather than Si-rich silicides, are formed during the M/SiC reactions is primarily attributed to the presence of metal-rich sources, as compared to the Si source (i.e., SiC). In contrast, during metallization of Si in VLSI technology, the amount of the existing metal source is limited as a thin film form. Based on the present results, however, as the location of the reaction zone changes from the metal side toward the SiC side, the relative concentration of Si to metal increases. In the Ni/SiC diffusion couple, layered reaction products of Ni_3Si and Ni_5Si_2 were formed from the Ni component toward the SiC component after reaction for 6 hrs at 1100°C.

4.3.5 Interfacial melting: The formation of metal silicides gives rise to interfacial melting during the metal/ceramic reactions in certain temperature ranges. The interfacial melting can be attributed to a combination of the formation of a low melting point silicide phase and a large enthalpy of mixing between the metals and Si. The former contribution may cause massive interfacial melting, while the latter one can only give rise to localized partial melting unless the reaction interface migrates at a fast rate. The contribution from the presence of C is believed to be minimal because of its inert activity in the systems. Considering the cases where overwhelming melting phenomena were observed, the formation of low melting point silicide phases is believed to be a major contributing factor. In the cases where localized melting was observed, a large enthalpy of solid state atomic intermixing may be responsible.

According to binary phase diagrams of Co/Si, Ni/Si and Pt/Si, eutectic reactions exist at various composition ranges. Specifically, the reaction products of Co(Si)+Co_2Si at Co75-Si25 (at%), Ni_3Si and Pt_3Si have melting points either lower than or comparable to the respective diffusion annealing temperatures in which they were formed. Their formation in the reaction zone may well explain the observed massive interfacial melting. Exceptional cases, nevertheless, were noted in the Co/SiC and Pt/SiC reactions at 1100 and 1000°C, respectively, in which localized and massive interfacial meltings were noted. In both systems, the melting points of the reaction products, namely Co_2Si and Pt_2Si respectively, are about 100°C higher than their respective formation temperatures. From the Pt/Si binary phase diagram, the stoichiometric Pt_2Si compound melts congruently at 1100°C. Nevertheless its liquidus line decreases drastically, as its composition deviates from stoichiometry, from 1100°C to around 850°C (the melting point of Pt_3Si). Since the formation of reaction products during a solid state reaction is facilitated through atomic interdiffusion, the effects of off-stoichiometry of the reaction product, and formation of a low melting point metastable phase on interfacial melting, cannot be ignored. A reasonable explanation for the massive interfacial melting observed in the Pt/SiC at 1000°C is that the Pt_2Si is not the first phase formed during the reaction. It is believed that Pt_3Si is the first phase formed during the Pt/SiC reaction at 1000°C. This hypothesis is supported by the observation that Pt_3Si forms first at 900°C. The Pt_3Si phase has a much lower melting point, 850°C, than the annealing temperature of 1000°C, which in turn gives rise to massive interfacial melting. The Pt_2Si phase is formed through further atomic interdiffusion. In the molten state, atomic diffusion rates of the constituents are expected to be high. In addition, the large enthalpy of Pt_2Si formation, ΔH = -44 kcal/mole [39], is also expected to contribute to the interfacial melting. Assuming that the heat capacity (C_p) of Pt_2Si is similar to that of Ni_2Si, C_p=20 cal/deg-mole [34], the temperature rise at the reaction interface resulting from Pt_2Si formation is on the order of 10^3 degree K, which alone is sufficient to cause interfacial melting during the Pt/SiC reactions at 1000°C.

On the other hand, the minor localized interfacial melting in the Co/SiC at 1100°C is believed to be primarily attributed to a large enthalpy of Co_2Si formation. The standard enthalpy of Co_2Si formation has been reported [34] to be about 28 kcal/mole. Assuming that C_p of Co_2Si is similar to that of Ni_2Si, the temperature rise at the reaction interface resulting from the formation of Co_2Si is in the range of 700 K which is sufficient to cause local interfacial melting. Moreover, it was recently reported that self-propagating, explosive, silicide formation in a room temperature environment is feasible in certain metal/Si multilayer structures, e.g., Rh/α-Si [40], Ni/α-Si [41], and Zr/α-Si [42] multilayers. The thermal driving force for such an explosive reaction originates from a sufficient amount of enthalpy from the silicide formation and, to a lesser extent, the crystallization of α-Si. The amount of enthalpy of silicide formation may be large enough to result in melting of Ni_2Si ($T_{m.p.}$=1565 K) at room temperature [41].

4.3.6 Carbon precipitation behavior: An intriguing phenomenon during the metal/ceramic reactions is that of the carbon precipitation behavior. In the Co/SiC and Ni/SiC systems, a C-PFZ is noted in the areas immediately adjacent to the metal component. Following the C-PFZ, a R-CPZ and M-CPZ were observed in the Ni/SiC samples, while only a R-CPZ was observed in the Co/SiC samples. In the Pt/SiC samples, both M-CPZ and R-CPZ were generated but no C-PFZ was formed. Although both M-CPZ and R-CPZ were generated in the Pt/SiC and Ni/SiC diffusion couples, there is a major difference in the locations of the M-CPZ and R-CPZ. In the Ni/SiC, the M-CPZ is formed adjacent to the SiC component. In the Pt/SiC, on the other hand, the M-CPZ is formed adjacent to the metal component. Furthermore, the microstructure of C precipitation layer is different between Pt/SiC and Ni/SiC.

The reaction patterns formed during the metal/ceramic reactions can be summarized as follows: Co/SiC ---→ Co/C-PFZ/R-CPZ/SiC; Ni/SiC ---→ Ni/C-PFZ/R-CPZ/M-CPZ/SiC; Pt/SiC ---→ Pt/M-CPZ/R-CPZ/SiC. The reason why the C precipitation behavior varies as a function of metal system, and position from the reaction interface is not clearly understood. It may involve several competing kinetic processes, e.g., overall nucleation and growth rate of silicide phases, rejection rate of C from the reaction front (which is also influenced by its solid solubility in various silicides), growth (or condensation) rate of C clusters, and diffusion rates of metals and Si. All these kinetic processes are known to be position and concentration dependent.

The structure of C precipitates also varies as a function of their location from the SiC reaction interface. Based on Raman spectroscopy, C precipitates exist in a mixed glassy/graphitic state. The position-dependent structural change of C is believed to result from the time sequence of their formation. Consider that C atoms originate from the decomposition of SiC. In the areas adjacent to SiC interface, C is freshly decomposed and, therefore, exhibits primarily a disordered state. For those C precipitates which form in areas farther from SiC reaction interface, they are decomposed earlier and therefore experience a longer heat treatment (i.e., a pyrolytic process). As a result, the C precipitates experience a longer structural rearrangement period, and tend to be more ordered.

The duration of thermal exposure of C precipitates also affects their microstructure as well as their distribution pattern, as a function of distance from the SiC interface. Experimentally, the microstructure of the C precipitates changes from fine-sized clusters in the areas close to the SiC interface into randomly-scattered, larger particulates in remote areas. The reason why discrete C layers form in the areas close to the SiC reaction interface, whereas C-decorated granular silicide layers form in remote areas, in the Pt/SiC reaction zone is attributable to the redistribution of C in the Pt-silicide matrix upon prolonged thermal annealing in the remote areas. The distribution pattern of carbon precipitates in the areas adjacent to the SiC reaction front may represent the decomposition behavior of SiC, since thermal relaxation and diffusion (rejection) of decomposed C is not significant.

4.3.7 Summary of Co, Ni and Pt Reactions with SiC: The reactions of the metals Co, Ni and Pt with ceramic SiC were studied in the temperature range 800 to 1200°C. The metal/ceramic reactions generate metal-silicides and C as reaction products. The silicides are primarily metal-rich instead of silicon-rich. The C, precipitated out in metal-silicide matrices, is found to exist in an unreacted form rather than a carbide form. The formation of metal-rich silicides gives rise to either massive or local interfacial melting at certain temperatures. Either planar or non-planar reaction interfaces are generated, depending upon the characteristics of metal/ceramic reactions. The thickness of the reaction zone on the metal side is always greater than that on the SiC side; a parabolic relationship between the thickness of the SiC reaction zone and annealing time is not observed. The kinetics of the metal/ceramic reactions are believed to be controlled by the decomposition of SiC, rather than by the interdiffusion of Si or metals. The patterns of the reaction products formed in the metal/ceramic reaction zones are different depending upon the specific metal system and their location from the reaction interface. A C-PFZ is generated in the Ni/SiC and Co/SiC, but not in the Pt/SiC. Although a CPZ is formed in all the Co/SiC, Ni/SiC, and Pt/SiC systems, both M-CPZ and R-CPZ are noted in the Ni/SiC and Pt/SiC systems. In contrast, only a R-CPZ is formed in the Co/SiC. The structure of the C precipitates varies as a function of their distance from the SiC reaction interface. The C existing close to the SiC interface is primarily in a glassy state. With increasing distance from the SiC interface, the C particulate size increases and forms a more graphitic structure. The structural evolution of the C precipitates is attributed to the duration of thermal exposure after they are dissociated from the SiC.

4.4 Reactions of stainless Steel with SiC

Solid state reactions of SiC with stainless steel produced layered structures of reaction zones. The nature of these solid state reaction products and the accompanying decomposition of SiC are discussed in the following sub-sections.

4.4.1 Solid State Reactions of SS/SiC: The 1st and 2nd layers consisted of C precipitates Massive interfacial melting was observed in the SS/SiC samples annealed at 1125°C for 8 h. Fig. 4.23 shows a typical cross-sectional view SEM micrograph of SS/SiC reaction pattern. The SiC reaction interface is noted to exhibit non-planar characteristics. Some areas of the reaction zone broke lose, as a result of weak bonding caused by melting/solidification, during sample preparation for characterization; horizontal cracks caused by melting/solidification shrinkage were found in the SS component. In the reaction zone, four reaction layers are clearly distinguishable and indicated in Fig. 4.24. Starting from the nonreacted SiC component, the four reaction layers can be characterized as: (1) modulated precipitation zone, (2) random precipitation zone, (3) multiple phase mixture zone, and (4) grain boundary precipitation zone. Fig. 4.25(a), (b), and (c) show high magnification SEM micrographs on the details of the microstructure in reaction zones 1, 2, and 3. It is found that multiple phases, as revealed by the regions with different contrast, start to appear in reaction zone 2.

X-ray analysis from the bulk SS/SiC reaction zone, in a powder form, indicated the presence of γ-iron, (Fe,C), which is the only phase detected from the as-received SS, and $Cr_{23}C_6$. In addition, a few unidentified minor peaks were also detected. EDS x-ray microanalysis indicated that the precipitates in reaction zones 1 and 2 were primarily carbon, while the metal matrices were rich in Ni and Fe but poor in Cr. In zone 3, four alloy phases, as revealed by backscattered electron micrographs, with varying concentrations of Ni, Cr, Fe, and Si were identified. These alloy phases are believed to contribute to those aforementioned unidentified x-ray peaks from the reaction products. One of these four alloy phases contained primarily Cr and Fe (with a small amount of Ni but no Si), while the rest of the three phases contained at least 20 at% Si. It is believed that these three phases are primarily metal silicides. Because of the complexity of these metal reaction products in the system, for convenience, the metal reaction products formed in the reaction zone will be represented by $(Ni,Fe)_xCr_ySi_z$ throughout this discussion. In zone 4, chromium carbide(s) precipitates were found to form along the grain boundaries of stainless steel.

Some precipitates in the reaction zone 2 were found to be Cr-rich. On the other hand, the amount of Fe and Ni contained in all the precipitates was fairly small which failed to substantiate the formation of Fe_3C or Ni_3C. To gain a better statistical ground for the determination of C precipitates, area x-ray mapping was performed on the C precipitates which were located progressively away from the SiC reaction front and shown in Figs. 4.26 through 4.29. It is clear that none of the precipitates can be attributed to either Ni_3C or Fe_3C. It is important to point out in Fig. 4.27 that the areas showing Cr-rich actually originate from the light areas, as indicated by the arrows in Fig. 4.27, rather than from the darker precipitates. For precipitates farther away from the SiC, some overlapping of C and Cr starts to show, as seen in Figs. 4.28 and 4.29. In some cases, nevertheless, the Cr and C signals were not generated from the same region. It appears that the formation of Cr-carbides in reaction zone 2 is

rather scarce. In summary, the tendency of forming Cr-carbide(s) appears to increase as a function of distance from the SiC reaction interface.

Reaction zones 3 and 4 were found to separate from each other by a diffuse boundary, as shown in Fig. 4.30(a). In the reaction zone 3, which is on the right of the boundary, Si was detected. In contrast, no Si was detected in the zone 4 which is located on the left of the boundary. Fig. 4.31(a) and (b) show EDS spectra obtained from the spots 1 and 2, respectively, shown in Fig. 4.30(a). Also noted in Fig. 4.30(a) are areas with grain boundary precipitates. EDS and WDS analyses of one of these G. B. precipitates, magnified in Fig. 4.30(b), are shown in Fig. 4.32. The G. B. precipitates were found to contain primarily Cr and C, and small amounts of Ni and Fe. To understand the elemental distribution in the G. B. precipitates, x-ray mapping was conducted on precipitates located at a triple grain boundary junction. Fig. 4.33(a) through (f) show a backscattered electron image of one such region and the corresponding x-ray maps for elements C, Cr, Ni, Fe, and Si, respectively. It is clear that the grain boundary precipitates are enriched in C and Cr, but depleted in Ni and Fe. No Si was detected in this region. Quantitative analyses of these precipitates suggested that they were likely to be $Cr_{23}C_6$.

It is interesting to note in Fig. 4.25 that both the distribution pattern and the size of C precipitates vary as a function of distance from the SiC reaction interface. In the areas adjacent to the SiC, alternating layers of C precipitates and metal phases were noted. The C precipitates show increasingly random scattering and larger particle size as their locations farther away from the SiC reaction front. Similar behavior has been observed during the solid state reactions of SiC with Ni, Co, Fe, and Pt [18,24,25]. Nevertheless, the C precipitates formed in the SS/SiC reaction zone exhibited highly anisotropic morphology, which is rather different from what was observed in the Pt/SiC [24], Ni/SiC [25], Co/SiC [25], and Fe/SiC [18]. In those previously studied systems, C precipitates showed more-or-less irregular shape.

There is an interesting correlation among the elemental distributions in Figs. 4.27 through 4.29. It is noted that the areas enriched of Cr are depleted of Ni, Si, and Fe. Furthermore, Ni and Si are present, more or less, in the same regions while Fe is primarily present in the other regions. It is suggested that Si has a stronger affinity for Ni, than for Fe, which in turn gives rise to an overwhelming Ni-Si reaction and the formation of Ni-based complex metal silicides (which has some solubilities for Fe and Cr) in the reaction zones 1 and 2. The formation of Ni-based complex metal silicides is believed to contribute to the observed massive interfacial melting because of the low melting point of nickel-rich silicides [35].

Interfacial melting as a result of solid state reactions has been previously observed in Pt/SiC, Co/SiC, and Ni/SiC systems [24,25] at reaction temperatures much lower than the melting points of the respective constituents. The interfacial melting can be attributed to either the formation of low melting point eutectic metal silicides in the reaction product(s), or a large negative enthalpy of the metal/Si solid

state reactions. To result in a massive interfacial melting phenomenon, it is believed that the former contribution is predominant. Recently, explosive, self-propagating silicide formation in a room temperature environment has been reported in some metal/Si multilayer structures, e.g., Rh/α-Si[40], Zr/α-Si [42], and Ni/α-Si [41] systems. The standard enthalpies of formation of common metal silicides in Ni-Si, Co-Si, and Pt-Si systems are typically in the range of -20 to -50 kcal/mole [34,39,41]. Assuming that the heat capacity (C_p) values of these metal silicides are comparable to that of Ni_2Si (C_p = 15.8 + 0.00329 T cal/deg-mole) [34], under the condition of adiabatic heating, the temperature rise associated with the formation of a silicide at the reaction interface may be estimated to be in the range of 10^2 degree K. Clearly, the contribution from highly exothermic metal/silicon reactions to interfacial melting occurring in metal/SiC solid state reactions can not be underestimated.

A strong Ni-Si chemical affinity is expected to give rise to a fast diffusion rate of Ni from the SS toward the SiC, which can result in enrichment of Ni (as compared to Fe and Cr) in the areas adjacent to the SiC reaction front. Table V shows a list of EDS analyses on the concentrations of Si, Ni, Fe, and Cr at locations 1 through 6, as indicated in Fig. 4.34, from the SiC to reaction zone 1 (M-CPZ). It is noted in the reaction zone 1 that Ni concentration increases progressively toward the SiC interface; an uphill concentration gradient was noted. In contrast, both Cr and Fe show an expected decreasing concentration gradient. The amount of Cr diffusing through the M-CPZ is much less than Fe or Ni, which is caused by the prevailing selective formation of Cr-carbides in the G.B. precipitation zone.

The selective reaction of C with Cr, rather than with Ni and Fe, is believed to originate from the highly negative Gibbs free energy of Cr-carbide formation. It is known that there exist four different types of Cr-carbides, namely $Cr_{23}C_6$, Cr_7C_3, Cr_3C_2, and Cr_4C. According to thermochemistry data [34,43], the Gibbs free energy of formation of various selected metal carbides were calculated and listed in Table VI. It appears that the most likely carbide to form in the present system is $Cr_{23}C_6$. The positive free energy of formation of Fe_3C suggests that its formation is not thermodynamically favored. Moreover, according to Marsh [44], and Brewer et al. [45], the addition of Ni and Si to C-Fe system further destabilizes the Fe_3C phase, although the cementite is already thermodynamically metastable.

The strong affinity of C for Cr gives rise to a faster apparent diffusion rate of C atom (than Si) toward the SS, which is characterized by the trailing of the Si diffusion front to the G.B.-PZ, as shown in Fig. 4.30(a). The diffusion of C atom proceeds from the SiC (a diffusion source), through the reaction zone, and into the SS (a diffusion sink). In view of the widespread C precipitation, the diffusion of C atom is believed to take place via both lattice and grain boundary. The reason why $Cr_{23}C_6$ precipitates form preferentially along the grain boundaries of SS may be attributed to the combination of minimizing the strain energy associated with their formation and the ease of nucleation at the grain boundaries. In contrast, the diffusion rate of C atom was identified to be slower in the Ni/SiC, Co/SiC, and Fe/SiC systems [18,25]; the diffusion front of Si atom was found to lead that of C, which is characterized by the

formation of a carbon precipitation free zone (C-PFZ) adjacent to the metals. In the present SS/SiC system, however, no C-PFZ was formed. A slower diffusion rate of C in the Ni/SiC, Co/SiC, and Fe/SiC systems is supported by the fact that all the Ni-carbide (Ni_3C), Co-carbide (Co_2C), and Fe-carbide (Fe_3C) are thermodynamically unstable [25,45] at elevated temperatures, and were not formed in the Ni/SiC, Co/SiC, and Fe/SiC systems, respectively.

4.4.2 Discontinuous decomposition of SiC: The formation of modulated (periodical) C precipitation in the present SS/SiC system is of great scientific interest. A similar structure was also generated during the solid state reactions in Ni/SiC [18,25] and Ni_3Al/SiC [24]. Since modulated C precipitation occurs only in areas immediately adjacent to the SiC, the amount of time provided for the dissociated C atoms (from the SiC) to redistribute within these regions is not expected to be sufficient. In contrast, the C precipitation exhibited a completely random pattern in areas remote from the SiC reaction interface. It is suggested that the modulation of C precipitation is directly related to the decomposition characteristics of the SiC when reacting with certain metal species, e.g., Ni.

Considering an overall reaction equation, SiC + SS(Ni, Fe, Cr) ---> $(Ni,Fe)_xCr_ySi_z + Cr_{23}C_6 + C$, a driving force resulting from a negative total Gibbs free energy of the reaction is required to proceed the SiC/SS reaction. In view of the global formation of the complex metal-silicides, $(Ni,Fe)_xCr_ySi_z$, as compared to the localized formation of $Cr_{23}C_6$, the driving force for the SiC/SS reactions is believed to originate from the negative free energy of the metal-silicides formation. Furthermore, it is important to consider that a prior decomposition of the SiC is required in order to proceed the SiC/SS reactions. Since SiC is thermally stable at the temperatures of study, the decomposition of SiC requires a certain amount of activation barrier to be overcome in addition to the thermodynamic driving force. The driving force is the negative free energy of the metal-silicides formation. To surmount the activation barrier for the decomposition of SiC, however, there exists a nucleation period. Without the presence of metal atoms on SiC interface, which is analogous to the case of thermal decomposition of SiC, the incubation time for SiC decomposition may be infinitely long. It is proposed that SiC exhibits discontinuous decomposition behavior when reacting with such metals as pure Ni or rich Ni-containing alloys, but not with Co or Fe. Recent studies on the reactions of SiC with pure Ni [18,25], Ni_3Al [24], and Ni alloys [32] indicated the formation of alternating layers of C and Ni-based metal silicides in the reaction zones. On the other hand, when SiC reacted with Pt [24], Co [25], and Fe [18], the C precipitation in the areas adjacent to the SiC was completely random.

According to ternary phase diagrams of Ni-Si-C [18] and Nb-Si-C [33], SiC is not in equilibrium with pure metals or metal-rich silicides. In other words, a metal-rich or even a pure metal layer next to the SiC is required for the continuation of the (Ni,Nb)/SiC reactions, i.e., the decomposition of SiC. It is believed that a similar requirement also applies to other systems, e.g., Co-Si-C, Fe-Si-C, Pt-Si-C, etc. Our previous studies of Ni/SiC [25] also indicated that the Ni-silicide formed adjacent to the SiC was Si-rich

compared to other Ni-silicides formed in the reaction zone. Clearly, the presence of a Ni-rich layer at the SiC reaction interface is a prerequisite to keep the system in a non-equilibrium state, which in turn promotes the decomposition of SiC and thereby continue the Ni/SiC solid state reactions. It is suggested that there exists a critical level of Ni concentration, above which the decomposition of SiC is possible. When the concentration of Ni falls below such a level, the decomposition of SiC is kinetically sluggish or essentially stop.

To explain the formation of a periodic structure during solid state reactions [46-48], the "supersaturation theory" proposed by Ostwald [49] is commonly adopted. According to the theory, the critical elements to constitute the formation of periodic C precipitates in metal/SiC reactions are: (1) a strong affinity of the metal specie for Si, but not C, to form a thermodynamically stable metal-silicide; (2) a critical metal concentration (C_m) at the SiC reaction interface is to be satisfied for the decomposition of SiC; (3) a low solid solubility (or rejection rate) of C atom in the silicide matrix. Based upon these criteria, periodic C precipitation is not expected to occur when SiC reacting with strong carbide forming metals, such as Nb, Ti, or Cr. On the other hand, although Ni, Co, Fe, or Pt have low affinity for C to form stable carbide at the temperatures of interest, periodic C precipitation occurred only in the Ni/SiC system. This may be attributed to the variation of the C rejection rate in those metal-silicide matrices. In this respect, the data of solid solubility or diffusivity of C in those metal silicides, although not available, is valuable to sort out the discrepancy. Table VII. summarizes a list of microstructural evolution in the reaction zone from selected metal/SiC reactions.

By examining the reaction zones of Ni/SiC under Raman microprobe, the first thin layer immediately adjacent to the nonreacted SiC is found to be primarily carbon, while no free nonreacted Si was detected. In the SS/SiC system, based on SEM micrographs, the immediate layer adjacent to the SiC was also found to contain predominantly C clusters. It is suggested that once a layer of SiC is decomposed, Si atoms, decomposition products of SiC, readily diffuse away and react with Ni to form a layer of Ni-silicide in front of the constituent C region. As a result, the Ni concentration at the SiC reaction interface decreases drastically, which in turn makes continuous decomposition of SiC more difficult. In order to further decompose SiC, a critical level of Ni concentration is to be satisfied, which takes time to establish. Concurrently, the dissociated C atoms, in front of the SiC reaction interface, form small clusters and aggregate as a layer to minimize their interfacial energy. The continuation of this process will give rise to the formation of alternating Ni-silicide and carbon layers. The boundary defining the layered structure, however, can be obscured by the diffusion kinetics of constituents and/or solid solubility of C in the matrices, which are known to be dependent upon metal systems, annealing parameters, and local concentration of the constituents (which is a function of distance from the reaction front). To give an example on the effects of those variables on the C precipitation behavior, our recent studies [50] of the NiAl/SiC reactions at 1300°C showed that the C precipitation in the reaction zone

was completely random although modulating C precipitation has been observed during the solid state reactions of SiC with Ni_3Al [24] and Ni alloys (containing 70 at.% Ni, 20 at.% Cr, and 10 at.% Al) [32].

4.4.3 Summary of SS/SiC Reactions: Solid state reactions of SiC with stainless steel produced four layered reaction zones. The 1st and 2nd layers consisted of C precipitates embedded in Ni-based metal silicides matrices. The 3rd layer contained multiple alloy phases. The 4th layer showed grain boundary precipitation of $Cr_{23}C_6$. On the basis of thermodynamic Gibbs free energy, C has the strongest affinity for Cr, which gives rise to a faster diffusion rate of C atom (as compared to Si) toward the stainless steel. As a result, the Si diffusion front trailed behind the C diffusion front, which prevented the formation of a C-PFZ adjacent to the SS, and $Cr_{23}C_6$ precipitates formed along the grain boundaries of the SS. On the other hand, it is demonstrated that Ni, Co, and Fe do not form thermodynamically stable carbides, which resulted in a slower C diffusion rate and was characterized by the formation of a C-PFZ in Ni/SiC, Co/SiC, and Fe/SiC systems. Ni atoms were found to have a strong affinity for Si and resulted in the formation of Ni-based metal silicides, which attributed to the observed massive interfacial melting. It has been found, so far, that the presence of Ni species in metals is essential to promote the formation of alternating C and metal-silicide layers in the reaction zone during metal/SiC reactions. Moreover, it appears that modulating C precipitation occurs only in systems which have a high Ni concentration; alternating carbon and nickel silicide layers were observed in Ni/SiC, Ni_3Al/SiC, and Ni alloys (containing 70 at.% Ni)/SiC, but not in NiAl/SiC. Based on Ni-Si-C and Nb-Si-C ternary phase diagrams, it is suggested that a critical concentration of Ni at the SiC reaction interface has to be satisfied in order to maintain the SiC at a nonequilibrium state. The formation of alternating carbon and nickel silicide layers in the reaction zone was explained in terms of discontinuous decomposition of SiC, as a result of the interplay of nickel silicide formation and a dynamic, time-dependent building up of the critical Ni concentration at the SiC reaction interface.

Section 5

SUMMARY

High temperature interactions of metallic matrices Nb, Co, Ni, Pt and stainless steel with SiC ceramic were examined in the temperature range 800 to 1200°C. Thin film couples were used in understanding the interfacial reactions of Nb with SiC and in evaluating the effectiveness of Al_2O_3 diffusion barriers in minimizing such reactions. It was found that Al_2O_3 layers in the 100 to 500 nm range are effective in slowing the interfacial reactions.

The reaction products and sequences of metal/SiC reactions can be summarized as follows:

Nb/SiC ---> Nb/NbC_x/$NbSi_yC_z$/NbC_x/SiC

Co/SiC ---> Co/Co_2Si+Co(Si)/Co_2Si+C/SiC

Ni/SiC ---> Ni/Ni_3Si/Ni_5Si_2+C/SiC

Pt/SiC ---> Pt/Pt-silicides (Pt_3Si, Pt_2Si, PtSi, $Pt_{12}Si_5$) + C/SiC

SS/SiC ---> S.S/G.B. $Cr_{23}C_6$/(Ni,Fe)Cr_xSi_y+C/SiC

Sequential annealings of Nb/SiC at 1200°C for 6, 18, 32, and 48 h indicated that the growth kinetics of layered reaction products obeyed a parabolic relationship with respect to annealing time, suggesting that the growth kinetics were limited by diffusion. The growth rate constants for reaction layers 1 and 2 were 6.7×10^{-13} and 5.3×10^{-12} cm^2/sec, respectively. In contrast, no parabolic growth rate was observed in Ni/SiC, Co/SiC, and SS/SiC. In most of the cases, the thickness of the reaction zone on the SiC side was always smaller than that on the metal side, suggesting that the decomposition rate of SiC was slow and may be a rate limiting step for the overall metal/SiC reactions.

The microstructure of C precipitates appears to be a function of distance from the SiC reaction front; coarsening of C precipitates was noted at locations farther from SiC. The distribution pattern of the C clusters showed either random or modulated patterns, depending upon the metal system as well as their location from the SiC interface. A model describing discontinuous decomposition of SiC is proposed to explain the formation of modulating C/metal-silicides structures. In general, metal silicide formation is detected in all the systems being studied. The formation of metal-rich silicides gives rise to interfacial melting in Ni/SiC, Co/SiC, and SS/SiC as a result of their relatively low melting points, as compared to the respective annealing temperatures. Non-planar interfaces were produced as a result of surface tension effects in the interfacial melt. The formation of liquid interfacial metal silicide phases is expected to degrade the overall properties of SiC reinforced metal matrix composites that contain Ni, Co and Pt.

Section 6

PUBLICATIONS AND PRESENTATIONS

1. A. Joshi, H.S. Hu, L. Jesion, J.J. Stephens and J. Wadsworth, "High Temperature Interactions of Refractory Metal Matrices with Selected Ceramic Reinforcements", Metallurgical Transactions A, Vol. 21A, pp.2829-37, (1990)

2. A. Joshi, H.S. Hu, and J. Wadsworth, "Interfacial Reactions of Refractory Metals Niobium and Tantalum with Ceramics Silicon Carbide and Alumina", Materials Research Society Proceedings 170, Interfaces in Composites, Eds. C.G. Pantano and E.J.H. Chen, MRS, Pittsburgh, PA, 1990, pp.149-154

3. D.L. Yaney and A. Joshi, "Reaction between Niobium and Silicon carbide at 1373 K", Journal of Materials Research, Vol. 5, pp.2197-2208, (1990)

4. A. Joshi, J.J. Stephens, and T.G. Nieh, "Interfacial reactions between Refractory Metals and Ceramic Reinforcements", Brown University Symposium on "Interfacial Phenomena in Composites: Processing, Characterization and Mechanical Properties", Salve Regina College, Newport, RI, June 1-3, 1988.

5. A. Joshi, H.S. Hu, and J. Wadsworth, "Interfacial Reactions of Refractory Metals Niobium and Tantalum with Ceramics Silicon Carbide and Alumina", Fall Meeting of the Materials Research Society, November 27-December 2, 1989, Boston, MA.

6. J. Wadsworth, "Ceramics and Intermetallics", University Research Initiative, Winter Group Meeting, Santa Barbara, CA, January 12, 1990.

7. A. Joshi, "Interfacial Reactions in Composite Materials", Second International Workshop on The Applications of Surface Analysis Techniques", Hong Kong, April 19-21, 1990

8. T.C. Chou and A. Joshi, "Solid State Interfacial Reactions of SiC with Ni, Co and Pt", paper prepared for Proceedings of "Symposium on Composites, Processing, Microstructure & Properties", November 13-15, 1990, Orlando, FL.

9. T.C. Chou, A. Joshi and J. Wadsworth, "Solid State Reactions of SiC with Ni, Co and Pt: Reaction Interfaces and Products, and carbon precipitation behaviors", article prepared for publication in J. Mater. Res., 1990.

10. A. Joshi, T.C. Chou and J. Wadsworth, "High Temperature Interfacial Reactions of SiC with Metals", Invited Keynote presentation at the 37th Annual Symposium of the American Vacuum Society, Symposium on "Composite Interfaces: Characterization and Properties", October 8-12, 1990, Toronto, Canada.

Section 7

REFERENCES

1. L.J. Ebert and P.K. Wright, "Mechanical Aspects of the Interface," in Interfaces in Metal Matrix Composites, edited by A.G. Metcalfe, Academic Press, New York, 1974, pp. 32-66.
2. A.G. Metcalfe, "Physical Chemical Aspects of the Interface", ibid., pp. 67-126.
3. A.G. Metcalfe, M.J. Klein, "Effect of Interface on Longitudinal Tensile Properties," in A.G. Metcalfe, op. cit., p. 151.
4. R. Naslain, R. Pailler and P. Martineau, in Physical Chemistry of the Solid State: Applications to Metals and their Compounds, P. Lacombe, Ed., Elsevier, Amsterdam, 1984, pp. 481-499.
5. P. Martineau, R. Pailler, M. Lahaye, R. Naslain, J. Materials Science, **19**, 2749 (1984).
6. M.B. Chamberlain, Thin Solid Films, **72**, 305 (1980).
7. C. Jones, C.J. Kiely and SS Wang, J. Mater. Res., **4**, 327 (1989).
8. C.G. Rhodes, R.A. Spurling, in Recent Advances in Composites in the United States and Japan, ASTM STP 864, J.R. Vinson and M. Taya, Eds., 1985, pp. 585-599.
9. R. Pailler, M. Lahaye, J. Thebault and R. Naslain, in Failure Modes and Processing in Composites - IV, J.A. Cornie and F.W. Crossman, Eds., The Metallurgical Society of AIME, New York, 1979, pp. 265-284.
10. D.J. Lloyd, in Composite Science and Technology, 1989, vol. 35, pp.159-179.
11. S.C. Chin and M.H. Richman, Army Materials and Mechanics Research Center Report, AMMRC TR 82-14, 1982.
12. S.R. Nutt and R.W. Carpenter, Materials Science and Engineering, **75**, 169 (1985).
13. L.D. Brown, C.L. Grove and H.L. Marcus, Interfaces in Metal Matrix Composites, Edited by A.K. Dhingra and S.G. Fishman, 1986, pp. 205-210.
14. T.G. Nieh, J.J. Stephens, J. Wadsworth and C.T. Liu, in Interfaces in Polymer, Ceramic, and Metal Matrix Composites, Edited by Hatsuo Ishida, Elsevier, Amsterdam, 1988, pp. 215-224.
15. R. Sherman, Surface and Interface Analysis, **10**, 23 (1987).
16. J.I. Ratliff and G. W. Powell, Research on Diffusion in Multiphase Ternary Systems: Reaction Diffusion in the Ti/SiC and Ti-6Al-4V/SiC Systems, AFML Techn. Report 70-42, 1970, US Department of Commerce, Nat. Tech. Inf. Serv. Springfield, VA.
17. P. Martineau, R. Pailler, M. Lahaye, and R. Naslain, J. Mater. Sci. **19**, 2749 (1984).
18. R. C. J. Schlepers, F. J. I. Van Loo, and G. De With, J. Am. Ceram. Soc. **71**, C-284 (1988).
19. C. S. Pai, C. M. Hanson, and S. S. Lau, J. Appl. Phys. **57**, 618 (1985).
20. Z. Zhang and K. Wei, Interfaces in Metal-Ceramics Composites, Eds. R. Y. Lin, R. J. Arsenault, G. P. Martins, and S. G. Fishman, TMS, Warrendale, PA, 1990, p.259.
21. A. Joshi, H. S. Hu, and J. Wadsworth, Mat. Res. Soc. Symp. Proc. **170**, 149 (1990).

22. D.L. Yaney and A. Joshi, J. Mater. Res., **10**, 2197 (1990).
23. A. Joshi, H. S. Hu, L. Jesion, J. J. Stephens, and J. Wadsworth, Met. Trans.A, **21A**, 2829 (1990).
24. T. C. Chou, J. Mater. Res. **5**, 601 (1990).
25. T. C. Chou, Scripta Met. et Mat. **24**, 63 (1990).
26. S. Krishnamurthy, Interfaces in Metal-Ceramics Composites, Eds. R. Y. Lin, R. J. Arsenault, G. P. Martins, and S. G. Fishman, TMS, Warrendale, PA, 1990, p.75.
27. D. R. Schuyler, M. M. Sohi, and R. Mahapatra, Interfaces in Metal-Ceramics Composites, Eds. R. Y. Lin, R. J. Arsenault, G. P. Martins and S. G. Fishman, TMS, Warrendale, PA, 1990, p.475.
28. C. Jones, C. J. Kiely, and S. S. Wang, J. Mater. Res. **5**, 1435 (1990).
29. T. C. Chou, Scripta Met. et Mat. **24**, 409 (1990).
30. T. C. Chou and T. G. Nieh, J. Mater. Res. **9**, 1985 (1990).
31. E. L. Hall, Y. M. Kouh, M. R. Jackson, and R. L. Mehan, Met. Trans. **14A**, 781 (1983).
32. M. R. Jackson, R. L. Mehan, A. M. Davis, and E. L. Hall, Met. Trans. **14A**, 355 (1983).
33. C.E. Brukl, Ternary Phase Equilibria in Transition Metal-Boron-Carbon-Silicon Systems, Technical Report No. AFML-TR-65-2, Part II, Vol. VII, Air Force Materials Laboratory, Wright Patterson Air Force Base, Ohio, 1966, p. 44.
34. O. Kubaschewski and C. B. Alcock, Metallurgical Thermochemistry, 5th ed. Pergamon Press, New York, 1979, p.350.
35. P. M. Hansen, Constitution of Binary Alloys, McGraw-Hill, New York, 1958, p.379.
36. T. Yamada, H. Sikiguchi, H. Okamoto, S. Azuma, and A. Kitamura, in Diffusion Bonding of SiC or $Si_{3N}{}^{4}$ to Metal, Proceedings of the 2nd International Symposium on Ceramic Materials and Components for Engines, Ed. W. Bunk and H. Hausner, Verlag Deutsche Veramische Gesellschaft, Lubeck-Travemunde, Federal Republic of Germany, 1986.
37. V. M. Bermudez, Appl. Phys. Letts. 42 (1983) 70.
38. V. M. Bermudez, J. Appl. Phys. 63 (1988) 4951.
39. L. Topor and O. J. Kleppa, Z. Metallkde. 77 (1986) 65.
40. J. A. Floro, J. Vac. Sci. Technol. A4 (1986) 631.
41. L. A. Clevenger, C. V. Thompson, and K. N. Tu, J. Appl. Phys. 67 (1990) 2894.
42. C. E. Wicksham and J. E. Poole, J. Vac. Sci. Technol. A6 (1988) 1699.
43. I. Barin and O. Knacke, Thermochemical Properties of Inorganic Substances, Springer-Verlag, New York, 1973.
44. J. S. Marsh, The Alloys of Iron and Nickel, McGraw-Hill, New York, 1938, V.1, Engineering Foundation, pp.58-82.
45. L. Brewer, J. Chipman, and S-G. Chang, Metals Handbook, Metals Park, OH, 1973, V.8, 8th ed., p.413.
46. K. Osinski, A. W. Vriend, G. F. Bastin, and F. J. J. van Loo, Z. Metallkd. **73**, 258 (1982).
47. P. C. Patnaik, Ph.D. Thesis, Mcmaster University (1984).
48. Y. S. Shen, E. J. Zdanuk, and R. H. Krock, Metall. Trans. **2**, 2839 (1971).

49. W. Ostwald, Z. Physik. Chem. 22, 365 (1897).

50. T. C. Chou, (unpublished research).

TABLE I. SELECTION OF METAL/CERAMIC COMBINATIONS

Matrix			Ceramic
Structure	Metal	T_m (K)	Reinforcements
FCC	Aluminum	933	SiC, Si_3N_4
FCC	Nickel	1726	SiC, Si_3N_4
HCP	Cobalt	1768	SiC
HCP	Titanium	1941	Si_3N_4
BCC	Niobium	2741	SiC, Al_2O_3
BCC	Tantalum	3014	SiC, Al_2O_3
HEX	Ti_3Al	1623	SiC, Si_3N_4, Al_2O_3
FCC	Stainless Steel		SiC

TABLE II. REPRESENTATIVE CHEMICAL ANALYSIS OF HEXOLOY (wt%)

SiC	Free Si	Al	Ca	B	Fe	Ti	Ni
99.2	0.07	0.10	0.01	0.45	0.01	0.01	0.01

Table III. ANNEALING CONDITIONS, DIFFUSION PHENOMENA, AND MAJOR REACTION PRODUCTS FOR VARIOUS DIFFUSION COUPLES.

Diffusion Couple	Annealing Temperature	Annealing Time (h)	Diffusion Phenomena	Reaction Product
Nb/SiC	1000°C	4	Planar interfaces	Nb_2C, Nb_5Si_3, NbC, Nb_5Si_4C
Nb/SiC	1100°C	4	Planar interfaces	Nb_2C, Nb_5Si_4C, Nb_5Si_3,
Nb/SiC	1200°C	6, 18, 32, 48	Planar interface, Homo- and heterogeneous nucleation/growth of reaction products	NbC_x, $NbSi_yC_z$, NbC_x
Co/SiC	1100°C	6	Localized interfacial melting, Planar interface, C-PFZ and R-CPZ	Co_2Si, C
Co/SiC	1210°C	4	Interfacial melting, Non-planar interface, C-PFZ and R-CPZ	Co(Si), Co_2Si, C
Ni/SiC	1100°C	6	Localized interfacial melting, Planar interface, C-PFZ, R-CPZ and M-CPZ	Ni_3Si, Ni_5Si_2, C
Ni/SiC	1170°C	4	Interfacial melting, non-planar interface, C-PFZ, R-CPZ and M-CPZ	$Ni_{31}Si_{12}$, C
Pt/SiC	800°C	12	Limited reactions No bonding	----
Pt/SiC	900°C	5	Interfacial melting, non-planar interface, M-CPZ and R-CPZ	Pt_3Si, C
Pt/SiC	1000°C	5	Interfacial melting, non-planar interface, M-CPZ and R-CPZ	Pt_2Si, C
Pt/SiC	1100°C	4	Interfacial melting, non-planar interface, M-CPZ and R-CPZ	Pt_3Si, $Pt_{12}Si_5$ Pt_2Si, PtSi, C
SS/SiC	1125°C	8	Interfacial melting non-planar interface, M-CPZ, R-CPZ and G.B.-CPZ	$Cr_{23}C_6$, C, $(Ni,Fe)Cr_xSi_y$

C-PFZ: carbon precipitation free zone
M-CPZ: modulated carbon precipitation zone
R-CPZ: random carbon precipitation zone
G.B.-CPZ: grain boundary carbide precipitation zone

Table IV. GIBBS FREE ENERGY OF DECOMPOSITION OF SIC AT VARIOUS TEMPERATURES

Reaction	Temperature(°C)	ΔG (kcal/mole)
	800	12.1
	900	12.0
SiC ---→Si + C	1000	11.9
	1100	11.8
	1200	11.7

Table V. EDS COMPOSITIONAL ANALYSIS OF SIC AND STAINLESS STEEL.
(All values in wt%)

	STAINLESS STEEL	MODULATED CARBON PRECIPITATION ZONE			SILICON CARBIDE		
(Location): --------->	(Bulk comp.)	6	5	4	3	2	1
Si	0	28.24	29.41	29.29	49.96	49.97	50.00
C	0	0	0	0	49.94*	49.97*	49.98*
Fe	44.8	32.35	28.78	23.38	0.04	0.03	0
Ni	30.1	35.45	39.10	45.52	0.06	0.03	0.02
Cr	23.73	3.96	2.72	1.81	0	0	0
Ti	0.5	0	0	0	0	0	0
Mn	0.9	0	0	0	0	0	0

* The concentration of C was obtained by ZAF calculations based on an assumption of stoichiometric SiC

Table VI. GIBBS FREE ENERGY OF FORMATION OF SELECTED METAL CARBIDES AT 1400 K

Carbides	Gibbs Free Energy (Kcal/mole)
$Cr_{23}C_6$	-111
Cr_4C	- 23
Cr_7C_3	- 17
Cr_3C_2	- 3
Fe_3C	+ 6
Co_2C	+ 2 at 1200 K data not available at T > 1200 K
Ni_3C	+ 7 at 1000 K data not available at T > 1000 K

Table VII. REACTION PATTERNS AND REACTION PRODUCTS FORMED IN SELECTED METAL/SIC SYSTEMS AT SPECIFIC TEMPERATURES#

---

1. SS/SiC ---> SS/ G.B.-PZ ($Cr_{23}C_6$)/ C-PFZ ((Ni,Fe)Cr_xSi_y)/ R-CPZ ((Ni,Fe)Cr_xSi_y)/ SiC
2. Ni + SiC ---> Ni/ C-PFZ (Ni_3Si)/ R-CPZ (Ni_5Si_2)/ M-CPZ (Ni_5Si_2)/ SiC
3. Co + SiC ---> Co/ C-PFZ (Co_2Si)/ R-CPZ (Co_2Si)/ SiC
4. Fe + SiC ---> Fe/ C-PFZ (Fe_4Si_1)/ R-CPZ (Fe_7Si_2)/ SiC
5. Nb + SiC ---> Nb/ NbC_x/ $NbSi_yC_z$/ NbC_x/ SiC
6. Ni_3Al + SiC ---> Ni_3Al/ NiAl*/ C-PFZ ($Ni_{5.4}Al_1Si_2$)/ M-CPZ ($Ni_{5.4}Al_1Si_2$)/ SiC
7. NiAl + SiC ---> NiAl*/ R-CPZ ($Ni_{14}Al_9Si_2$)/ SiC

Reaction temperatures (°C): 1 (1200), 2 (1100), 3 (1100), 4 (850), 5 (1200), 6 (1000), 7 (1300)

* significant amount of Si diffused into the NiAl phase

@ references: 4 (Ref.8), 6 (Ref.30), 7 (Ref.50).

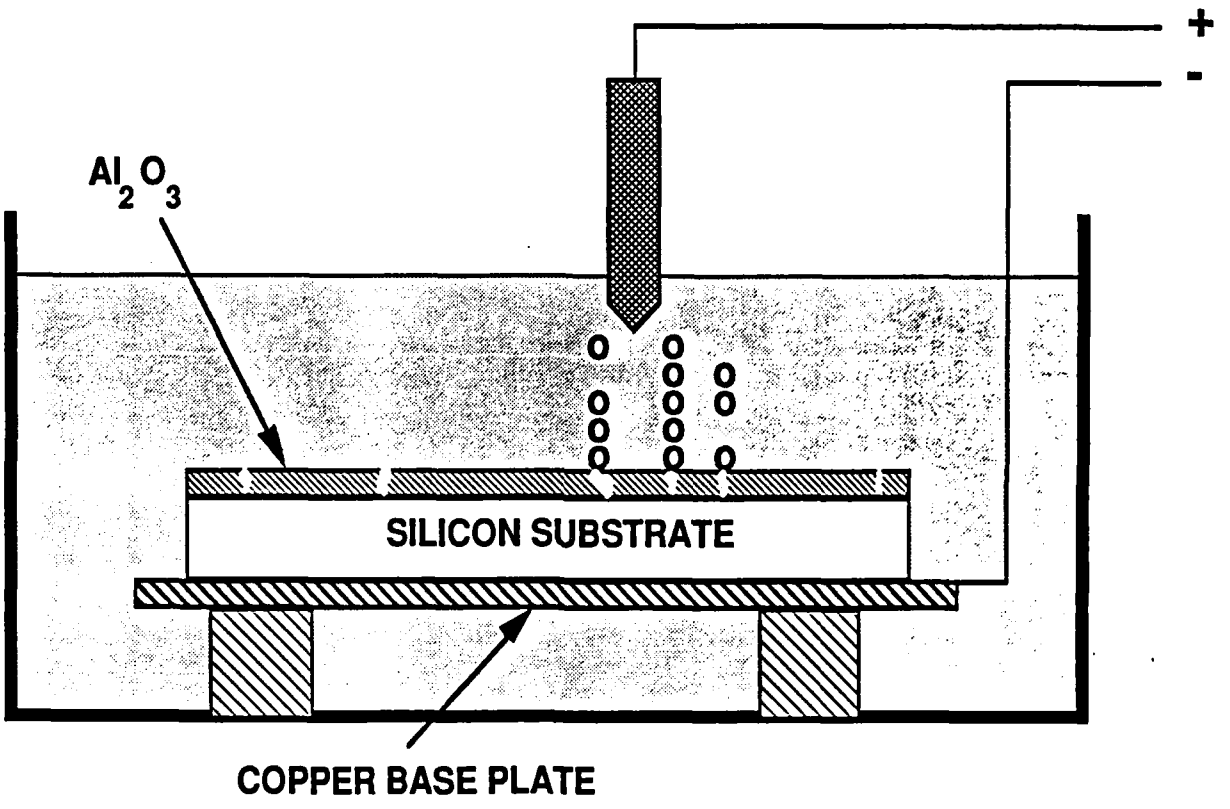

Fig. 3.1 Schematic of the electrochemical set up used to measure the pin hole densities of Al_2O_3 layers deposited on silicon substrates.

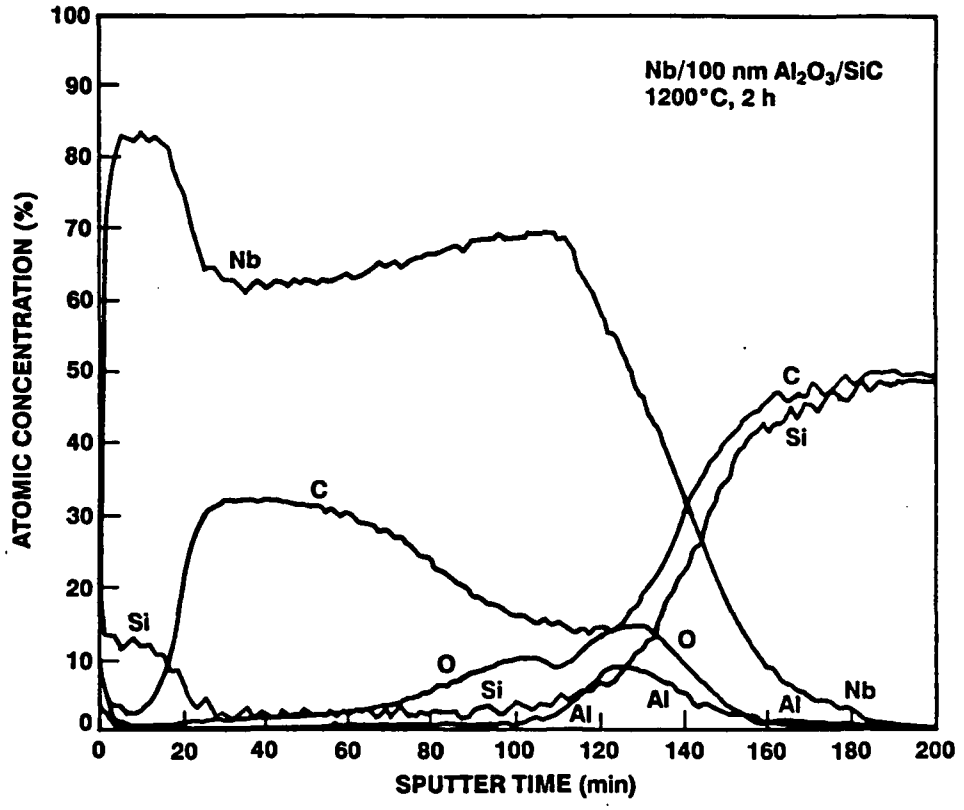

Fig. 4.1 AES depth profile of $Nb/Al_2O_3/SiC$ specimen annealed 2 h at 1200 °C, with Al_2O_3 layer thickness of (a) 100 nm, and (b) 200 nm. [Equivalent Ta_2O_5 sputter rate is 12 nm/min].

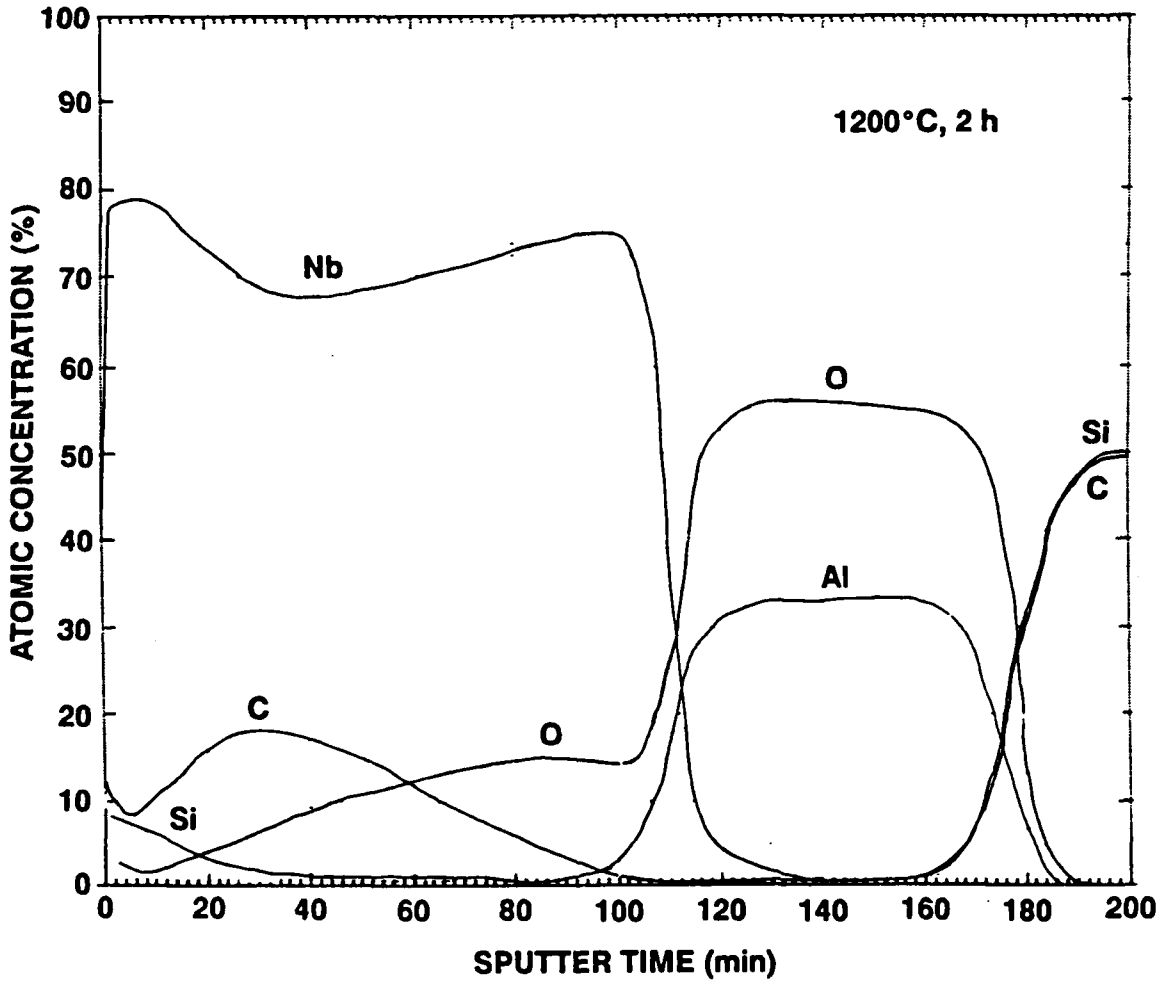

Fig. 4.2 AES depth profile of Nb/Al_2O_3/SiC specimen annealed 2 h at 1200°C, with Al_2O_3 layer thickness of 500 nm. [Equivalent Ta_2O_5 sputter rate is 12 nm/min].

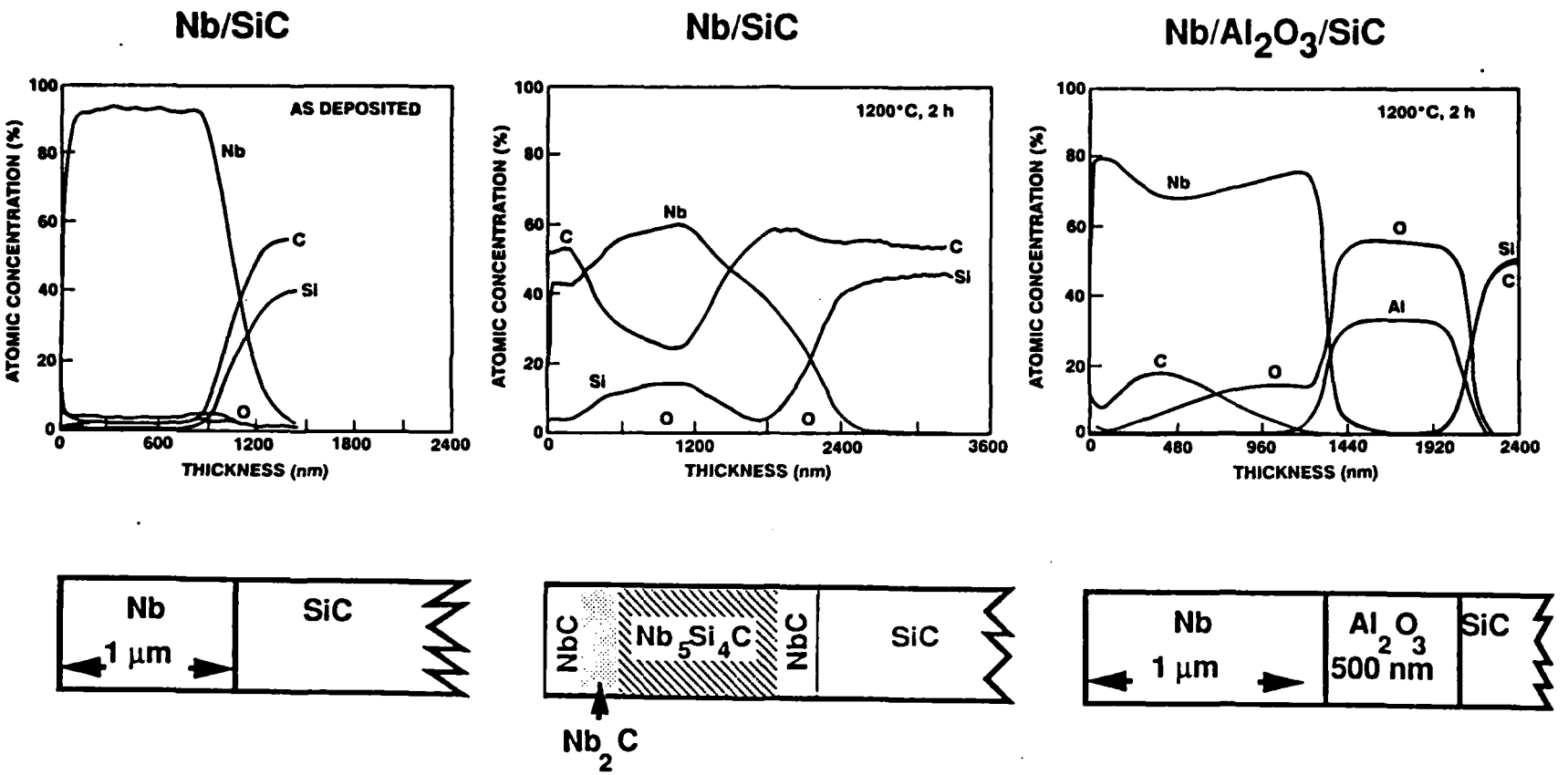

Fig. 4.3 AES depth profiles of specimens (a) Nb/SiC in the as-deposited condition, (b) Nb/SiC annealed 2 h at 1200 °C, and (c) Nb/500nm Al_2O_3/SiC annealed 2 h at 1200 °C. [Equivalent Ta_2O_5 sputter rate is 12 nm/min].

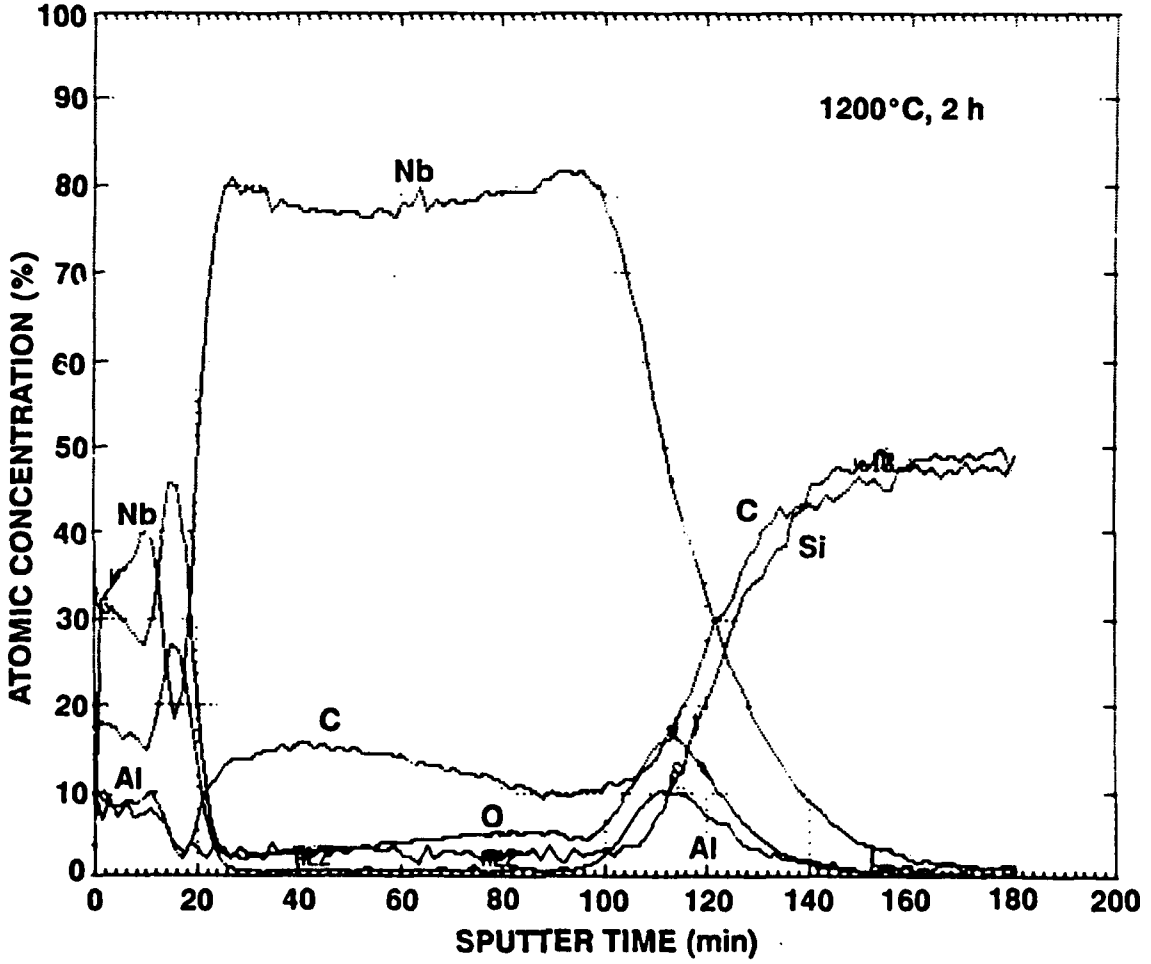

Fig. 4.4 AES depth profile of $Al_2O_3/Nb/Al_2O_3/SiC$ specimen annealed 2 h at 1200°C, with Al_2O_3 layer thickness of 20 nm for cap and 100 nm for the diffusion barrier. [Equivalent Ta_2O_5 sputter rate is 12 nm/min].

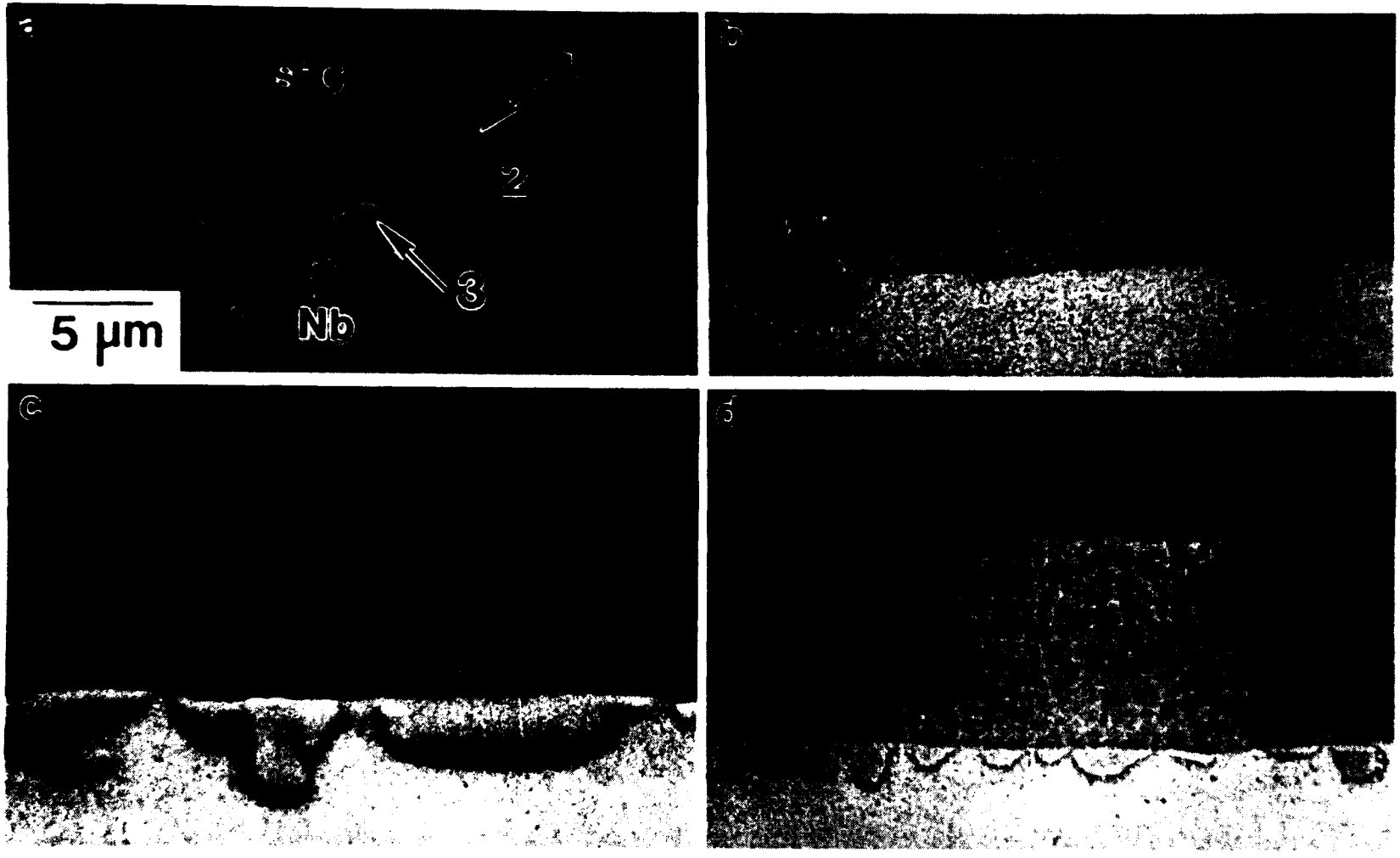

Fig. 4.5 Cross-sectional view SEM micrographs showing the growth of layered reaction products, from the Nb/SiC reactions at 1200°C, as annealing time increases from (a) 6, (b) 18, (c) 32, to (d) 48 h. The SiC and Nb components are indicated, and the original joining interfaces are marked by arrows.

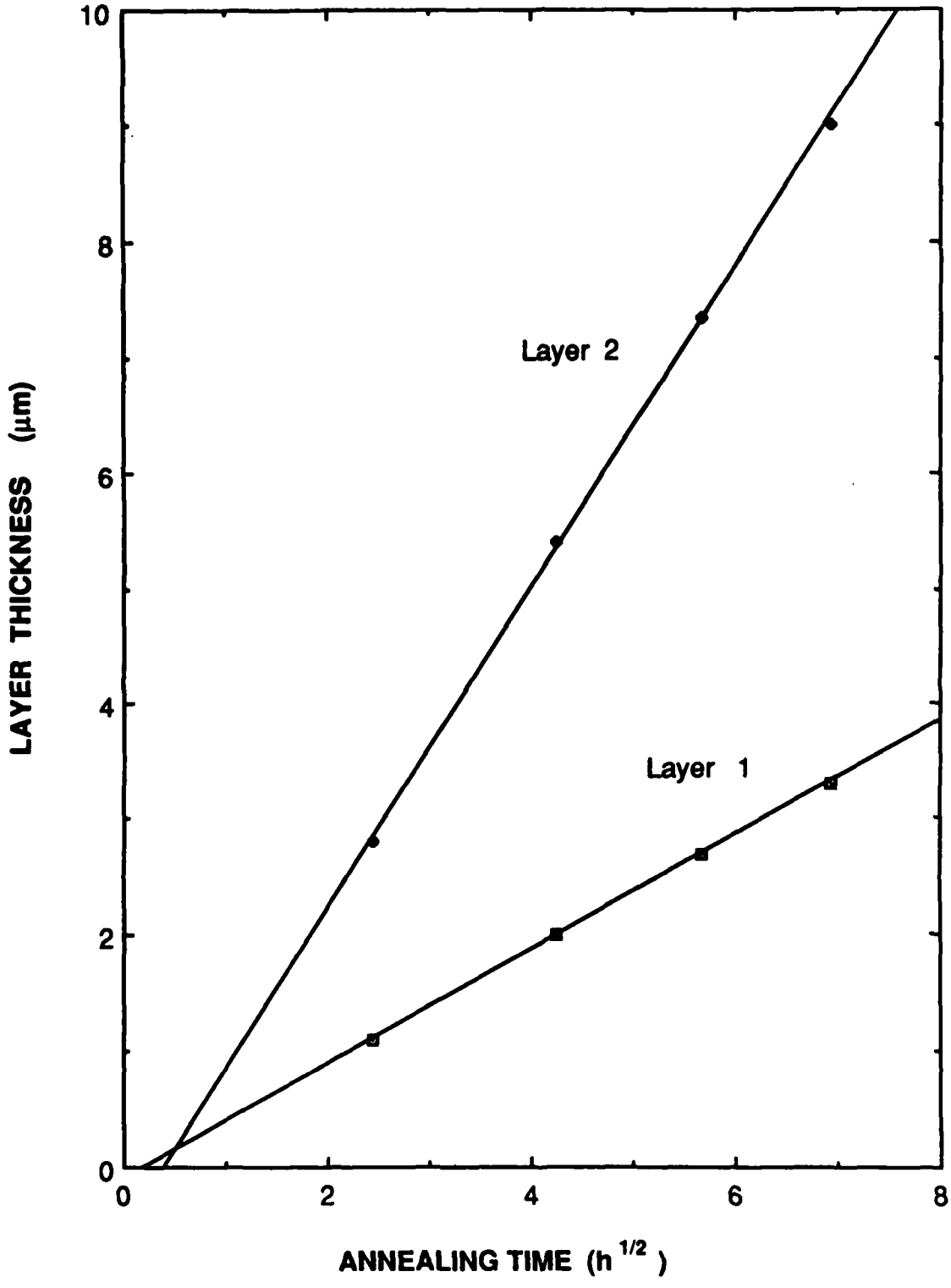

Fig. 4.6 Growth of the thicknesses of layers 1 and 2 in Nb/SiC diffusion couples at 1200 °C.

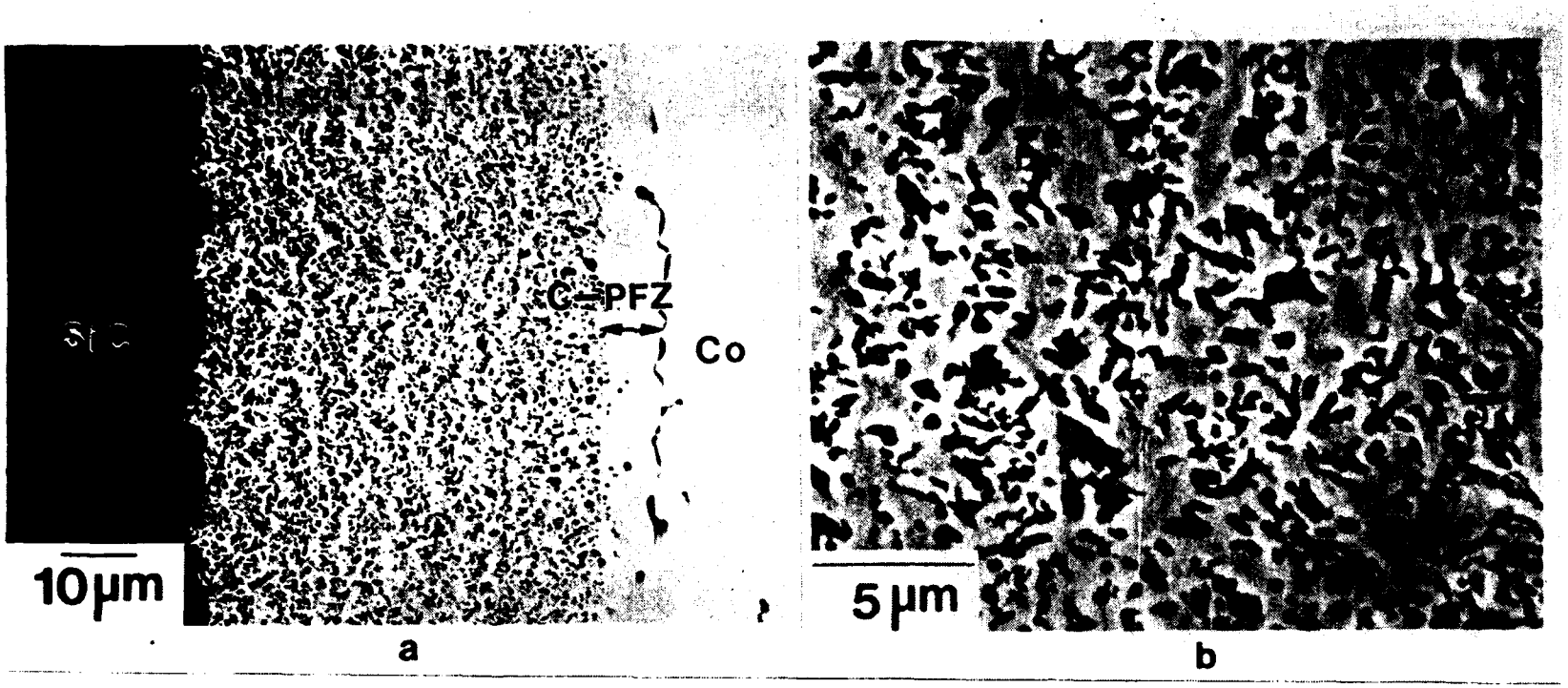

Fig. 4.7 (a) A cross-sectional SEM micrograph showing the Co/SiC reaction zone after annealing for 6 hrs at 1100°C. The location of the phase boundary is indicated by arrows. (b) A high magnification SEM micrograph showing the microstructure of the random carbon precipitation zone.

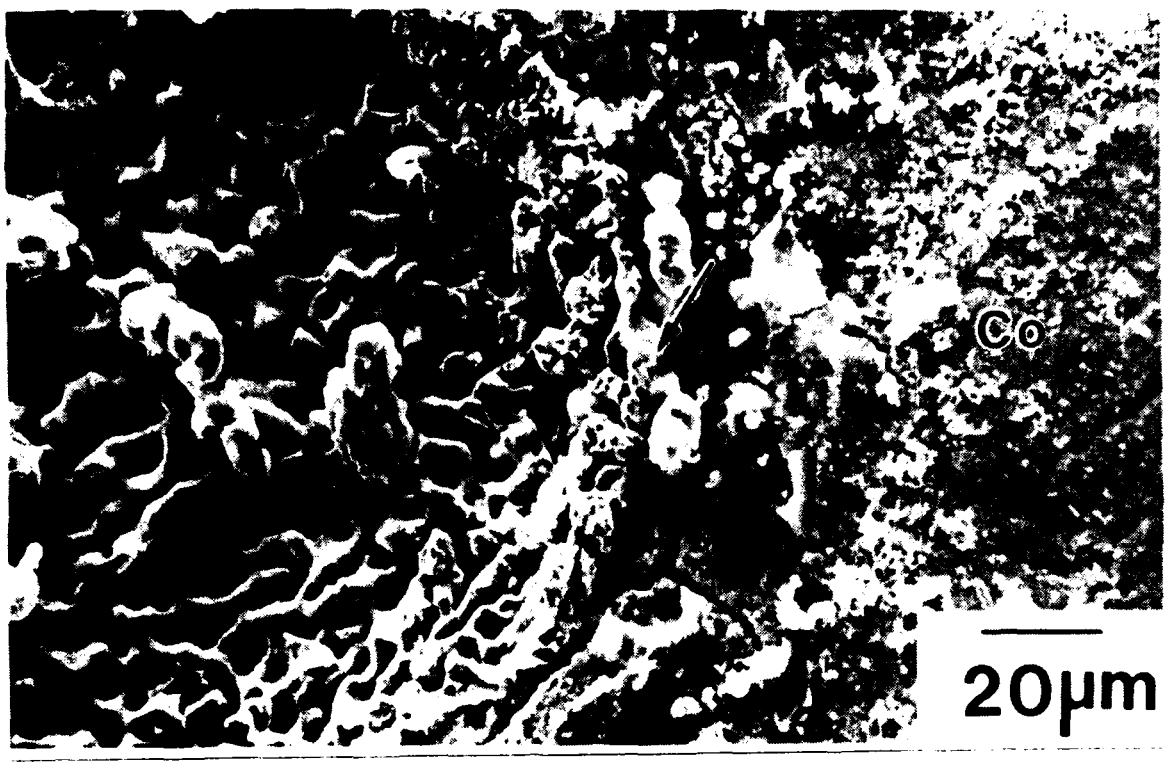

Fig. 4.8 A SEM micrograph showing the microstructure of the ex-situ fractured SiC interface. The boundary between the unreacted and reacted regions is indicated.

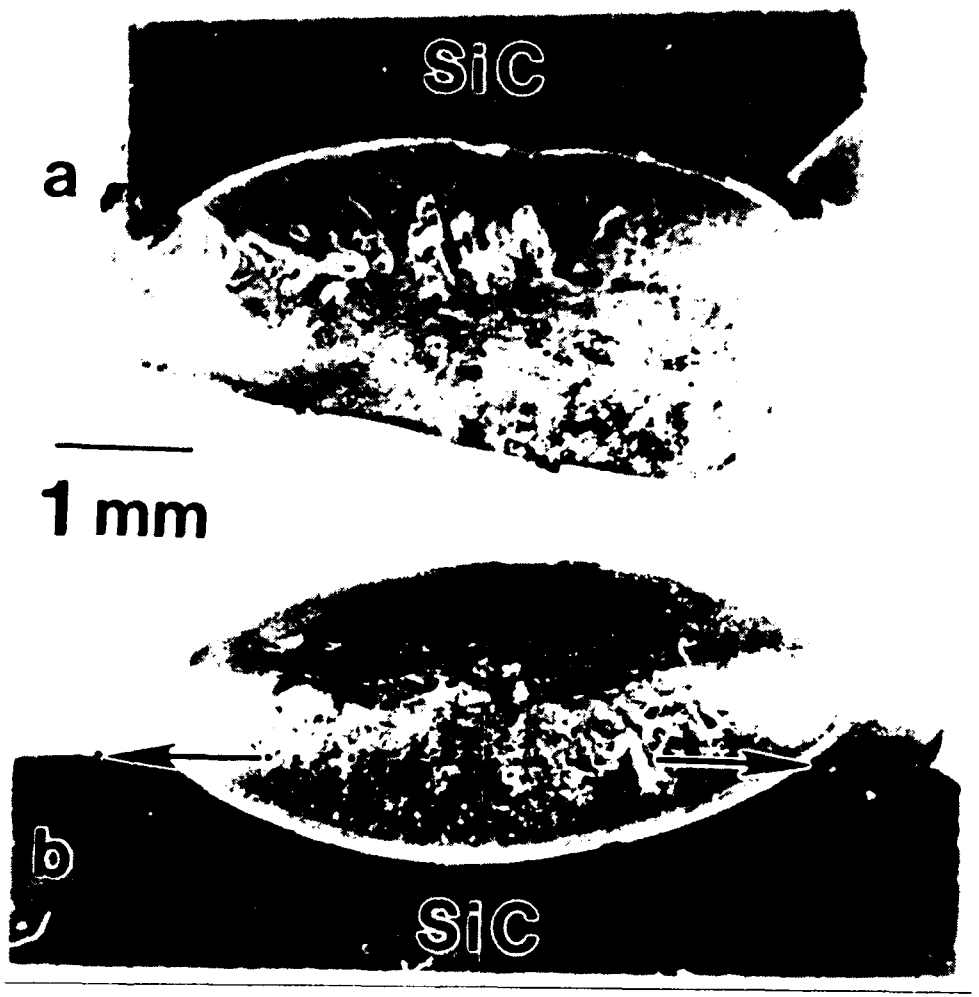

Fig. 4.9 Optical micrographs showing cross-sectional views of the Co/SiC reactions based on the reaction geometries of: (a) SiC on top of Co, and (b) Co on top of SiC after 1210°C annealing for 4 hrs. The original SiC/Co joining interface is indicated in (b).

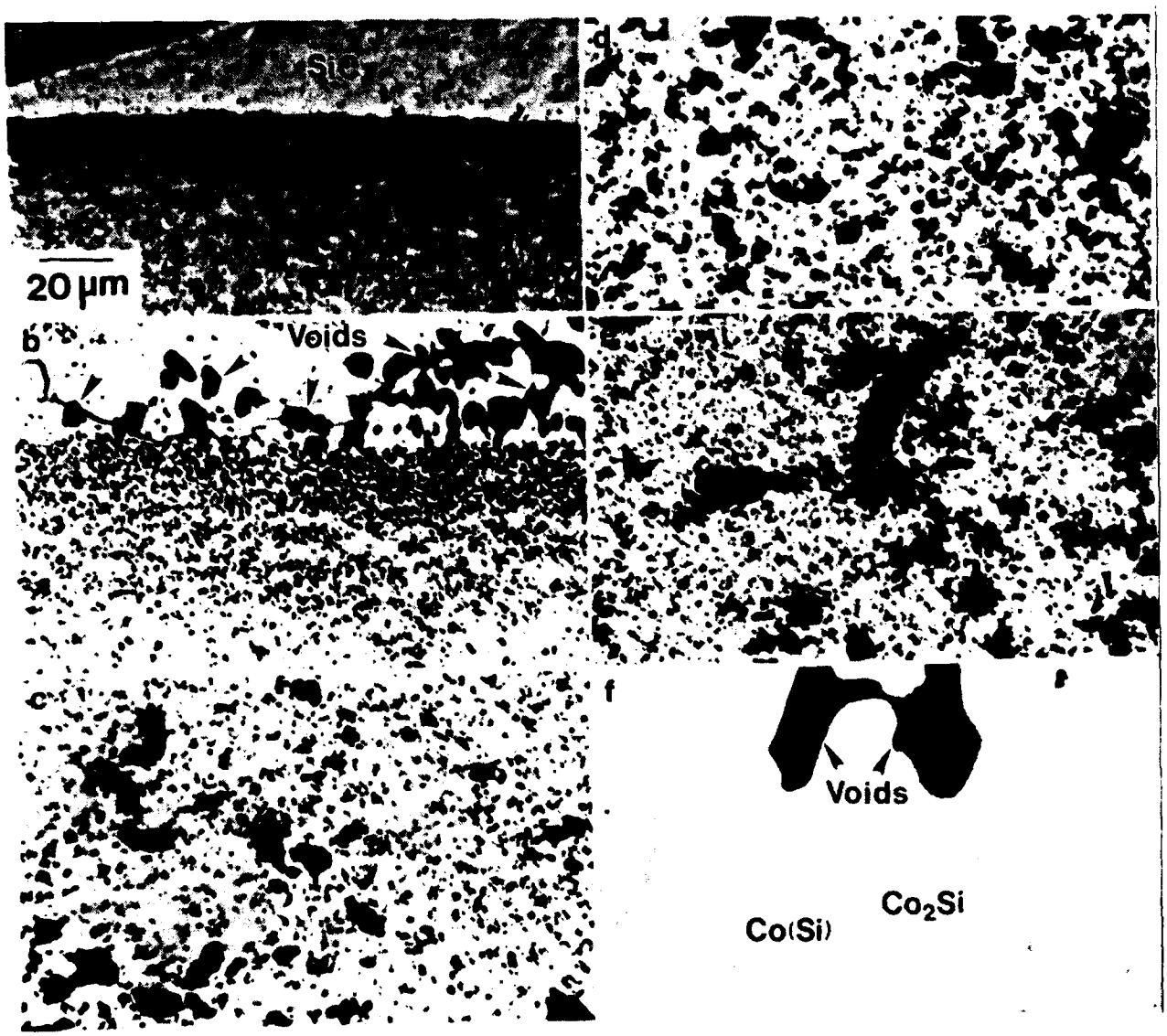

Fig. 4.10 A series of optical micrographs showing cross-sectional views of the Co/SiC reaction zone. (a) Co/SiC interface,(b)-(e) random C precipitation zone, (f) Co(Si) (light matrix) and Co_2Si (gray areas) two phase mixture region. The dark areas, as indicated and shown on top of the (b) and (f), are voids.

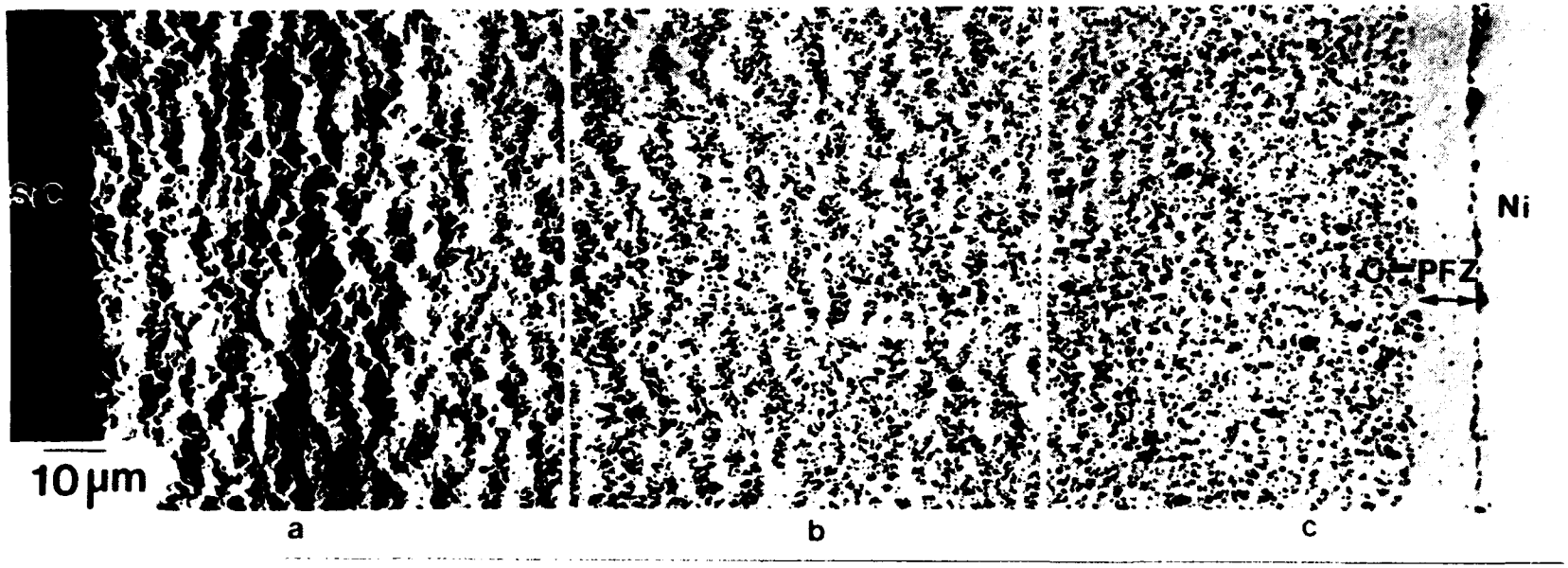

Fig. 4.11 A cross-sectional SEM micrograph of the Ni/SiC reaction zone after annealing for 6 hrs at 1100°C.

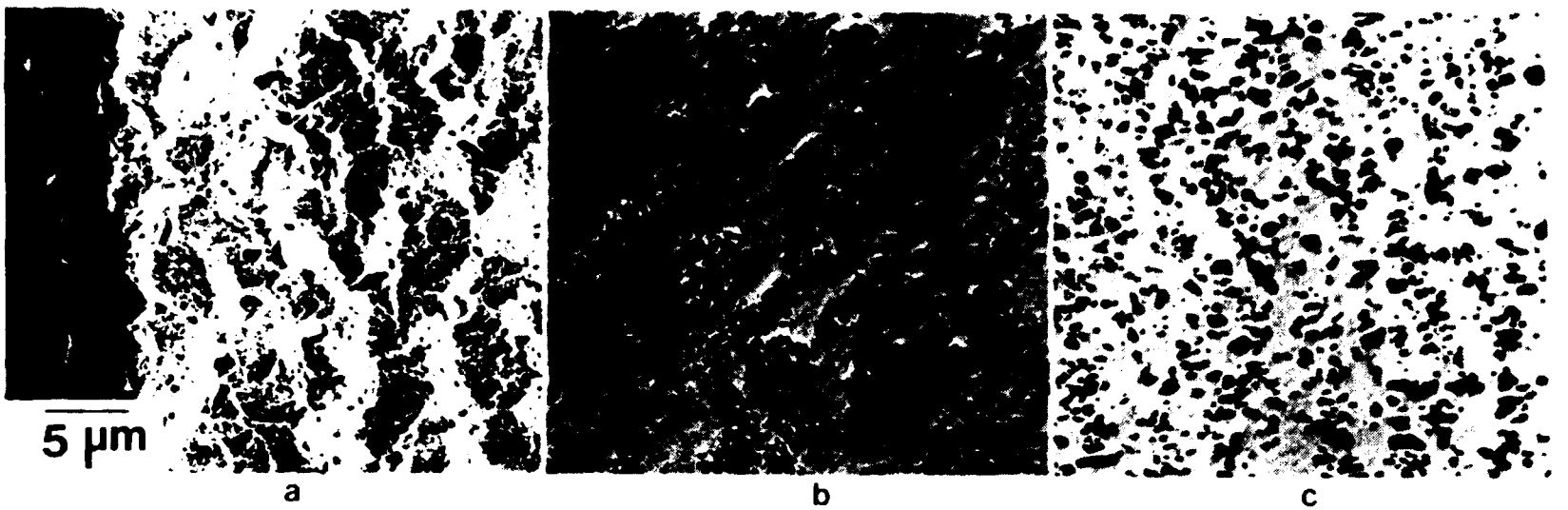

Fig. 4.12 High magnification SEM micrographs of the Ni/SiC reaction zone.

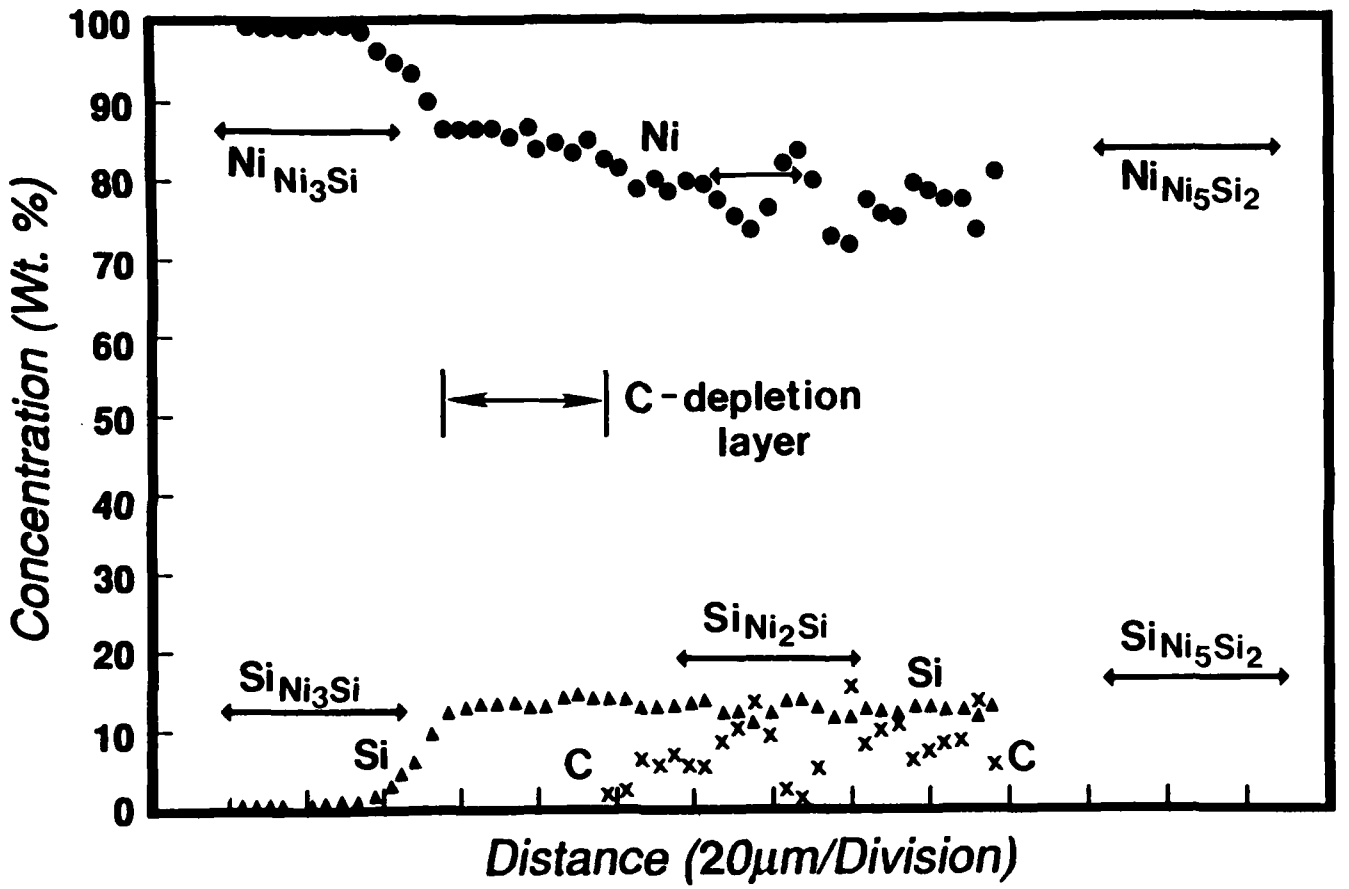

Fig. 4.13 Quantitative electron microprobe concentration profiles of Ni, Si, and C across the reaction zone from the Ni/SiC diffusion couple after annealing for 6 hrs at 1100°C. The relative concentrations of Ni and Si for Ni_3Si and Ni_5Si_2 are indicated. The locations of the unreacted Ni component, C-PFZ, and CPZ are marked.

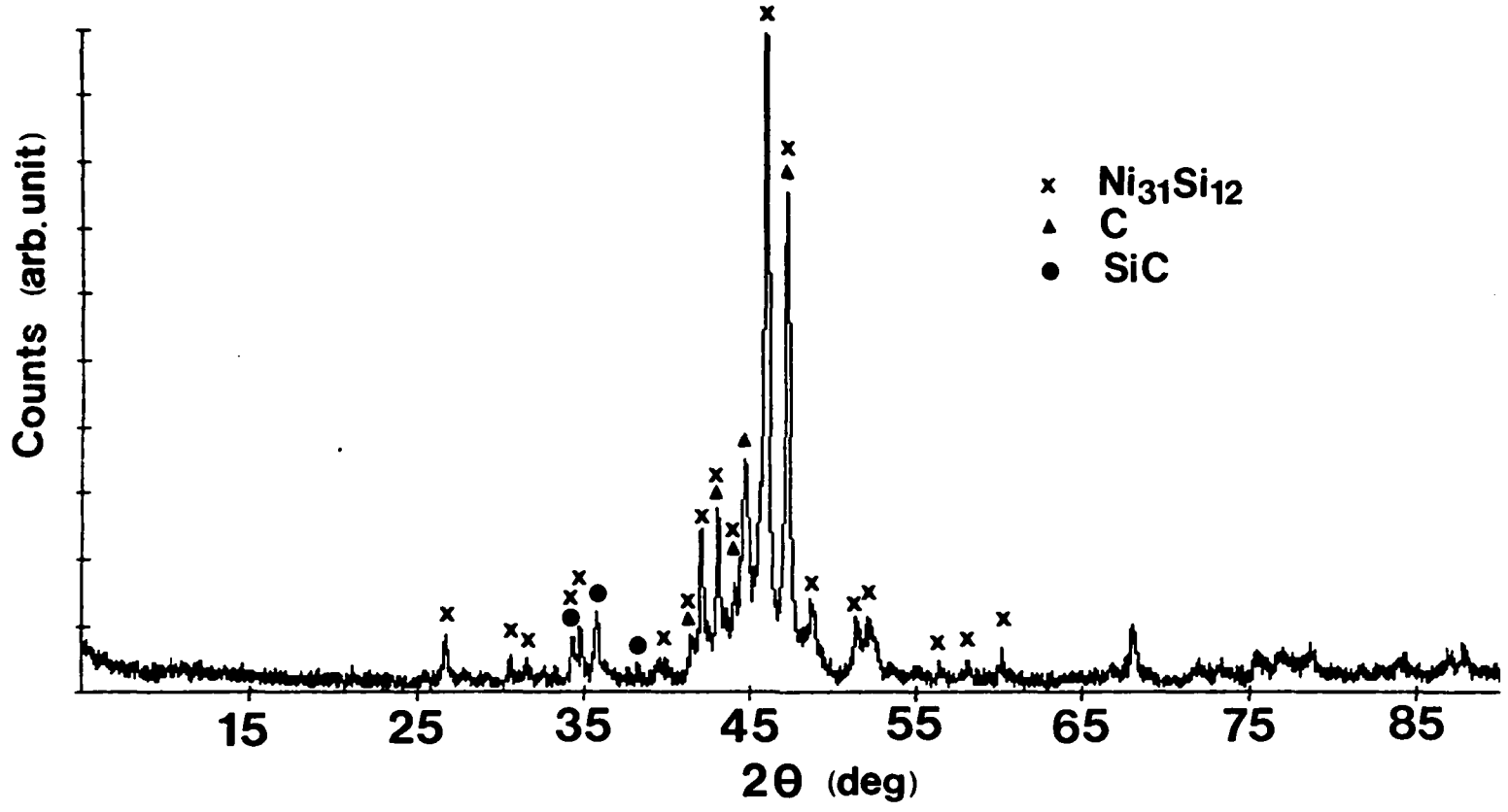

Fig. 4.14 XRD spectra of the reaction products generated from the Ni/SiC reaction at 1170°C.

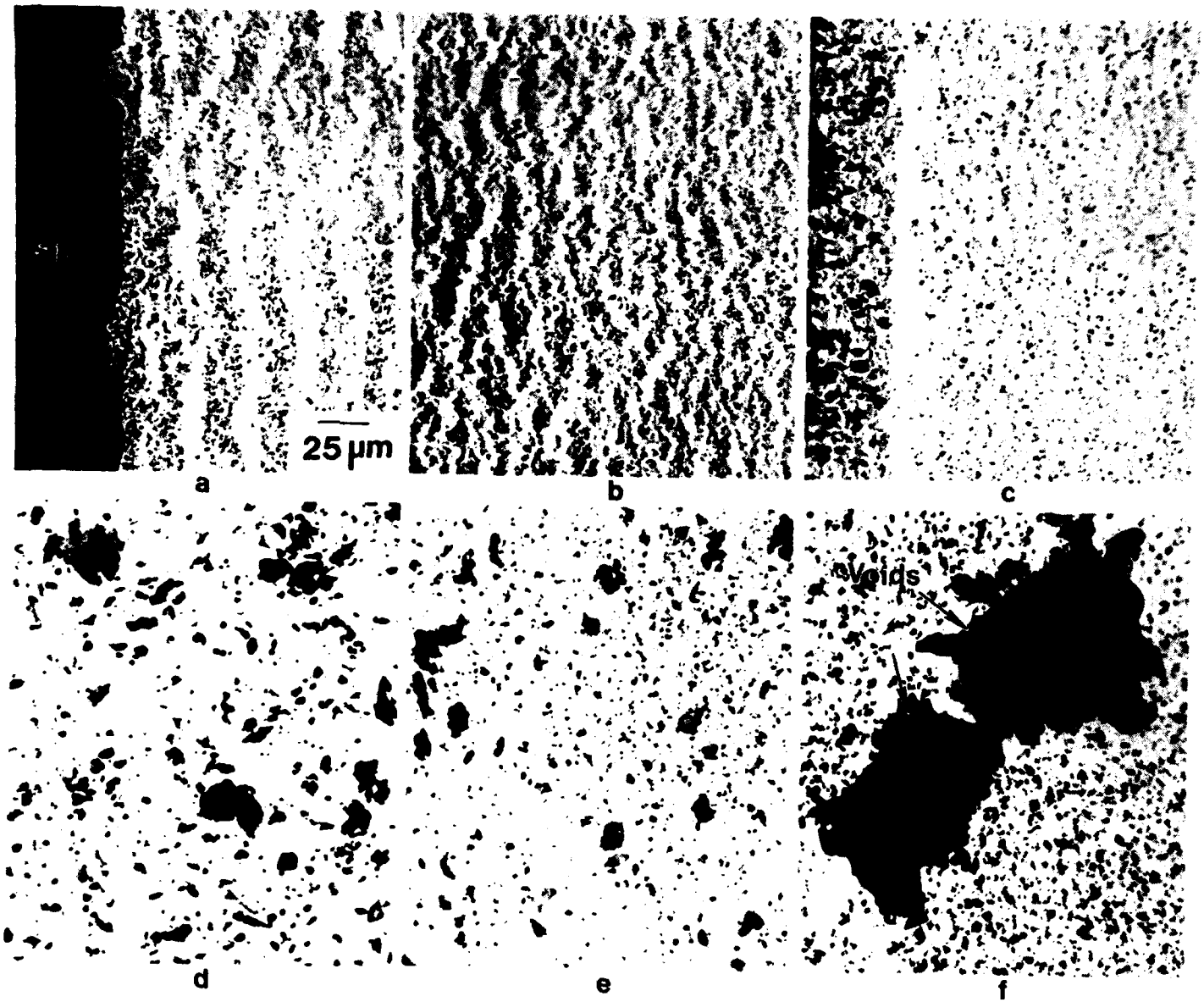

Fig. 4.15 Optical micrographs showing cross-sectional views of the Ni/SiC reaction zone after annealing for 4 hrs at 1170°C. Porosity, as a result of melting/ solidification, is noted and indicated in the reaction zone.

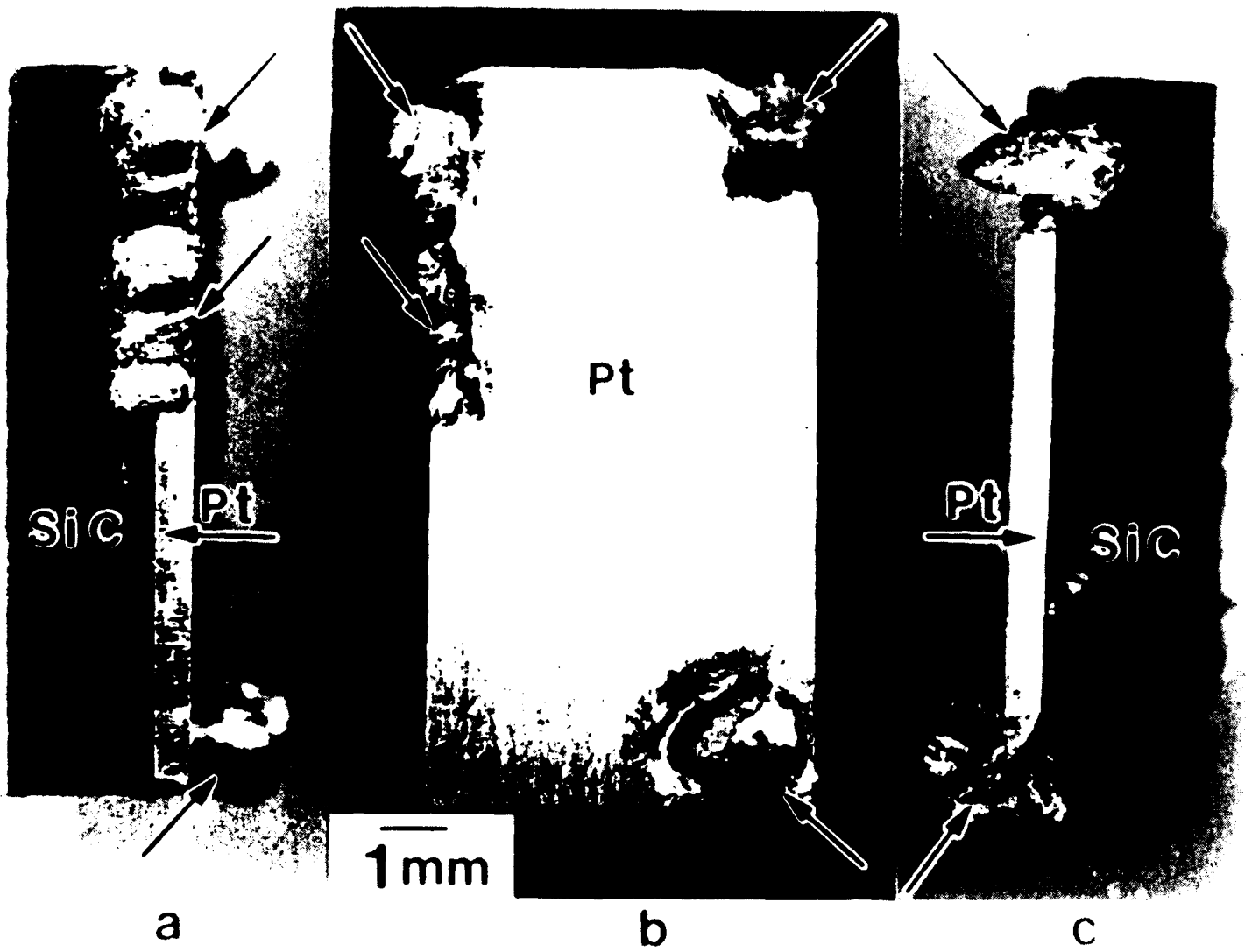

Fig. 4.16 Optical micrographs showing different views of the melting/solidification phenomena from the Pt/SiC diffusion couple after annealing for 5 hrs at 900 °C.

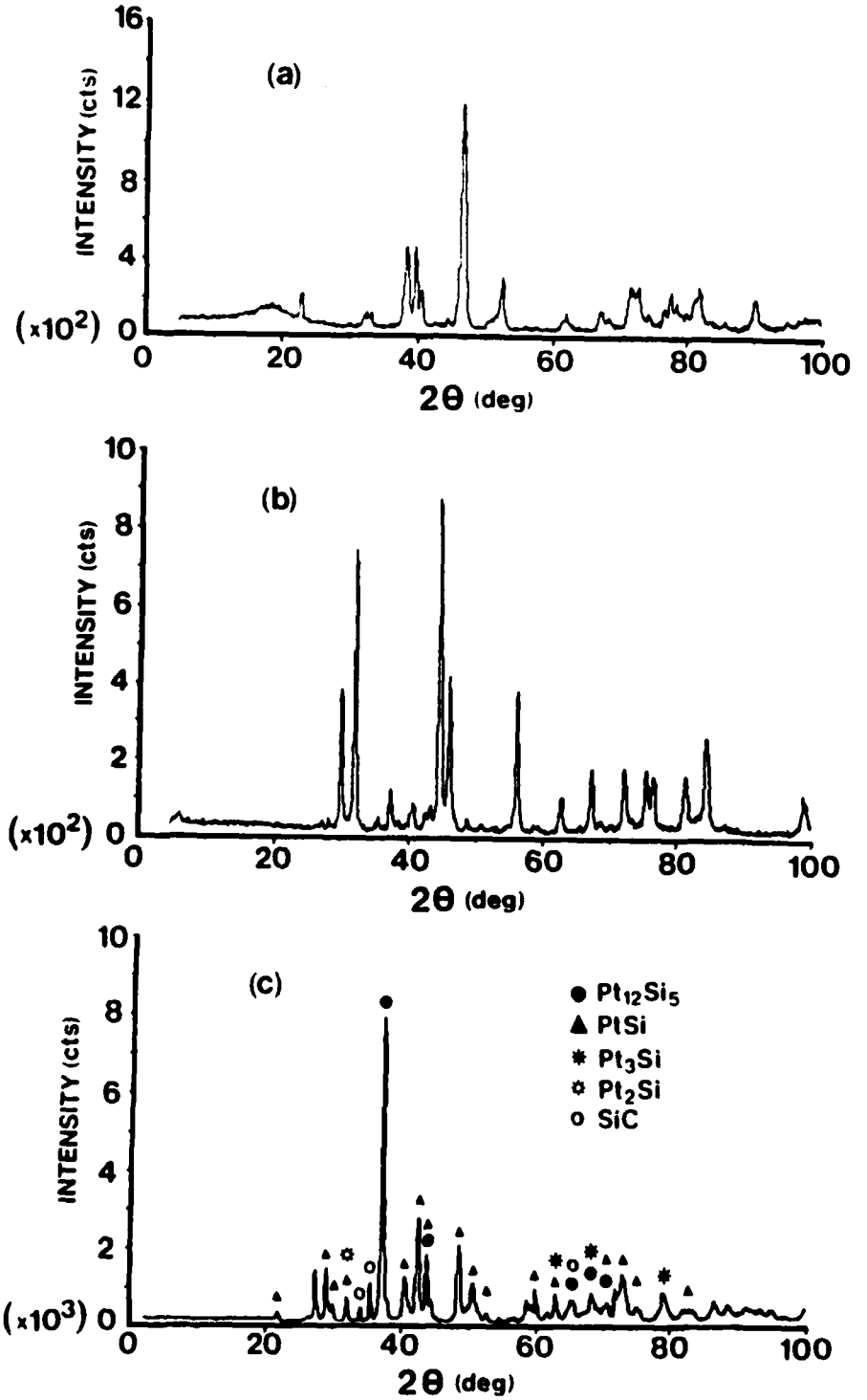

Fig. 4.17 XRD spectra of the Pt/SiC reaction products after (a) 900, (b) 1000, and (c) 1100°C reactions.

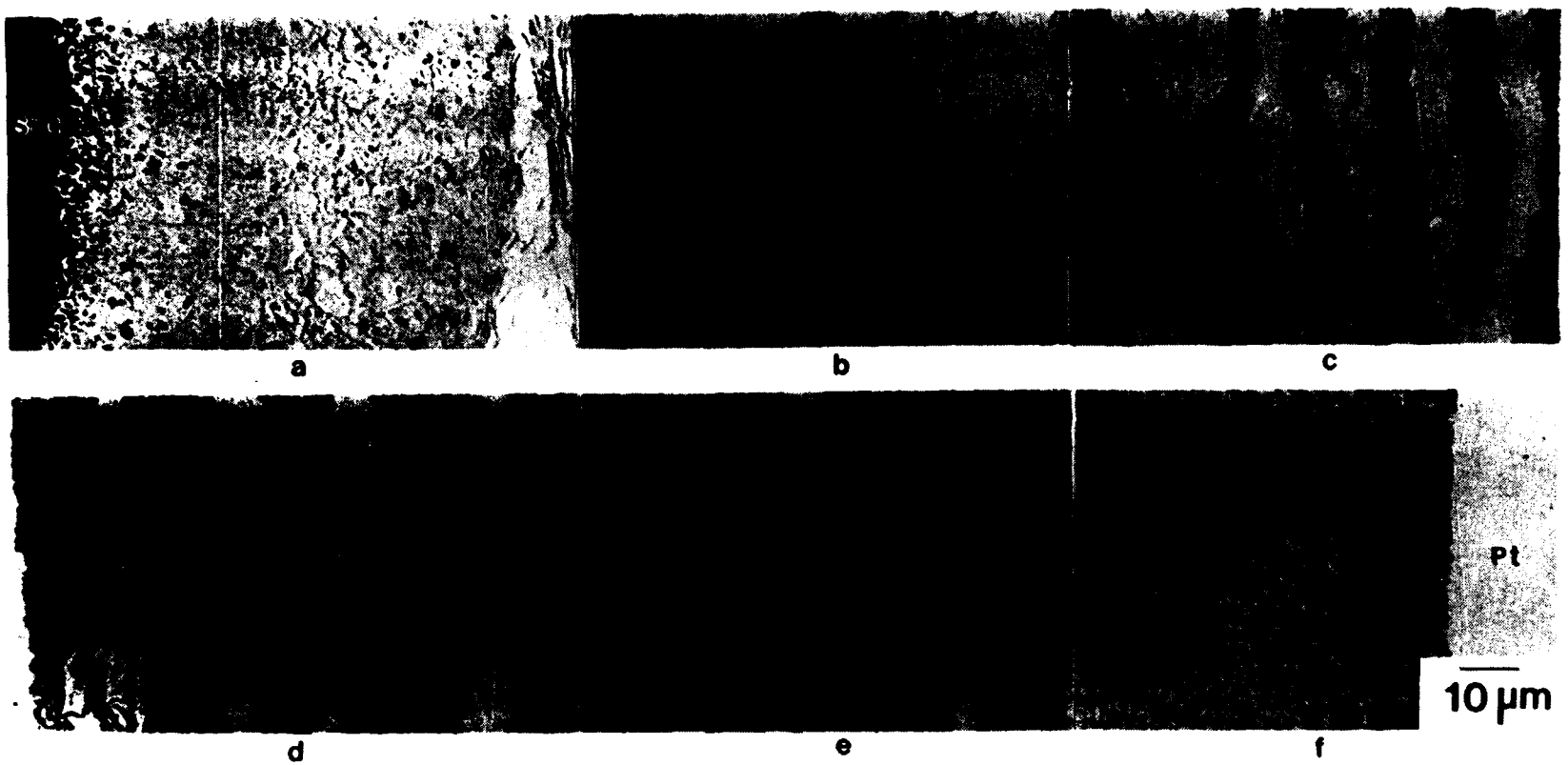

Fig. 4.18 A series of SEM micrographs showing microstructure of the Pt/SiC reaction zone after annealing for 4 hrs at 1100°C.

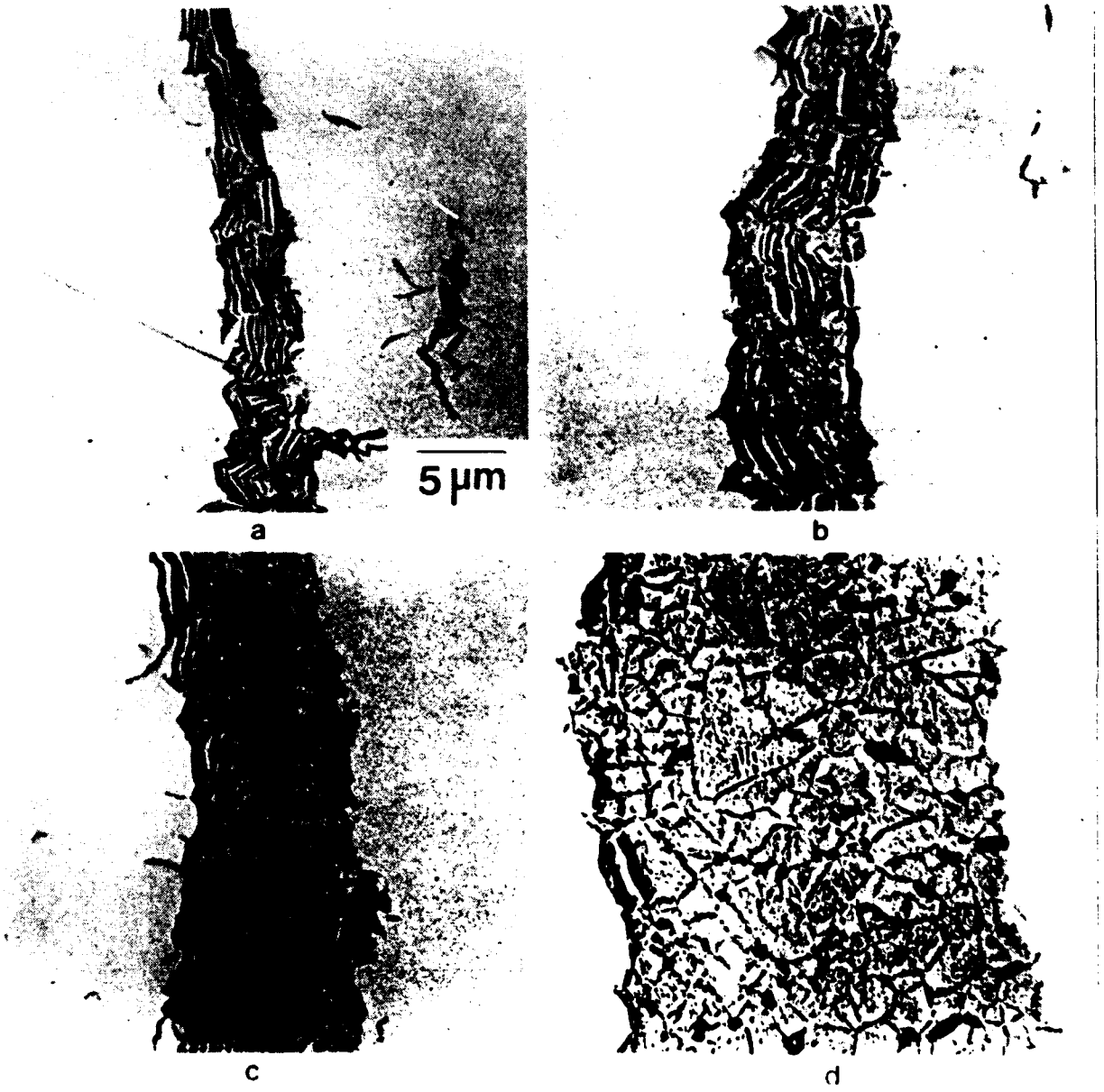

Fig. 4.19 SEM micrographs showing the microstructural change of the C bands, as a function of distance from the SiC reaction interface, from the as-reacted Pt/SiC diffusion couple after annealing for 4 hrs at 1100 °C. As the distance increases, from (a) to (d), the thickness of the clustered C bands increases and the discrete C layers transform into C-decorated, granular Pt-silicide layers.

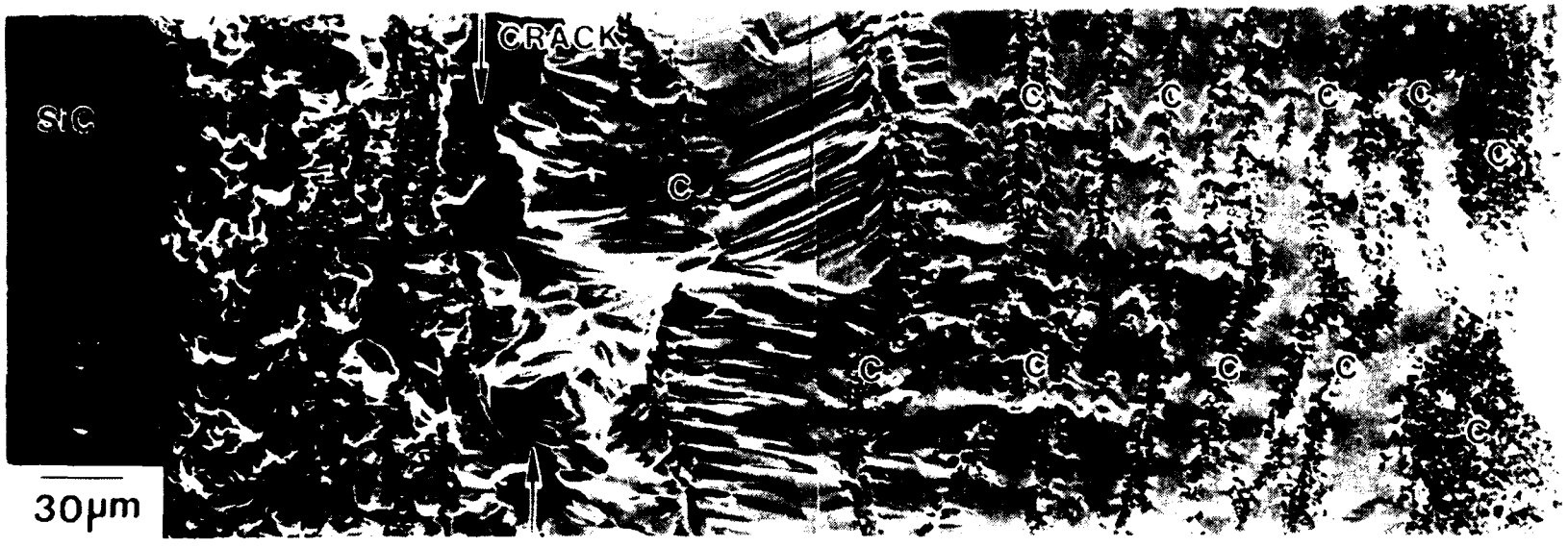

Fig. 4.20 SEM micrographs showing the microstructural evolution in the reaction zone from the as-reacted Pt/SiC diffusion couple after annealing for 4 hrs at 1100°C.

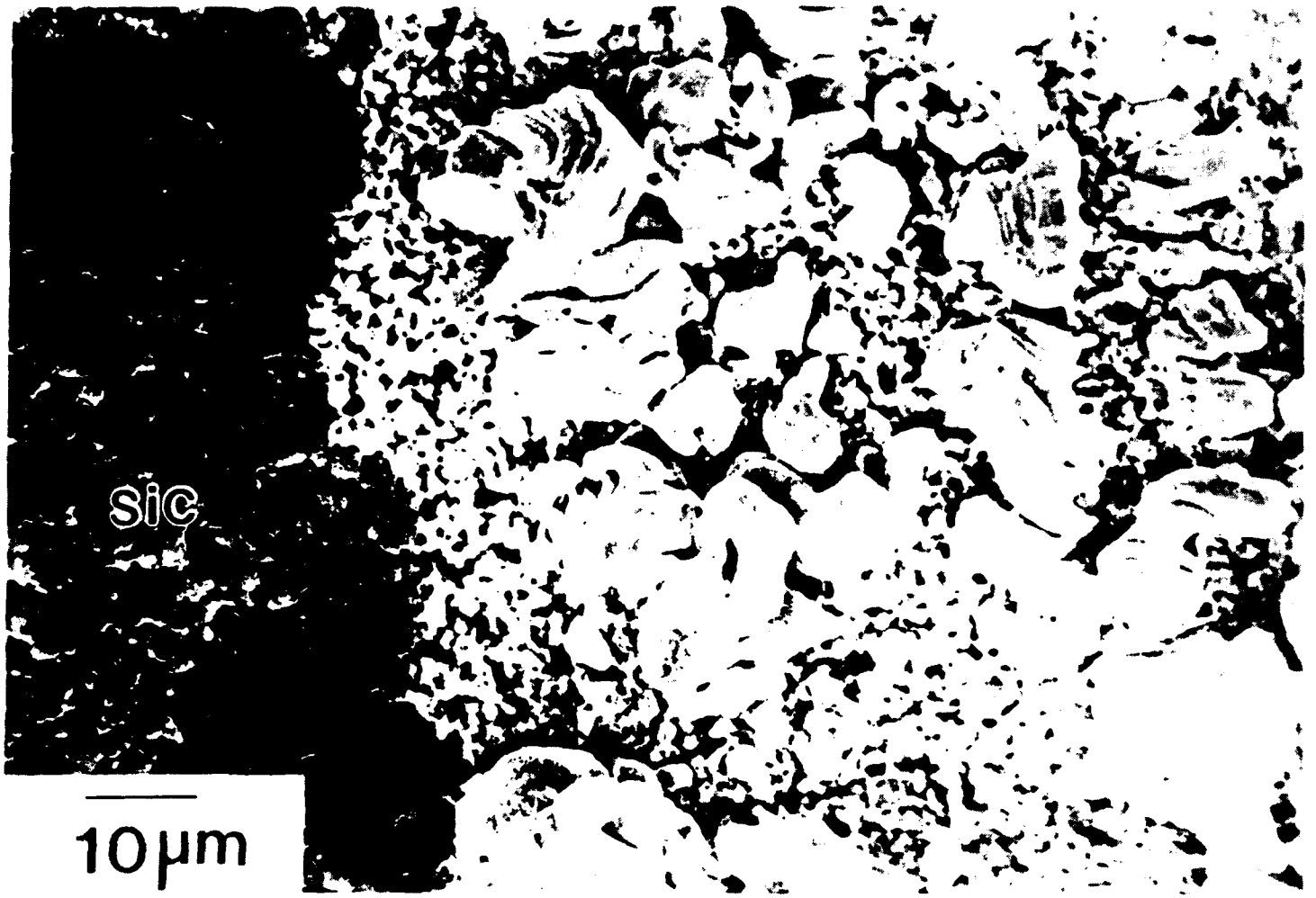

Fig. 4.21 A high magnification backscattered electron image showing the microstructure of the 3rd layer, and the morphology of the melted/solidified particulates formed on top from the as-reacted Pt/SiC diffusion couple after reactions at 1100°C for 4 hrs.

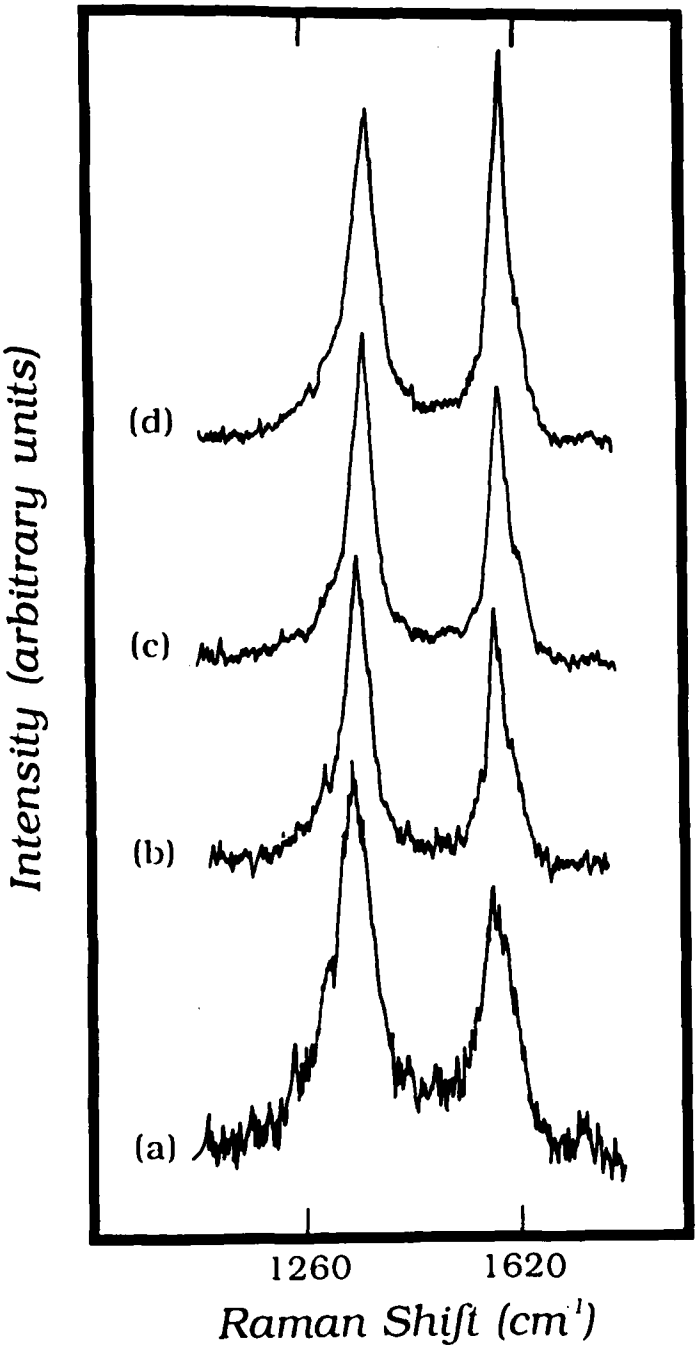

Fig. 4.22 A series of Raman spectra from the modulated C bands precipitated in the the SiC/Pt reaction zone after annealing for 5 hrs at 1000°C. The spectrum, (a), from the SiC reaction interface indicates the existence of glassy carbon, which is characterized by the presence of a Raman peak at 1354 cm^{-1}. As the locations of the C bands are farther removed from the SiC interface, from (b) to (d), graphitization of the C occurs, which is characterized by the decrease of the intensity ratio between the 1354 and 1585 cm^{-1} Raman peaks.

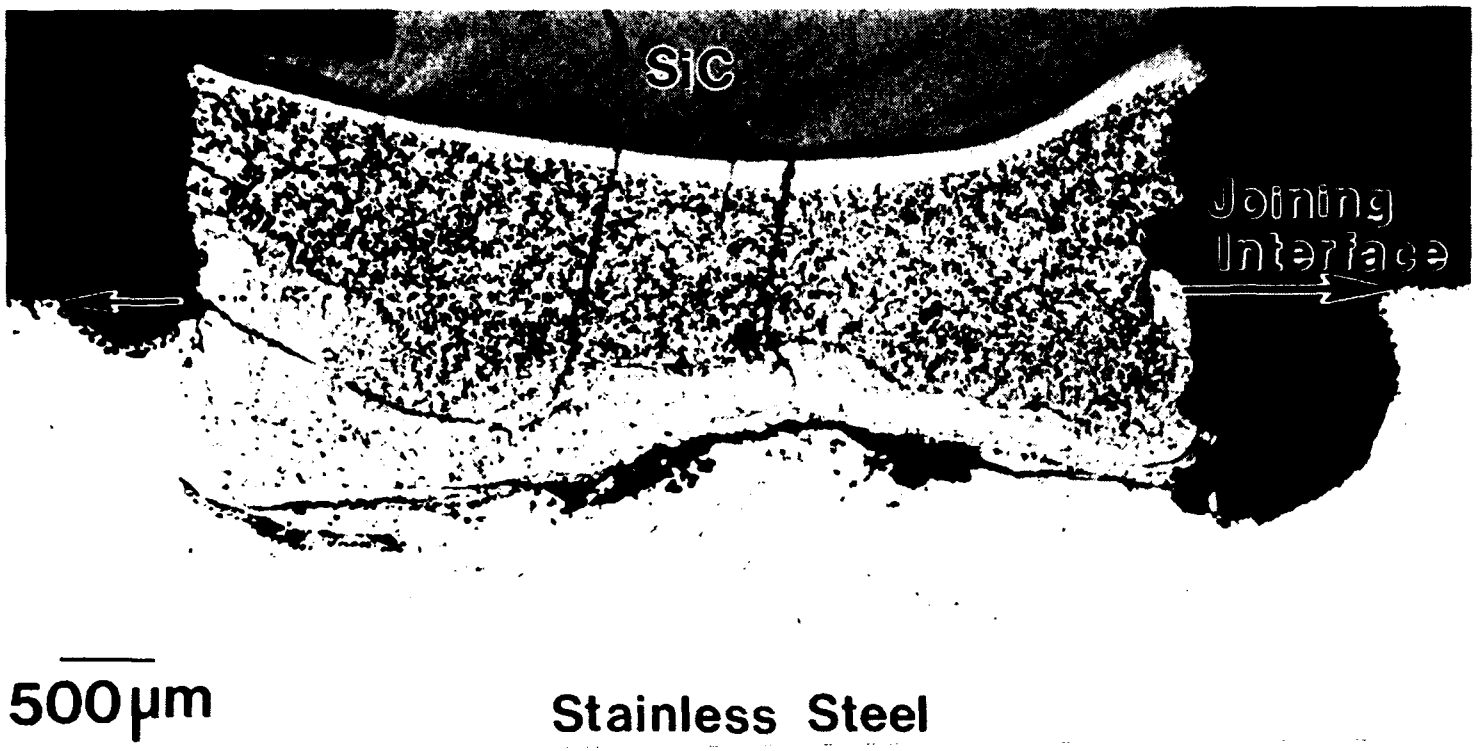

Fig. 4.23 A cross-sectional view SEM micrograph showing the reaction zone of a SS/SiC diffusion couple upon annealing at 1125°C for 8 h.

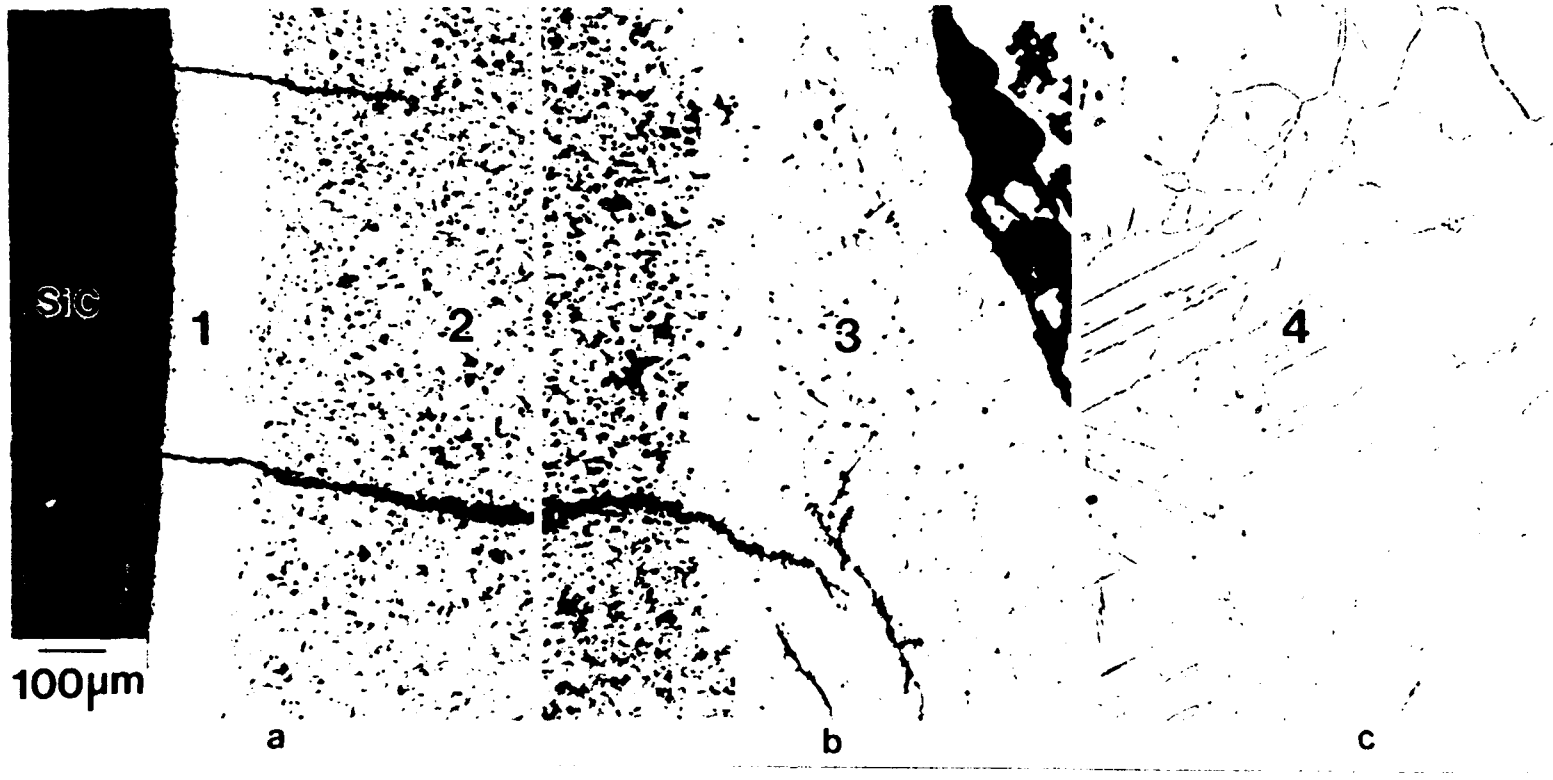

Fig. 4.24 High magnification SEM micrographs showing the formation of 4 layered reaction zone. The four layers are indicated as 1, 2, 3 and 4.

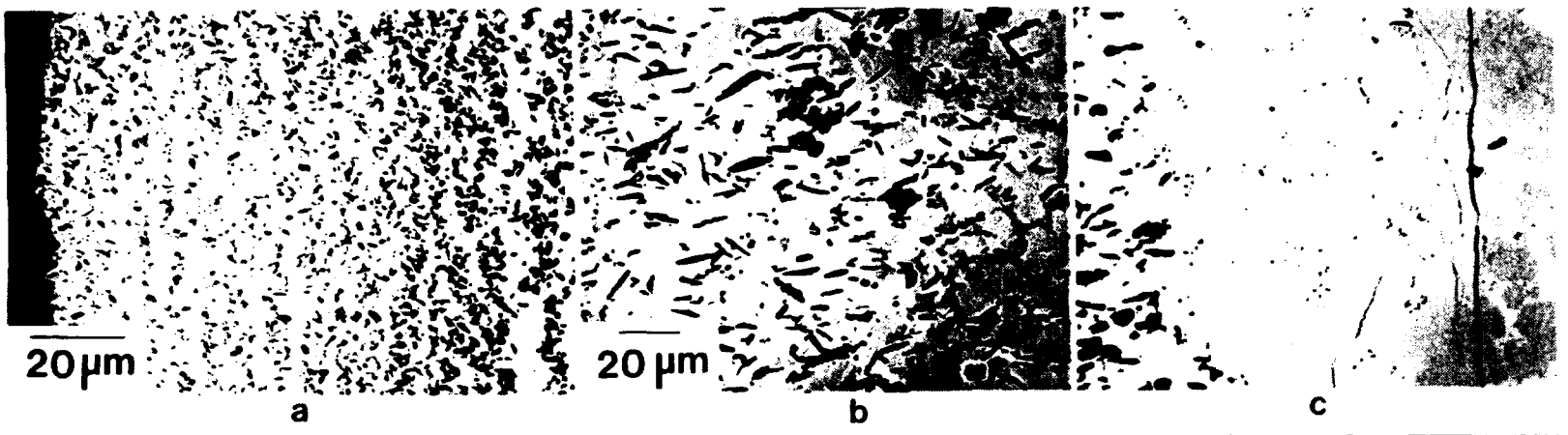

Fig. 4.25 High magnification SEM micrographs showing detailed microstructures in reaction zones 1, 2, and 3. Highly anisotropic C precipitates were observed in reaction zones 1 and 2.

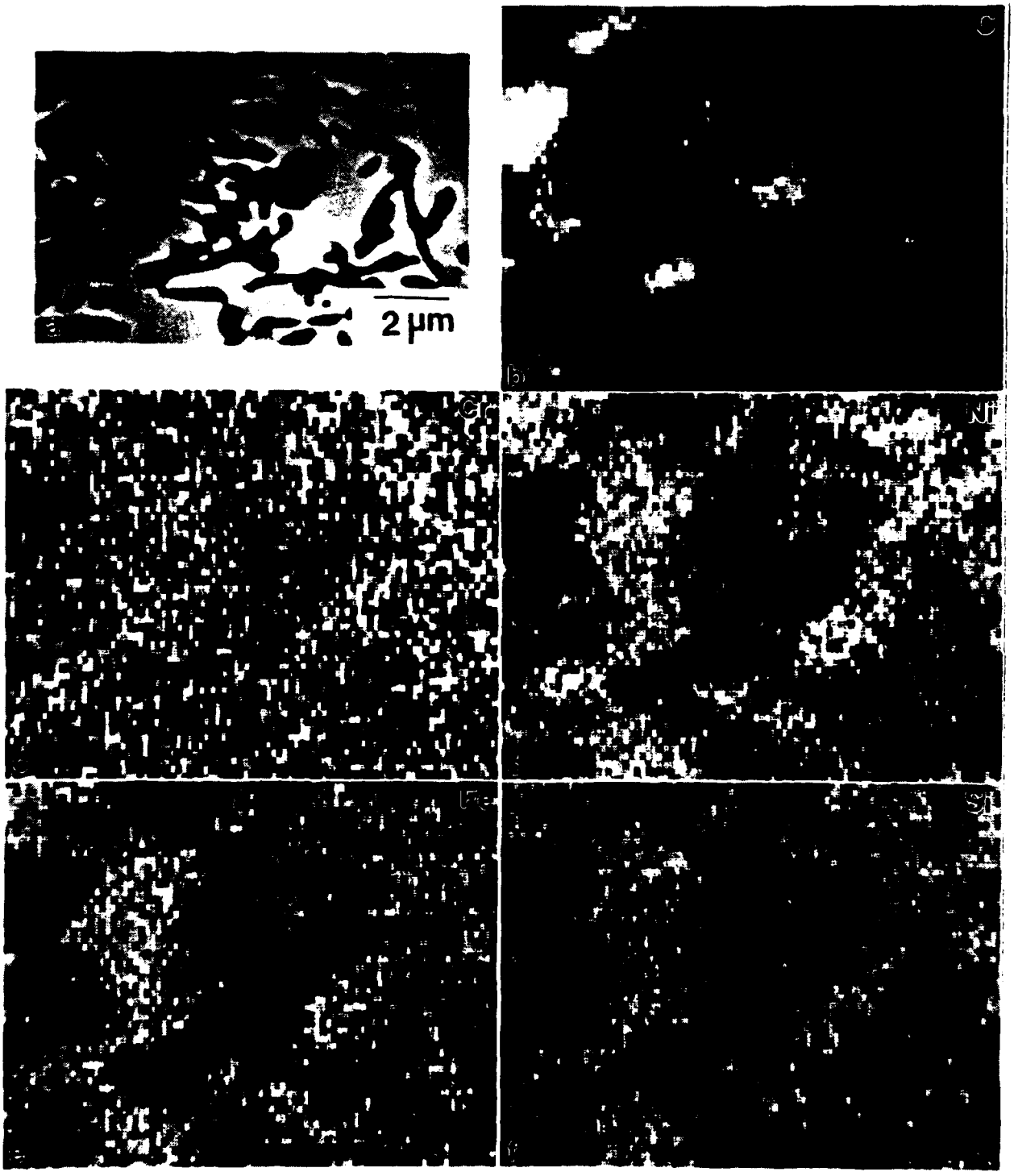

Fig. 4.26 (a) A backscattered electron image, and the corresponding elemental x-ray maps of (b) C, (c) Cr, (d) Ni, (e) Fe, and (f) Si from an area in reaction zone 1.

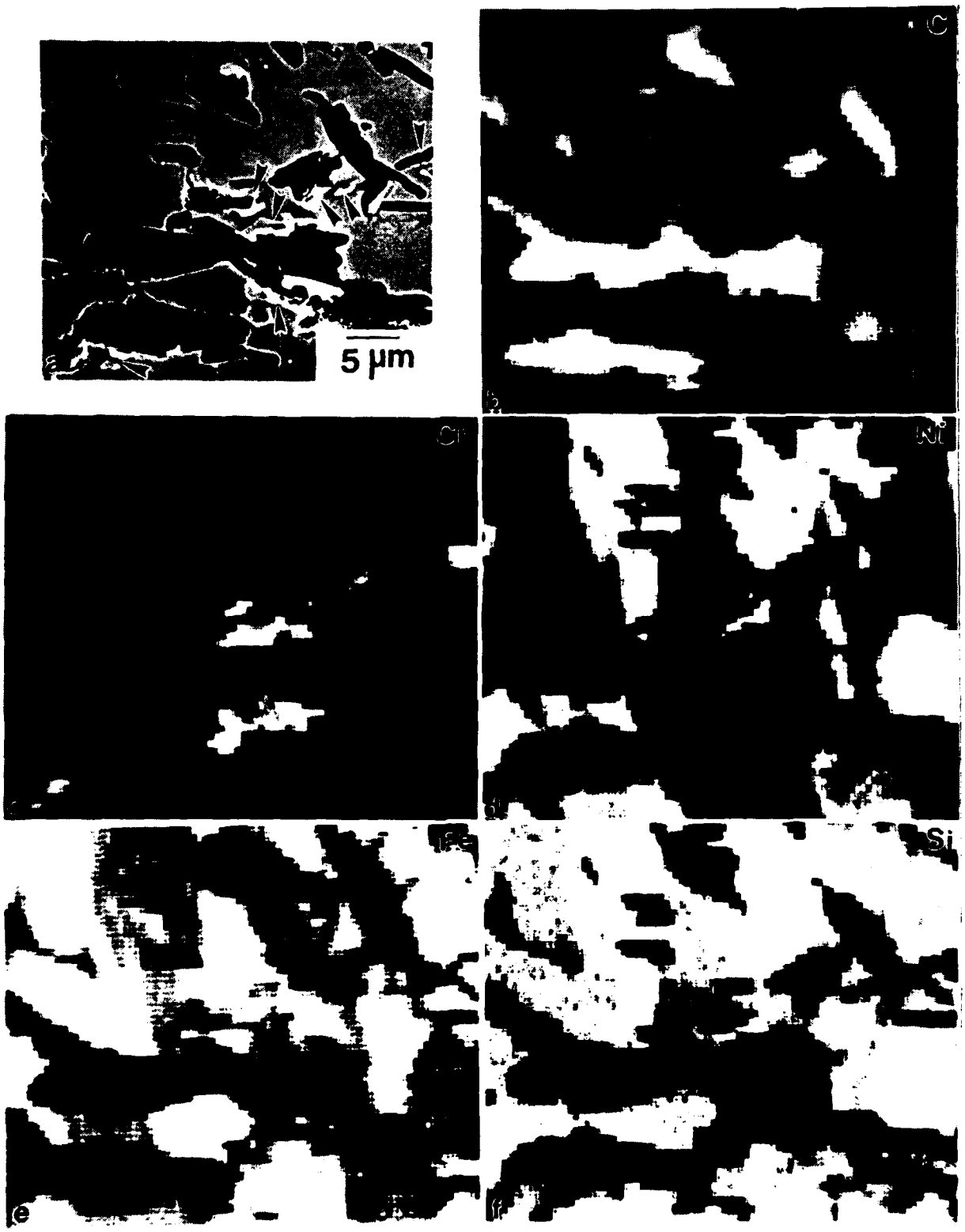

Fig. 4.27 (a) A backscattered electron image, and the corresponding elemental x-ray maps of (b) C, (c) Cr, (d) Ni, (e) Fe, and (f) Si from an area in reaction zone 2.

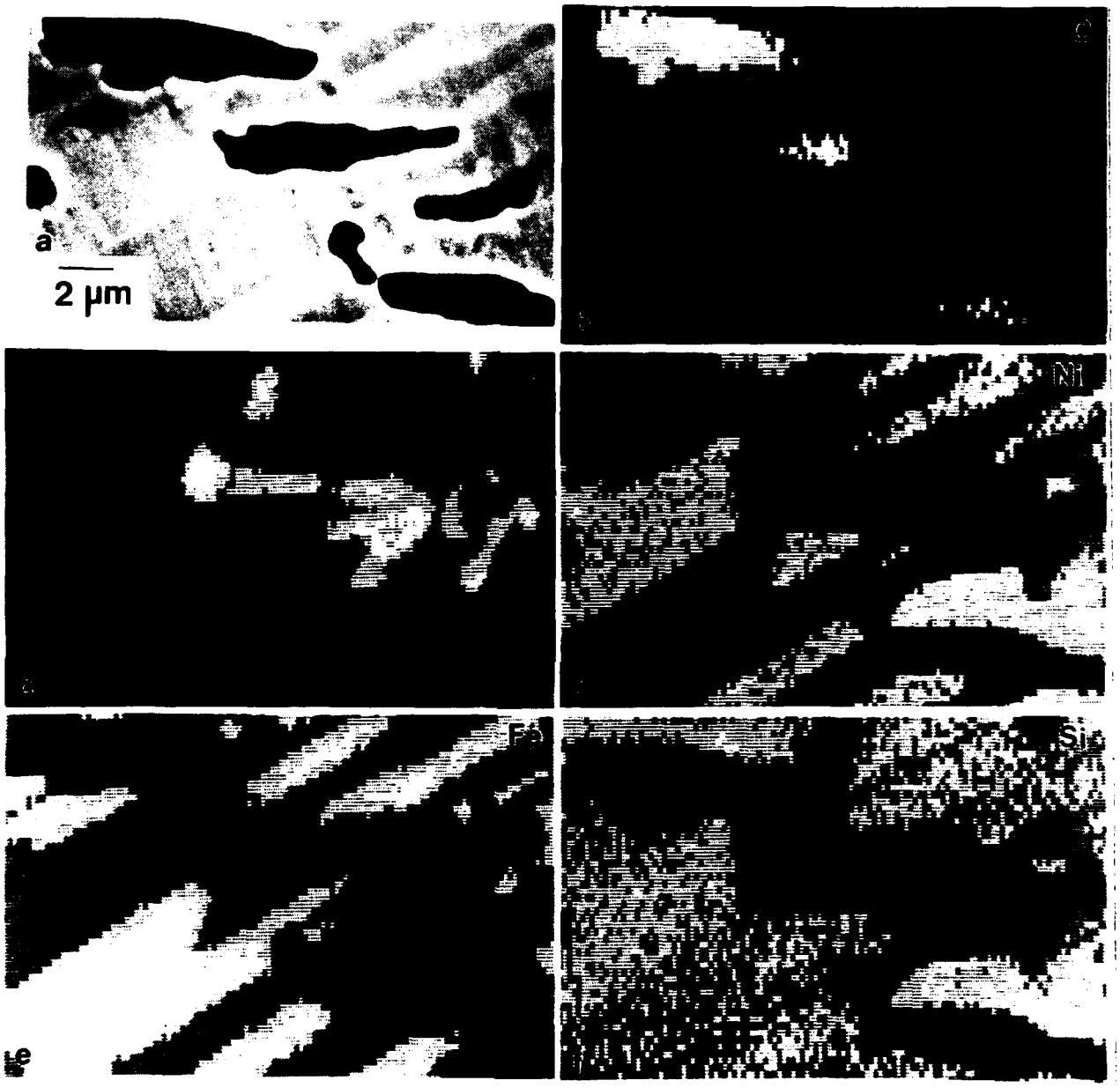

Fig. 4.28 (a) A backscattered electron image, and the corresponding elemental x-ray maps of (b) C, (c) Cr, (d) Ni, (e) Fe, and (f) Si from a farther area in reaction zone 2.

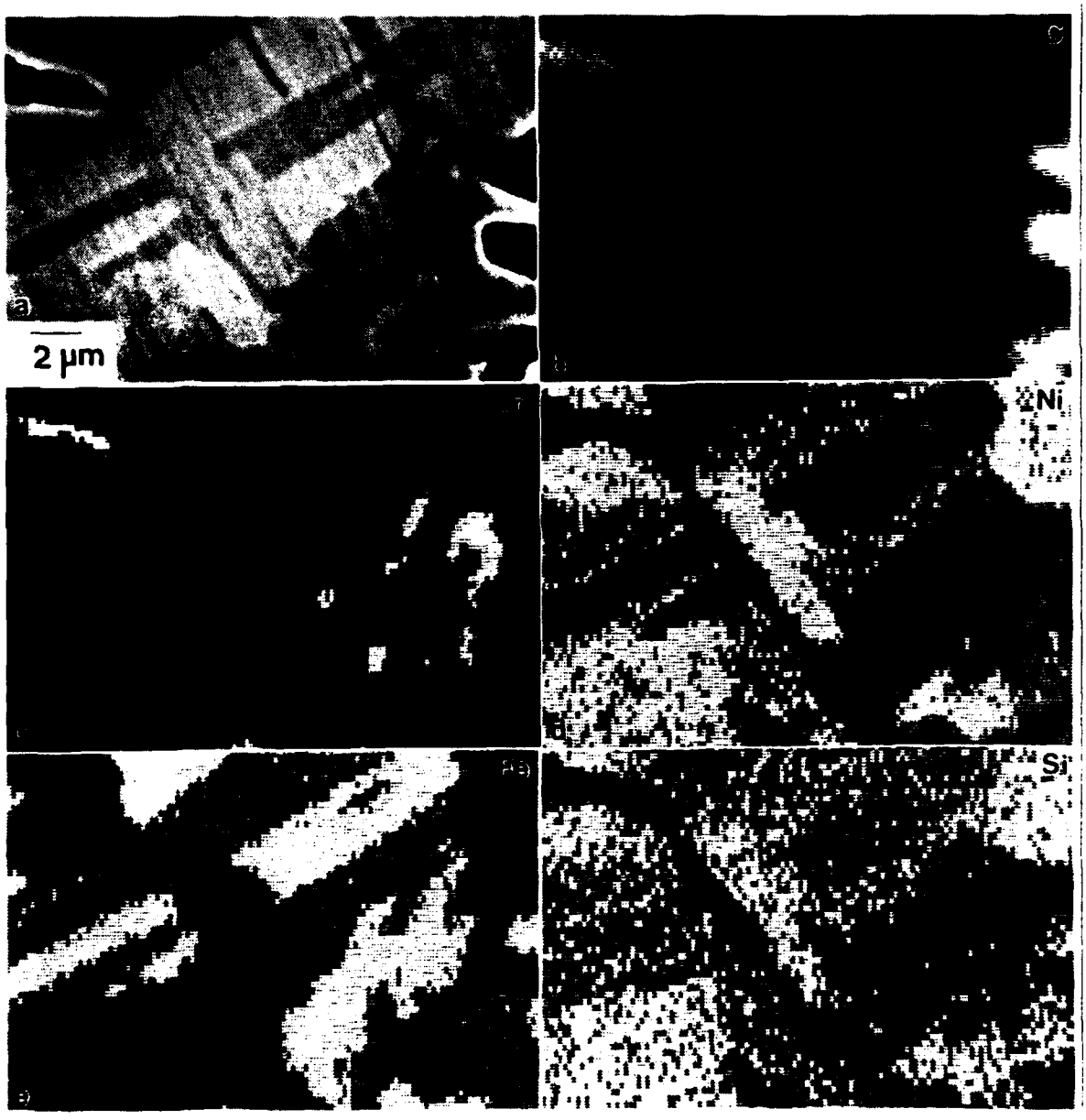

Fig. 4.29 (a) A backscattered electron image, and the corresponding elemental x-ray maps of (b) C, (c) Cr, (d) Ni, (e) Fe, and (f) Si from an even farther area in reaction zone 2.

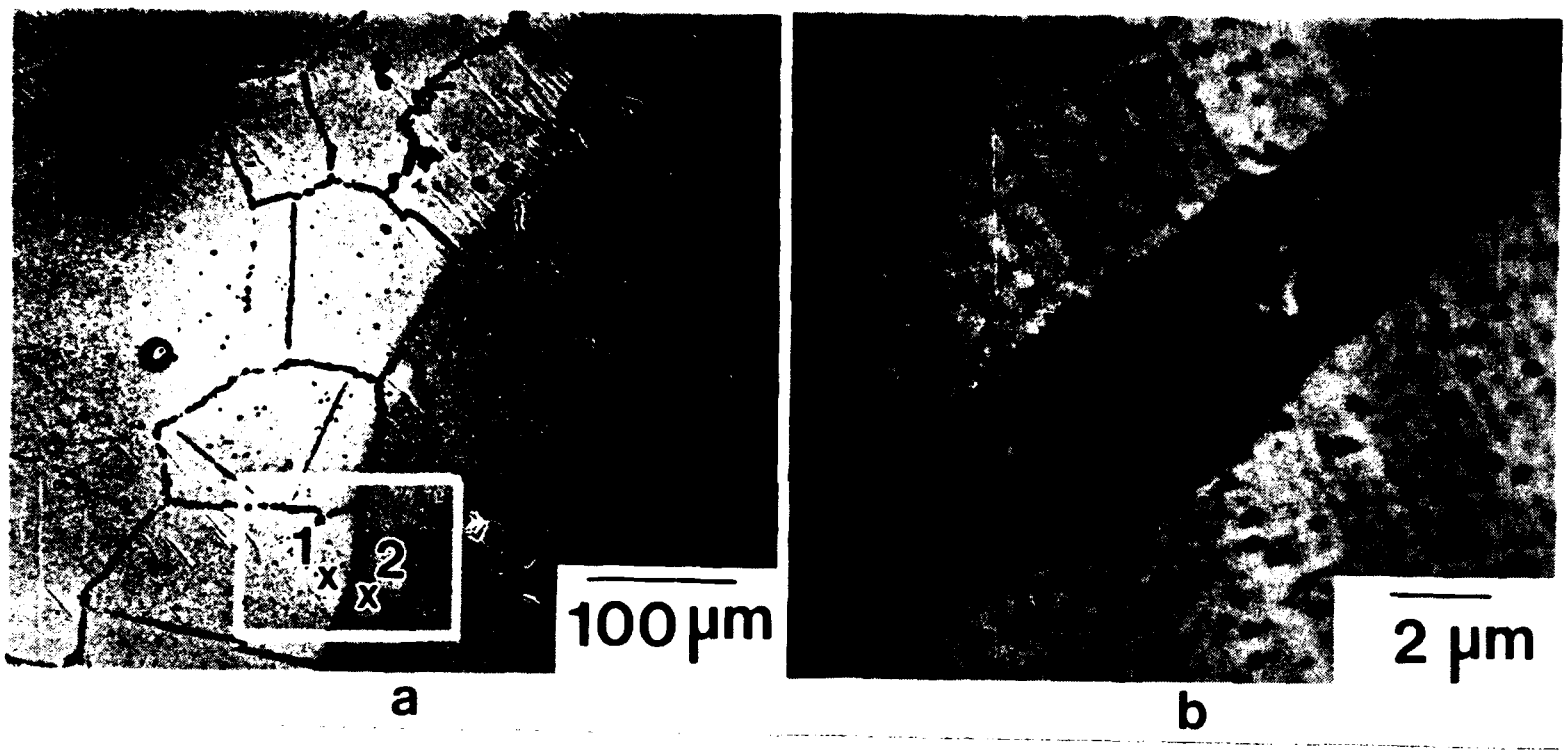

Fig. 4.30 SEM micrographs showing (a) the Si diffusion front and the G.B.-PZ; (b) a high magnification of the grain boundary precipitates. The Si diffusion front is indicated by arrows.

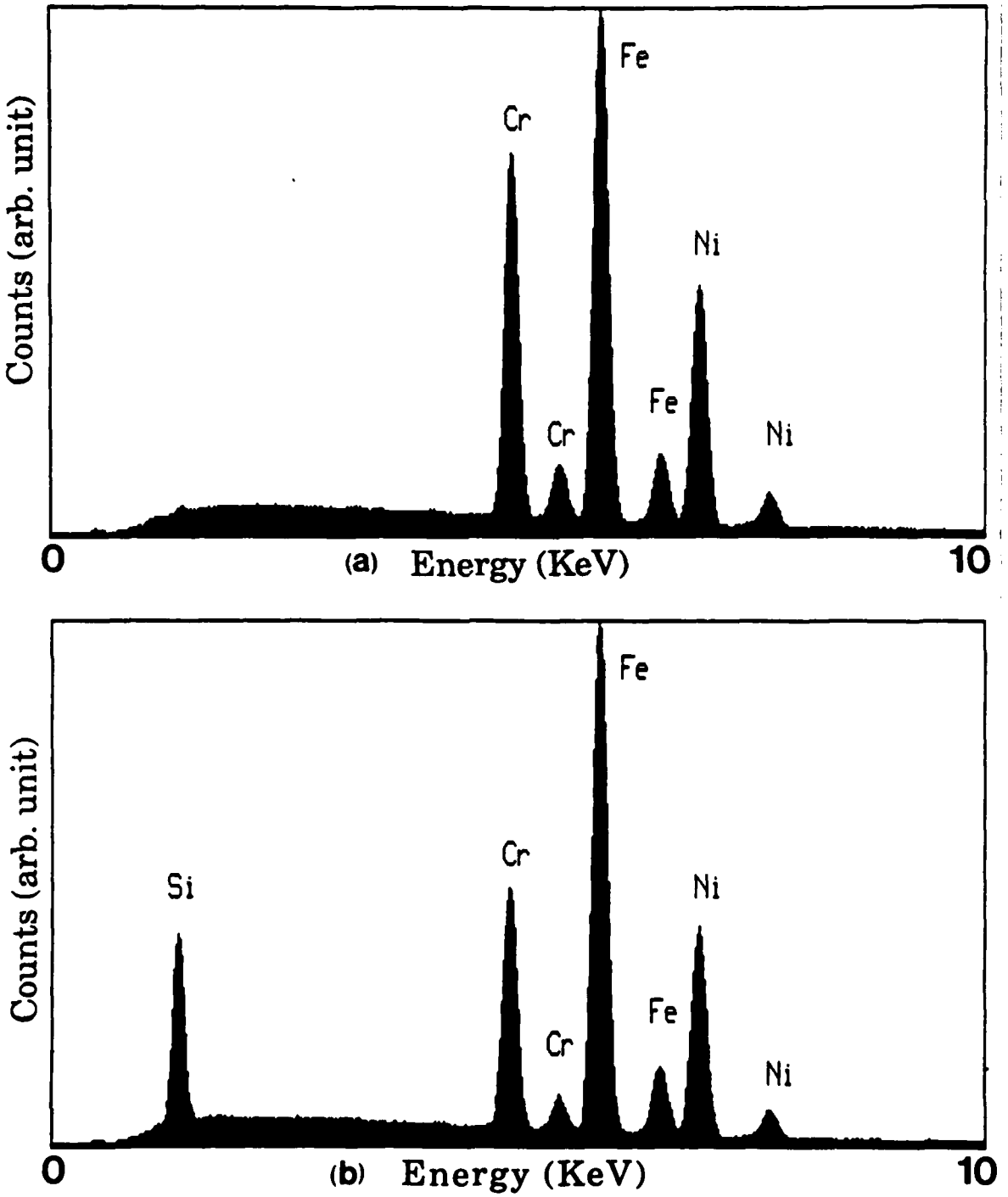

Fig. 4.31 EDS spectra collected from (a) point 1 and (2) point 2, as indicated in Fig. 4.30(a), showing the diffusion of Si is limited by the diffusion front.

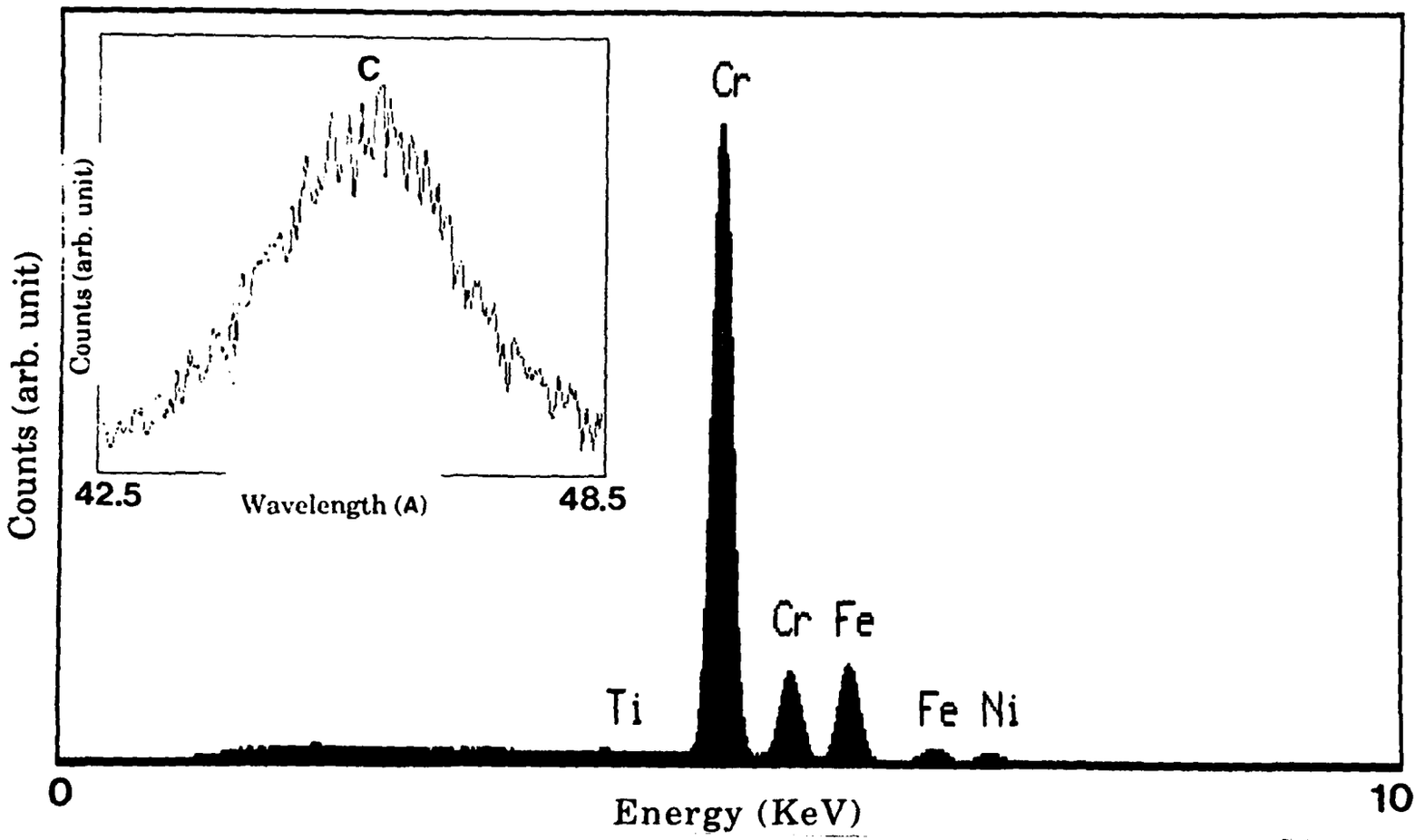

Fig. 4.32 EDS and WDS (the inset) spectra obtained from the grain boundary precipitates, as shown in Fig. 4.30(b), indicating the precipitates are Cr-carbide(s).

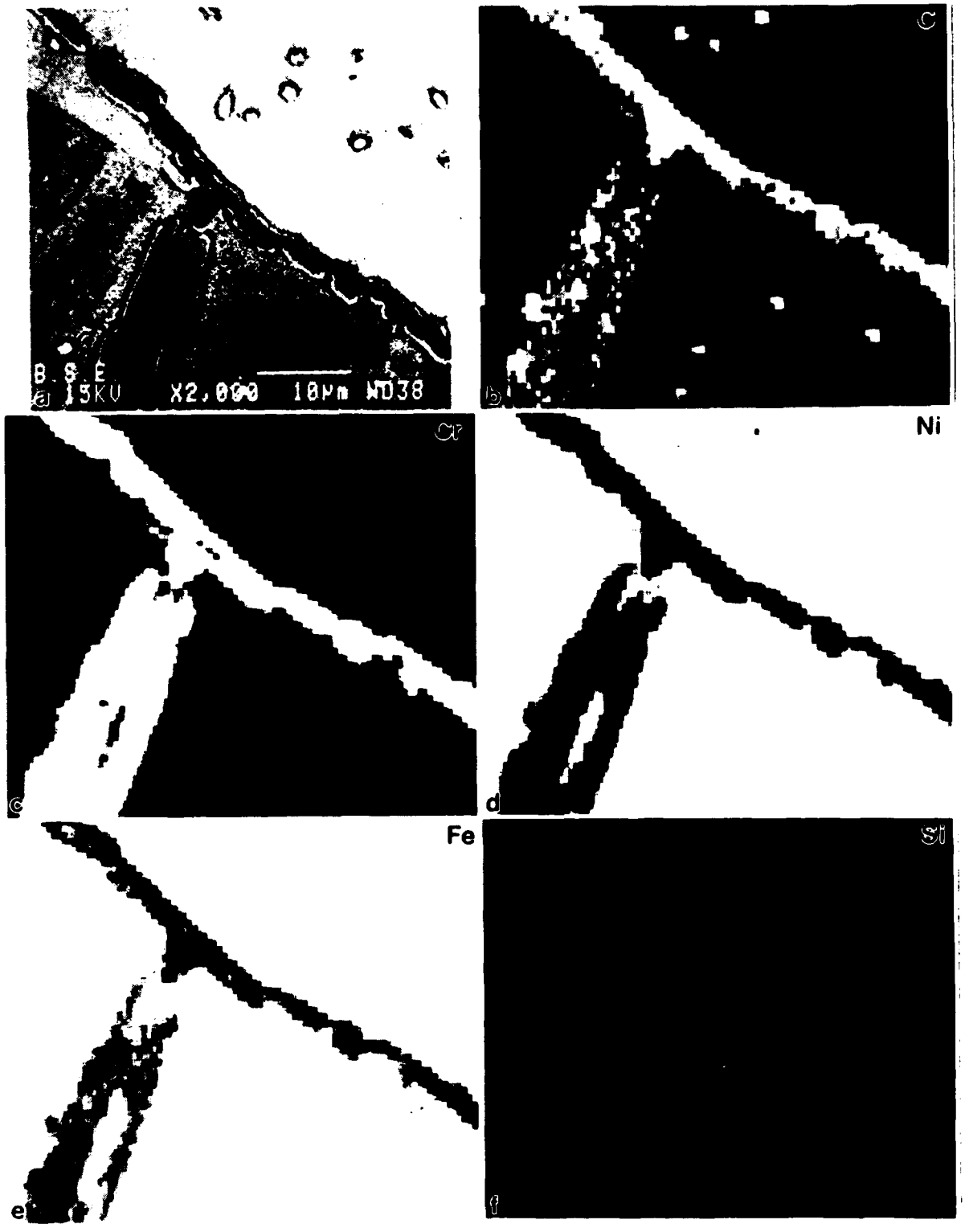

Fig. 4.33 (a) A backscattered electron image, and the corresponding elemental x-ray maps of (b) C, (c) Cr, (d) Ni, (e) Fe, and (f) Si from precipitates located in a triple grain boundary junction.

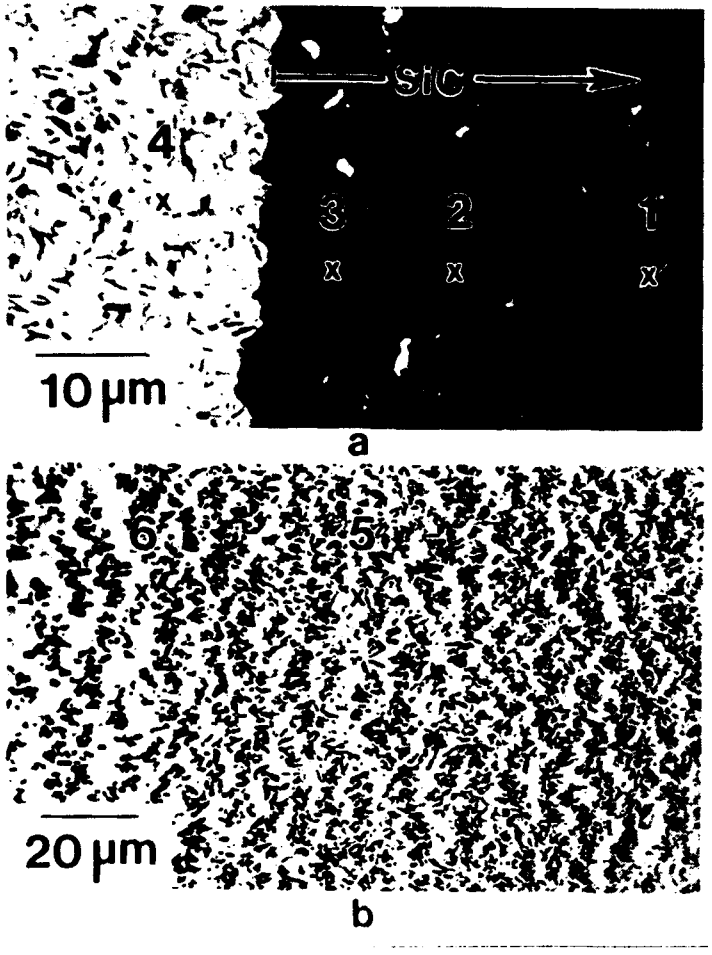

Fig. 4.34 SEM micrographs showing the locations from which systematic EDS analyses were conducted to establish the concentration gradients of Ni, Fe, and Cr.